Partitioning of platinum-group elements between metal and sulphide melt in the Cu-S and Ni-S systems.

by

Henriëtte Ueckermann

Submitted in partial fulfillment of the requirements
for the degree of Master of Science in Applied Mineralogy
at the Faculty of Natural Sciences and Engineering
University of Pretoria
Study leader: Prof. R.K.W. Merkle

February 2002

CONTENTS

LIST OF TABLES

LIST OF FIGURES

LIST OF ABBREVIATIONS AND SYMBOLS

σ	standard deviation
AEC	Atomic Energy Corporation
at%	Atomic percent
bd	below detection
D	Nernst partition coefficient
D_X	Nernst partition coefficient for element X
ED	energy dispersive
Exp	experiment number
eV	electron volt
EPMA	electron probe micro analyser
FWHM	full width at half maximum
KeV	kilo electron volt
LLD	lower limit of detection
MeV	mega electron volt
mss	monosulphide solid solution
nA	nano Ampére
n	number of analyses per experiment
nd	not determined
NAC	National Accelerator Center
nC	nano Coulomb
pA	pico Ampére
PGE	platinum-group element(s)
PIXE	particle induced X-ray emission
PRF	pre-reaction furnace
ppm	parts per million
SEM	scanning electron microscope
Temp	temperature
WD	wavelength dispersive
wt%	weight percent

LIST OF MINERAL FORMULAE - ALL PHASES SYNTHETIC

Cu	Copper
CuS	Covellite
$Cu_{2-x}S$	Digenite
Cu_2S	Chalcocite
$CuFeS_2$	Chalcopyrite
Fe	Iron
FeS	Troilite
FeS_{1+x}	Pyrrhotite
FeS_2	Pyrite
$(Fe,Ni)_9S_8$	Pentlandite
Ni	Nickel
NiS	Millerite
NiS_2	Vaesite
Ni_3S_2	Heazlewoodite
Ni_9S_8	Godlevskite
Ni_3S_4	Polydymite

1. Introduction and aim of study

The platinum-group elements (PGE - Ru, Rh, Pd, Os, Ir, and Pt) are often considered to be strongly siderophile and geochemically coherent (Fleet and Stone, 1991; Schmitt *et al.*, 1989). PGE patterns in undepleted mantle xenoliths (lherzolites and peridotites) compared to chondrites show relatively uniform depletion of the PGE during the primary differentiation of planetary material (Barnes *et al.*, 1985; Walker *et al.*, 1996). However, numerous natural examples of fractionation and preferential concentration of PGE have been recorded through the years. Palme and Wlotzka (1976) reported extreme enrichment of Os, Ir, Ru, Rh and Pt in metallic and sulphide phases in refractory inclusions in C3V chondritic meteorites, while fractionation of PGE during geological processes is shown by the substantial enrichment of Rh, Pd and Pt compared to Os, Ir and Ru in crustal mafic intrusions (Naldrett *et al.*, 1979; Naldrett, 1981). In contrast, deposits related to ultramafic rocks (komatiites) characteristically have comparatively much lower contents of Rh, Pd and Pt compared to Os, Ir and Ru. Enrichment of Os, Ir and Ru in ophiolites in chromitites (Page and Talkington, 1984; Barnes *et al.*, 1985; Legendre and Auge, 1986; Walker *et al.*, 1996) can be attributed to partial melting of mantle material, which results in a residue rich in the refractory elements Os, Ir and Ru (concentrated in the chromitite) and a melt enriched in Rh, Pd and Pt, depending on the S saturation of the source. This melt could then form the cumulate upper portions of the ophiolite which are enriched in Rh, Pd and Pt (Page and Talkington, 1984). During partial melting of peridotites, Pt and Pd are mobilised with Cu, while Ir and Ru are refractory, and the behaviour of Rh varies (Gueddari *et al.*, 1996; Pattou *et al.*, 1996). Cu-rich sulphide ores are characteristically enriched in Pt, Pd and Au, and depleted in Os, Ir, Ru and Rh compared to spatially-related Ni ores (Naldrett *et al.*, 1982; Naldrett, 1989; Barnes *et al.*, 1997). This latter enrichment is believed to be the result of equilibrium partitioning during fractional crystallisation of a sulphide melt and its change into a more Cu-rich residual liquid.

All these fractionation processes are controlled by the partition coefficients of the PGE between various phases, and can be characterised by these coefficients. A partition or distribution coefficient (D) is the ratio of the content of an element in two co-existing

phases: for example the ratio of the Pt content in metal, measured in wt%, to Pt content in co-existing sulphide. Exact knowledge of partition coefficients provides quantitative data necessary to evaluate precious metal behaviour in high temperature magmatic processes in nature, as well as in technical processes such as smelting and refining. Their application allows a better understanding of the chemistry of these trace elements in metal-matte systems in metallurgical practice (Schlitt and Richards, 1975).

The phases in which PGE most frequently occur in nature consist of base-metal sulphides, mainly Cu, Fe and Ni sulphides, so that the PGE are normally extracted and refined together with these and a large range of minor elements. The simplified Cu-Fe-Ni-S system is already very complex, and to fully understand and to permit prediction of the behaviour of the PGE in such complex systems, their behaviour in binary and ternary systems needs to be known. Potential developments in the beneficiation of PGE may involve further reduction of the S-contents in the mattes compared to present practice. Presently alloys of varying composition (Cu-Ni±Fe) are formed during slow cooling, but the behaviour of PGE in the systems Cu-S, Ni-S and Fe-S are poorly understood. Although a fair amount of research has been published on the more complex systems resembling natural conditions (e.g. Fleet *et al.*,1993, Li *et al.*, 1996, Barnes *et al.*, 1997), very little information is available on the partitioning of PGE in the binary and ternary systems. It was therefore decided to quantify the partitioning of Rh, Pd and Pt between the metals and selected sulphide phases and melt compositions in the Ni-S, Cu-S and Fe-S systems. Due to insurmountable technical problems that were experienced in the investigation of the Fe-S system (discussed in detail in section 5.3.), this system was not investigated as comprehensively as the other systems.

1.1. Choice of PGE contents for investigation

The aim of this investigation set out as the determination of the behaviour of PGE at trace concentrations, comparable to typical PGE matte contents, and higher than natural concentrations, in the Cu-Fe-Ni-S system. The concentrations of PGE in nature are very low (e.g. Barnes *et al.*, 1985) and, although somewhat higher in metallurgical mattes (e.g. Schlitt and Richards, 1975), they still occur in trace amounts. Stone *et al.* (1990) underlined the

importance of trying to keep experimental conditions as close as possible to the conditions to which the results would be applied. Initial experiments were prepared to contain 500 ppm, 1000 ppm and 2000 ppm PGE. Although these concentrations are higher than typical PGE contents in nature, and somewhat high for metallurgical comparison, they were chosen because quantitative analyses would still be practical.

To determine if interpolation and extrapolation of partition coefficients from low to much higher PGE concentrations would be meaningful, additional experiments with PGE contents of 6000 ppm and 10000 ppm were prepared. Jones and Drake (1983) and Willis and Goldstein (1982) observed that the Ni partition coefficient in the Fe-Ni-S system (with minor impurities) is influenced by the bulk Ni content of the system. Crocket *et al.* (1997), in an investigation of PGE partitioning between sulphide and basalt melt, reported that variation of partition coefficients for some PGE was related to initial PGE concentration in charges. Barnes *et al.* (1997), however, compared their partition coefficients, calculated from experiments performed with PGE at percent levels, with experiments reported in the literature where PGE contents were at ppm levels and found no significant difference. The investigation of PGE partitioning in this study using at least three different PGE concentrations makes it possible to determine whether the partition coefficient of a specific PGE remains constant from low to high concentrations.

To determine how the presence of other PGE influence the partitioning behaviour of a single PGE, each PGE was investigated in the absence of other PGE, as well as in combination with them. Sulphur content in liquid was found to influence the partition coefficients of siderophile elements, such as Ir (Jones and Drake, 1983), and Schlitt and Richards (1975) determined that in the region of liquid immiscibility in the Cu-Ni-S system, an increase in Ni content caused a systematic change in the Ag partition coefficient between alloy and melt. The influence of PGE on each other was not expected to be as severe as in these examples.

Considering that each PGE would be investigated at at least three different concentrations at a chosen bulk composition, as well as isolated from other PGE, it was considered

impractical to include all six PGE in the investigation. Rh, Pd and Pt were chosen, as these are economically the most important PGE. Furthermore, Pt is a heavy PGE, while Rh and Pd are light PGE, and Pt and Pd traditionally behave similarly in mss systems as opposed to Rh.

1.2. Choice of major element compositions of experiments

1.2.1. The Ni-S system at low S contents

Kullerud and Yund (1962) reviewed all the previous work on the binary system Ni-S and discussed a low temperature Ni_7S_6 phase that transforms to a high temperature Ni_7S_6 phase. Further research by Kulagov *et al.* (1969), Naldrett *et al.* (1972) and Fleet (1987, 1988) established that stoichiometrically and structurally, low temperature Ni_9S_8 (godlevskite) was the low temperature Ni_7S_6 phase of Kullerud and Yund (1962). Godlevskite occurs at temperatures below that of interest to the present investigation.

The thermodynamic properties and phase relations of the system Ni-S were also studied by Lin *et al.* (1978), Sharma and Chang (1980) and Cemic and Kleppa (1986). Except for native Ni, five mineral phases are now known to exist within the Ni-S system: heazlewoodite (Ni_3S_2), godlevskite (Ni_9S_8 - see above), millerite (NiS), polydymite (Ni_3S_4) and vaesite (NiS_2). Additionally, high temperature modifications are known for Ni_3S_2 (above 533°C), Ni_9S_8 (above 397°C) and NiS (above 282°C) (Sharma and Chang, 1980). Of all these phases, only heazlewoodite is commonly found in slow-cooled metallurgical mattes, which are relatively low in sulphur.

The phase diagrams by Sharma and Chang (1980) and Cemic and Kleppa (1986) were used to determine the bulk compositions of experimental charges. All experiments were designed to contain co-existing nickel and sulphide melt. The charges were equilibrated from 1200°C to 700°C, at 100°C intervals. The weight percentages of elements in the experimental charges are given in the Appendix, Tables A1 to A6.

1.2.2. The Cu-S system at low S contents

The phase relations and compositions of the Cu-S system have been investigated by a number of authors; the most relevant publications include Kullerud (1960), Morimoto and Gyobu (1971), Schlitt and Richards (1973) and Chakrabarti and Laughlin (1986).

Bulk compositions for experimental charges were determined based on the phase diagram by Chakrabarti and Laughlin (1986). Experiments were designed from 1200°C to 700°C at 100°C intervals, at compositions which would allow the investigation of co-existing copper and digenite, co-existing Cu-rich melt and digenite, co-existing digenite and S-rich melt, and immiscible Cu-rich melt and S-rich melt. Weight percentages of elements in the experimental charges are given in the Appendix, Tables A7 to A12.

1.2.3. The Fe-S system at low S contents

The phase diagrams by Kullerud and Yoder (1959), Kullerud (1961), Chuang *et al.* (1985), supported by the later phase diagram by Fleet and Stone (1991), were used to determine the bulk major element compositions of the experimental charges for the investigation of this system. Experiments were designed from 1200°C to 700°C at 100°C intervals, at compositions that would contain co-existing iron and troilite, co-existing iron and quenched melt, and co-existing pyrrhotite and quenched melt. Weight percentages of elements in the experimental charges are given in the Appendix, Tables A13 to A18.

1.3. Previous investigations of PGE partition coefficients

1.3.1. The Ni-S system

Urban *et al.* (1995) investigated three nickel-sulphide buttons obtained from different nickel sulphide fire-assay extraction methods, containing traces of PGE. Heazlewoodite (Ni_3S_2) was the dominant phase, with lesser PGE-sulphides and PGE-Ni alloys. It was found that Rh, and to a lesser degree Ru, display a strong affinity for the PGE-sulphides (with

differing compositions in different buttons), with PGE sulphide / heazlewoodite partition coefficients between 25 and 55. The authors suggested that the same behaviour could be expected for Pd. Ir, Os and Pt tend to alloy with each other and Ni, with metal / heazlewoodite and metal / PGE-sulphide partition coefficients in the order of 500 to 1000 for Ir, 100 to 400 for Os and 100 to 1000 for Pt.

1.3.2. The Cu-S system

Gerlach *et al.* (1972) investigated the partitioning of Pt and Au at 1200°C in several systems, including the Cu-S system, and determined a D_{Pt} of 2000 for Cu / Cu sulphide. Schlitt and Richards (1975) determined an experimental D_{Pd} of 167 and D_{Pt} of 2500 at 1200°C. Taylor (1983) investigated the thermodynamics involved in the partitioning of trace elements between Cu bullion (99 % Cu) and Cu matte (roughly Cu_2S), using experiments equilibrated at 1200°C. He found a D_{Rh} of 110 from the experiments, and calculated D's of 11 for Rh, 25 for Pd, 550 for Ru, 5400 for Ir, and 6800 for Pt. He also quoted D's of 70 for Ru (Romanov *et al.*, 1973), 80 for Pd (Burylev *et al.*, 1974), 340 for Ir (Romanov *et al.*, 1973) and 2000 for Pt (Burylev *et al.*, 1974).

1.3.3. The Fe-S system

The classical study by Noddack *et al.* (1940) on partitioning of minor amounts of PGE between iron and sulphide are now known to be suspect due to impure separation of the phases (Fleet and Stone, 1991). Partition coefficients for the iron and sulphide liquid at 1300°C to 985°C were about 8 to 13 for Ru, Rh, Os, Ir and Pt, and 2.6 for Pd, with all PGE preferring the iron. For iron and FeS at 985°C, the partition coefficients for all six PGE were found to be between 10 and 16 (all PGE preferring iron). Analyses were performed on bulk mechanical separates, and the FeS is now known to have contained about 6 wt% iron, which influenced the calculated D's.

Jones *et al.* (1986) reported an iron / troilite partition coefficient of 150 for Pd, and Jones and Drake (1986) an iron / sulphide partition coefficient of 83 for Ir.

The investigation by Fleet and Stone (1991) on the Fe-Ni-S system contained very low contents of Ni, with some experiments containing no Ni at all, so that these results are applicable to the Fe-S system. In co-existing iron and sulphide liquid assemblages, Os, Ir and Pt were reported to be concentrated in the alloy phases (strongly siderophile), with Pd less so. Alloy / sulphide liquid partition coefficients reported for 1000°C are 1 to 2 for Pd, 30 to 110 for Rh and >1000 for Os, Ir, Pt and Ru. In co-existing troilite and sulphide liquid assemblages Ru, and to a lesser degree Rh, are the only PGE with a significant solubility for troilite, while Pd partitions strongly into the liquid, confirming the minimal substitution of PGE in stoichiometric troilite.

Chabot and Drake (1997) experimentally investigated the metal / liquid D for Pd along with Ag. D_{Pd} changed from slightly incompatible in metal to slightly compatible (0.5 to 2), as the S content of the liquid increased.

1.3.4. The Fe-Ni-S system

Fleet and Stone (1991) investigated the partitioning of minor amounts of all six PGE in the Fe-Ni-S system at 1000°C to 1400°C at low pressure. They reported distinctly different partitioning behaviour for the light and heavy PGE. Os, Ir and Pt are preferentially concentrated into the alloy phases, while Pd is depleted in alloys and relatively enriched in sulphide liquid. Pd varies from siderophile to chalcophile in assemblages with Fe-containing alloy, but is chalcophile in all other alloy-containing assemblages. The reported partition coefficients for Fe alloy / sulphide liquid are 1 - 2 for Pd (comparable to Ni), 30 - 110 for Rh, and >1000 for Pt, Ir and Os. The overall affinity for Fe-rich alloy is Os >> Ir > Pt > Ru > Rh >> Pd. Ru, and to a lesser extent Rh, are the only PGE with significant solubility in troilite co-existing with sulphide melt, while Pd partitions strongly into the melt. Minor amounts of Ru, Rh and Pd were reported in Ni-bearing troilite.

Distler *et al.* (1977) investigated the distribution of Ru, Rh and Pd between pyrrhotite, pentlandite and sulphide melt, again observing enrichment of Pd in the melt, while Ru and Rh partitioned into co-existing sulphide.

The partitioning of minor amounts of Ir in the Fe-Ni-S system was investigated by Willis and Goldstein (1982) and Jones and Drake (1983), who found the D_{Ir} to be dependent on the S content in the liquid. Jones and Drake (1986) adopted an Fe-rich alloy / sulphide liquid partition coefficient of 83 for Ir, and Jones and Malvin (1990) constructed a positive linear relationship between the S content in the liquid and the Ir partition coefficient in solid metal.

Fleet *et al.* (1999) investigated the partitioning of PGE and Au between solid metal and liquid metal sulphide, and reported high solid metal / liquid metal partition coefficients for the most refractory metals (D_{Os}: 249 to 6180, D_{Ir}: 367 to 4180), intermediate for Ru (41 to 164) and Pt (40 to 300), and near unity for the least refractory metals (D_{Pd}: 0.7 to 1.47, D_{Ni}: 1.40 to 2.77, D_{Au}: 1.32 to 3.87). They report variation in bulk composition as the most important cause for the variation in the partition coefficients.

1.3.5. The Cu-Fe-Ni-S system

Many nickel-copper sulphide ore bodies contain Cu-rich and Fe-rich portions, with the Fe-rich ore typically enriched in Os, Ir, Ru and Rh, and the Cu-rich ore enriched in Pt, Pd and Au (Li and Barnes, 1996; Barnes *et al.*, 1997). The Fe-rich ore represents the first phase to crystallise from a sulphide melt - the monosulphide solid solution (mss), while the Cu-rich ore represents the fractionated liquid. Fleet *et al.* (1993) crystallised mss from Cu- and Ni-enriched sulphide liquid at 1000 – 1040°C, and determined partition coefficients (weight % metal in mss / weight % metal in sulphide liquid) of 4.3 for Os, 3.6 for Ir, 4.2 for Ru, 3.0 for Rh, 0.21 for Pt and 0.21 for Pd. Barnes *et al.* (1997) reported D_{Pd}: 0.005 to 0.435, D_{Rh}: 0.045 to 7.43, D_{Pt}: 0.013 to 0.46 and D_{Ir}: 0.429 to 17, depending on temperature and S content. Barnes *et al.* (1994) and Li *et al.* (1996) found D_{Pd}: 0.14, D_{Pt}: 0.1, and D_{Rh}: 4 to 7. For their low fS_2 experiments they found D_{Pd}: 0.02 and D_{Rh}: 0.3 to 0.4, comparable to the

low fS_2 partition coefficients by Fleet and Stone (1991) of D_{Pd}: 0.02 and D_{Rh}: 0.2 to 0.3. According to Peregoedova (1997), the most important difference between Pt and Pd behaviour during crystallisation of Cu-Fe-Ni-S melt is that Pt tends to form its own compounds, including sulphides at high fS_2, whereas Pd prefers (Fe,Ni,Cu)-sulphide solid-solutions.

1.3.6. Other relevant systems

1.3.6.1. Pd-Fe-S system

Makovicky *et al.* (1986), Makovicky *et al.* (1988) and Makovicky and Karup-Møller (1993) investigated this system. S-rich pyrrhotite dissolved more than 12 wt% Pd while troilite contained no detectable Pd at 900°C. At 500°C Pd in troilite was below detection, up to 0.5 wt% Pd was measured in S-rich pyrrhotite, and less than 0.01 wt% Pd measured in pyrite. Previous research in this system is recorded in publications by Skinner *et al.* (1976), Distler (1980) and Bryukvin *et al.* (1985).

1.3.6.2. Pt-Fe-S system

At 900°C up to 2.2 wt% Pt was measured in S-rich pyrrhotite, and Pt in troilite was below detection (Makovicky *et al.*, 1986). Pt-rich pyrrhotite was found to co-exist with PtS and PtS_2. At 500°C Pt was below detection in pyrrhotite of all compositions and pyrite.

1.3.6.3. Rh-Fe-S system

It was found that pyrrhotite can contain up to 44 wt% Rh at 900°C, while still retaining its essential X-ray characteristics (Makovicky *et al.*, 1986). At 500°C, up to 6.7 wt% Rh was found in pyrrhotite, which decreased to around 1.1 wt% Rh at lower S contents. Rh in pyrite was below detection.

1.3.6.4. Pd-Ni-S system

This system was investigated by Karup-Møller and Makovicky (1993). They found that at 900°C up to 4.9 wt% Pd was present in $Ni_{1-x}S$, and up to 2.1 wt% Pd in NiS_2. At 725°C they detected up to 2.6 wt% Pd in $Ni_{1-x}S$, 4.3 wt% Pd in Ni_3S_2 and 1.0 wt% Pd in NiS_2. At 500°C $Ni_{1-x}S$ contained up to 0.5 wt% Pd, Ni_3S_2 up to 13.7 wt% Pd, Ni_7S_6 up to 1.1 wt% Pd and NiS_2 up to 0.3 wt% Pd. Pd in $Ni_{1-x}S$ and NiS_2 was below detection at 400°C, while up to 0.4 wt% Pd was detected in Ni_3S_2, and up to 0.2 wt% Pd in Ni_7S_6.

1.3.6.5. Cu-Pd-S system

Karup-Møller and Makovicky (1999) investigated this system at 900°C, 725°C, 550°C and 400°C. $Cu_{2-x}S$ dissolved up to 0.7 at% Pd at 900°C and up to 0.9 at% Pd at 725°C, but at 550°C Pd was below detection in $Cu_{2-x}S$, and at 400°C Pd was below detection in both $Cu_{2-x}S$ and CuS.

1.3.6.6. Cu-Rh-S system

This system was investigated at 900°C, 725°C and 500°C by Makovicky and Karup-Møller (1994). At 900°C $Cu_{2-x}S$ was found to contain up to 0.04 at% Rh, while containing only traces of Rh at lower temperatures. Rh in CuS at 500°C was also below detection. Copper metal was found to contain up to 10 at% Rh at all temperatures.

1.3.6.7. Fe-Ni-PGE systems

Blum *et al.* (1989) investigated phase boundaries and tie lines in the Fe-Ni-Ru system at 1000°C, 800°C and 600°C, as well as the partitioning behaviour of Pt and Ir between phases in this system. Pt was found to be more compatible with face-centred cubic Ni-Fe alloy, while Ir was more compatible with close-packed hexagonal Ru-Fe alloy, even though pure Pt and Ir both have face-centred cubic crystal structures.

1.3.6.8. Fe-Ni-PGE-S system

The Fe-Ni-PGE-S system was investigated at 500°C by Makovicky *et al.* (1986). No Pt, but up to 12.5 wt% Pd and up to 12.4 wt% Rh was detected in pentlandite. It was concluded that Pd and Rh, along with Ru, can fully occupy the octahedral metal positions in pentlandite, while Pt cannot enter the pentlandite structure. It was also observed that at low fS_2 PGE prefer alloy with Fe to troilite. With moderate increase in fS_2 the solubility of Rh in pyrrhotite increased sharply.

The Pd-Fe-Ni-S system was investigated by Distler *et al.* (1977). Makovicky and Karup-Møller (1995) and Makovicky *et al.* (1990) experimentally investigated the systems Fe-Ni-Pd-S and Fe-Pt-Pd-As-S.

2. Experimental technique

2.1. Sealed quartz glass tube technique

This technique was described by Kullerud (1971) and was also used for experimental work by Bruwer (1996) in the experimental sulphide laboratory of the Geology Department at the University of Pretoria. Experiments were carried out in high purity quartz glass tubes. Pure SiO_2 does not react with sulphur or the relevant metals at the temperatures under investigation, making it a suitable, as well as affordable, container for this type of investigation. The walls of the tubes have to be thick enough to withstand high S pressure from the inside during heating, but also thin enough to allow for very fast cooling of the contents during quenching. In this study, all quartz glass tubes used had an inside diameter of 4 mm and a wall thickness of 1 mm.

One end of a short tube (usually between 8 and 10 cm - Figure 1A) was heated over a natural gas - oxygen flame until it softened and melted to form a closed end (Figure 1B). To ensure that no contaminants were present in the tube, it was then thoroughly cleaned. Contaminants would have influenced the experiments, or reacted with quartz at high temperatures to weaken the glass. The tube was rinsed with cleaning solution (Extran), followed by thorough rinsing with clean water, and lastly rinsing with acetone to reduce the amount of static electricity built-up during later weighing-in of the powders. Static electricity was observed to cause the powders to cling to the walls of the tube, so that not all the reactants would reach the bottom where reactions and equilibration take place. When the tube was dry, the starting materials were weighed in (Figure 1C). A short quartz glass rod, with a diameter of slightly less than 4 mm and a length of about 2 cm, was placed on top of the contents in the tube (Figure 1D). The open end of the tube was then connected to a vacuum pump and the system evacuated down to between 10 and 60 milliTorr (1.3 to 8 Pa). During evacuation the rod reduced the volume in the tube to allow faster evacuation, and protected the contents of the tube by partly blocking the opening of the tube, preventing the powder inside from being sucked out. A wet cloth was wrapped around the bottom end of the tube where the experimental charge was located. The tube was then heated in the gas

flame at a position above the rod (Figure 2), rotated evenly while remaining under vacuum until the tube wall collapsed on the rod and sealed the contents of the tube (Figure 1E). The wet cloth protected the charge from the heat during this process.

2.2. Starting material

Fe, Cu and Ni with purity of ≥ 99.98% and S with purity of at least 99.99% were used for all experiments, as well as specpure Pt, Pd and Rh.

Before the elements were weighed in, Cu and Ni were reduced to eliminate all oxygen that might have been introduced through surface oxidation. The reduction process is illustrated in Figure 3. A tube furnace was fitted with a quartz glass tube. One end of the tube was connected to a H_2 and Ar gas inlet, and the other end to a rubber tube which was led through a beaker filled with water. No openings were left where atmospheric gases could infiltrate the system. Powder of the pure element was placed in a quartz glass boat and inserted into the tube in the tube furnace. The powder was then heated at 600°C for 6 hours in an atmosphere of H_2 and Ar gas. The gas entered the tube through the inlet, and exited on the other end, where the pressure of the gases could be monitored by checking the speed of the gas bubbles as they rose through the water. After six hours the elements were allowed to cool in an Ar atmosphere, before they were removed from the tube. The elements usually had to be crushed, sometimes in acetone to prevent oxidation as best as possible, before they could be weighed into the tubes. The reduction process was performed immediately before the elements were weighed into the tubes, to limit oxidation as much as possible.

The reduction technique described above was found to be ineffective for Fe. An abnormally high number of the Fe-containing experiments failed and were oxidised. This is believed to be due to oxidation of the Fe after reduction and before weighing-in, resulting in FeO formation and reaction with the quartz glass. Consequently, reduced Fe was first weighed into tubes, and these tubes were again heated in the tube furnace under Ar + H_2 atmosphere (Figure 4). After reduction, S and PGE were weighed in and the tube sealed as quickly as possible. The weight difference before and after reduction due to oxygen loss was found to

be approximately 0.5 wt% (~0.002 g loss from 0.400 g). The Fe weight after reduction was used to calculate the amount of S and PGE to be added. Different reduction times, temperatures and H_2 pressures were evaluated to determine a possible effect on the success of the experiments, but no clear conclusions could be drawn. The higher success rate achieved for later experiments could be the result of reduction of Fe after weighing-in, allowing much less time for the Fe to oxidise. However, experience obtained through the preparation of hundreds of experiments in the laboratory suggests that quality differences exist between quartz tube batches, which led to many cracked tubes even in Fe-free experiments.

Sulphur was dried at 95°C and stored in a desiccator.

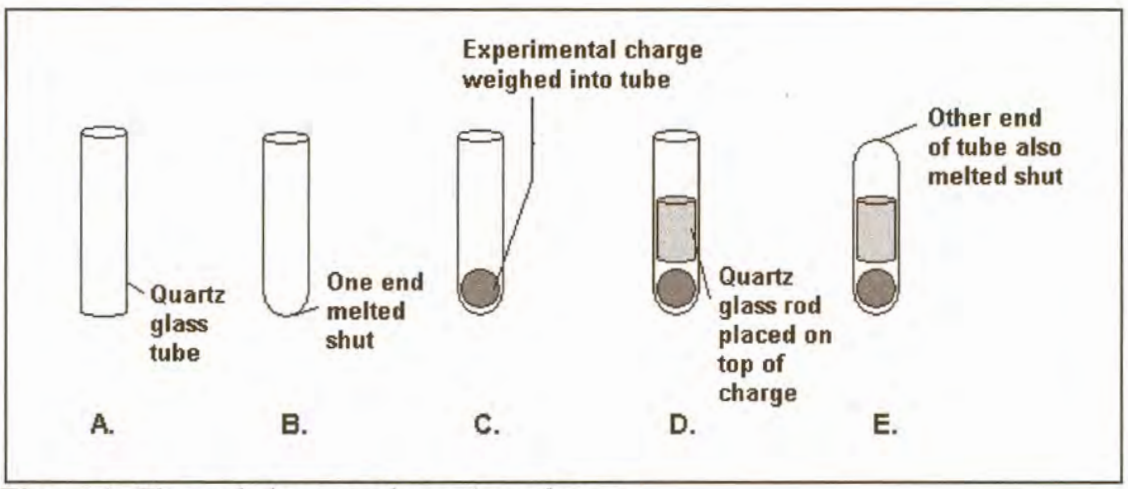

Figure 1. *The sealed quartz glass tube technique.*

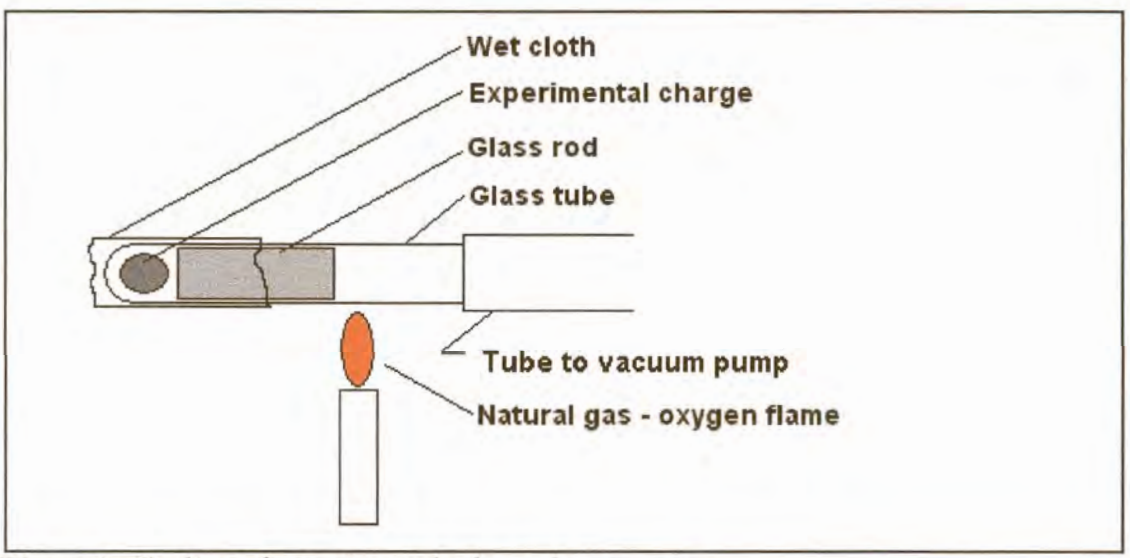

Figure 2. *Sealing of experimental tube under vacuum.*

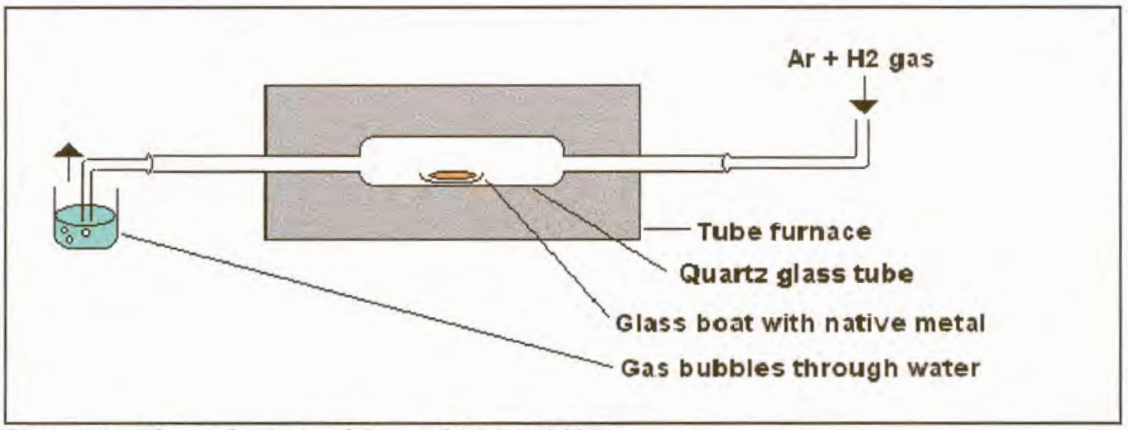

Figure 3. *The reduction of Cu and Ni at 600°C.*

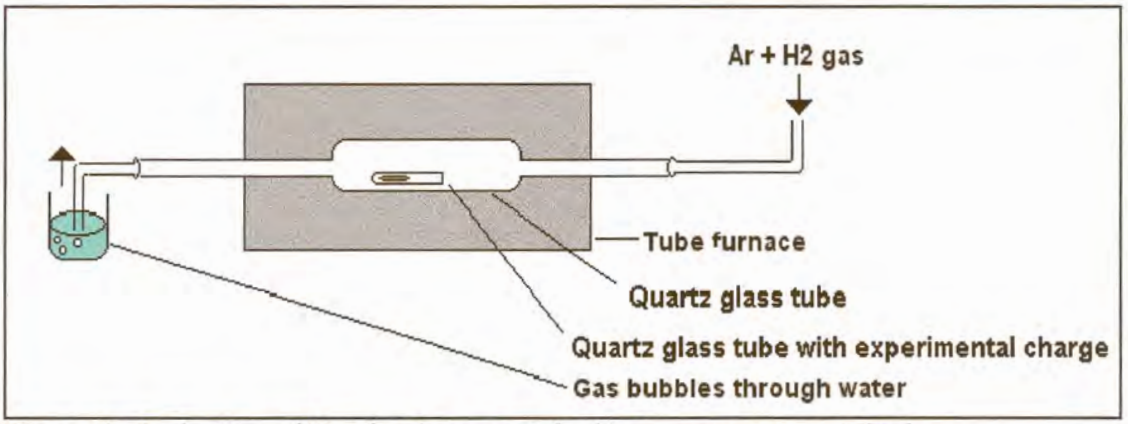

Figure 4. *Reduction of Fe after being weighed into an experimental tube.*

Very low concentrations of PGE were investigated. To be able to accurately weigh 500 ppm of PGE into an experiment, charges with a total weight of 2 grams had to be prepared. The 2 gram Fe-S experiments proved very difficult to prepare, as both Fe and S are light and the length of 2 grams of material weighed into a 4 mm diameter tube was about 20 cm. To obtain proper equilibration along the entire length of the tube was very difficult. These long tubes also cracked very easily, and the contents always separated during reaction. Experimental charges of 1 gram were prepared to investigate PGE contents of 1000 ppm, and 0.5 gram charges were prepared to investigate higher PGE contents. All the experimental charges prepared to investigate the Cu-S, Ni-S and Fe-S assemblages at all temperatures are shown in the Appendix, Tables A1 to A18.

2.3. Equilibration of experiments

2.3.1. Pre-reaction

After the tubes were sealed, they were heated in a pre-reaction furnace at 700°C to 800°C for at least one day. This allowed the pure sulphur powder to react with the metals, which prevented explosion of the tubes due to high sulphur vapour pressure at higher temperatures. According to Kullerud and Yoder (1959), pure sulphur pressure is between 15 and 35 bar at 700°C to 800°C. Sulphur pressure increases logarithmically with increasing temperature, and at higher temperatures pure sulphur pressure would crack the quartz glass tubes very easily. By pre-reacting the experiments at low temperatures, the presence of pure sulphur inside the tubes at higher temperatures was avoided.

2.3.2. Equilibration

Two large chamber furnaces, each fitted with six horizontal tubes reaching from the front door to the back of the furnace, were used for equilibration at the desired temperatures (Figure 5A). The temperature gradients along the length of the tubes were measured with a calibrated thermocouple. An experimental charge was inserted horizontally into one of the tubes and left at a position where the desired temperature was measured before and during equilibration over the entire length of the charge. A thermally isolating plug was inserted into the open front end of the tube to prevent heat loss. When the temperature in a tube was measured, a plug with a small hole was placed into the front end of the tube, and a calibrated hand-held thermocouple was inserted through this hole (Figure 5B). The temperature around the charge was considered unacceptable if it varied by more than 2°C from the desired temperature. Some of the lower-temperature experiments were placed vertically in holders and reacted in a smaller chamber furnace. A thermocouple was inserted through a small hole in the door of the furnace to ensure that the reaction temperature was satisfactory. When not used, the hole was filled with thermally isolating material.

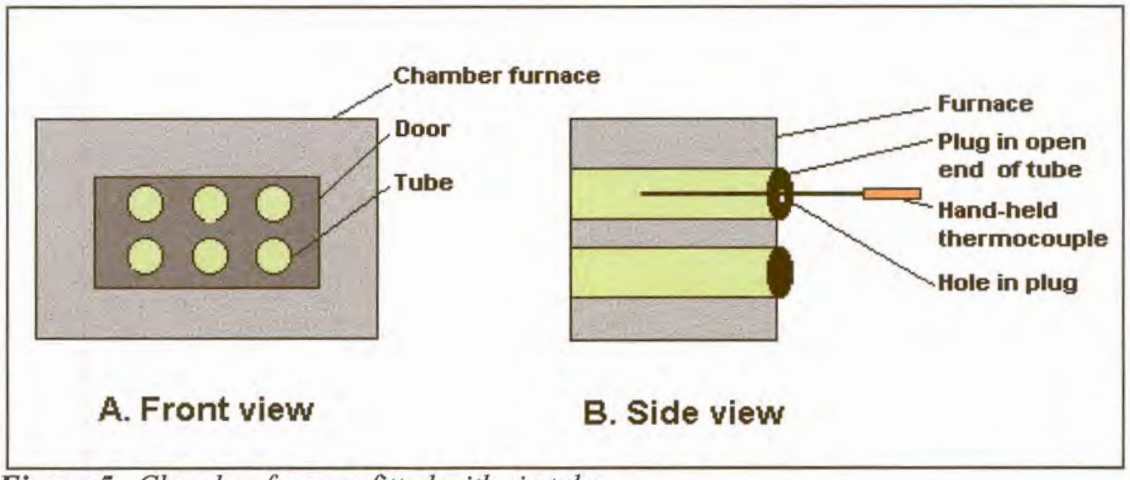

Figure 5. *Chamber furnace fitted with six tubes.*

All the experiments in this investigation were reacted at temperatures between 1200°C and 700°C. The high temperature experiments reached equilibrium much faster than the low temperature experiments, and were removed from the furnace after shorter time periods. Lengthy exposure of quartz glass to high temperatures (~1200°C) results in recrystallisation and weakening of the tubes. When these experiments were exposed to the higher temperatures for long time periods, the tubes tended to crack, which resulted in oxidation of the charges in the furnace, or cracking of the tubes when the experiments were quenched.

2.3.3. Quenching

When the charges were assumed to have reached equilibrium, they were quenched. As sulphide liquid crystallises into lower temperature phases during quenching, it is of great importance to cool the charge as fast as possible to limit the crystallisation time and therefore the crystallite sizes. A tall cylinder filled with cooled water was placed at the open end of a furnace tube, and the charge was then dropped into the cylinder and allowed to fall through the water, in this way preventing the formation of a heated or isolating boundary layer. Other cooling mediums that were tested by Bruwer (1996) were water and ice, supercooled brine and liquid nitrogen, but no systematic improvement on the quenching speed was observed. It is believed that the low thermal conductivity of the quartz glass limits the quenching speed more than the quenching medium does. The low temperature

experiments were taken directly out of the furnace in their holders, and tipped over into a large, deep, water-filled container.

2.4. Preparation of experiments for further investigation

The tube of a quenched experiment was broken open and the charge removed and split open to expose a cross-section. One half of the freshly exposed cross-section was mounted in epoxy under vacuum. The other half was kept as reference. Mounting under vacuum ensured that all air bubbles were removed from the epoxy, and that the epoxy filled all the pore spaces and cracks in the charge, so that a very good polish could ultimately be achieved. After polishing, each section was studied microscopically to ensure that representative areas of all the desired phases were visible. In binary systems no more than two phases can co-exist, and for this investigation all experiments were prepared to contain two phases in equilibrium. Sections were then photographed and prepared for analytical investigation. If one of the expected phases was not visible, grinding and polishing was continued. In some experiments, for example HU397, the PGE contents were very low, and the presence of a separate PGE alloy was suspected. This experiment was systematically polished away in 100 μm layers, but no alloy was found.

Total experimental charge weights varied from 0.25 gram to 2.0 gram, and more than one cross section was prepared from the larger experiments. In a number of experiments separated drops were found when the tubes were broken open. These drops, usually very small, could have separated before or during quenching. Drops formed during quenching would have equilibrated with the remainder of the experiment, and the composition would resemble that of the similar phases in the rest of the experiment. Drops formed before quenching probably did not equilibrate with the rest of the experiment. Each separated drop was investigated microscopically as well as analytically, to determine its relevance to each individual experiment.

Mounting and polishing difficulties were experienced due to hardness differences of co-existing phases. Metal is very malleable and co-exists in the different systems with sulphides such as digenite and pyrrhotite, both of which are very brittle. It was sometimes impossible to achieve a good polish of both the metal and the co-existing sulphide. Smearing of copper at very low concentrations was observed. This aspect is covered in a publication by Franklyn *et al.* (2001). In an investigation by Franklyn and Merkle (2001) tests were performed to determine the extend of smearing in various materials during polishing. Extensive smearing of PGE metals has also been reported by Makovicky *et al.* (1986) and Makovicky *et al.* (1990), but no discreet PGE phases were detected in this investigation, so that this possible complication could be ignored.

3. Microscopical Observations

3.1. Optical properties of quenched phases

3.1.1. Ni-S system

3.1.1.1. Nickel

White, very bright, isotropic (Figure 6).

3.1.1.2. Ni-S melt

Greenish cream, with exsolutions of nickel (Figure 6).

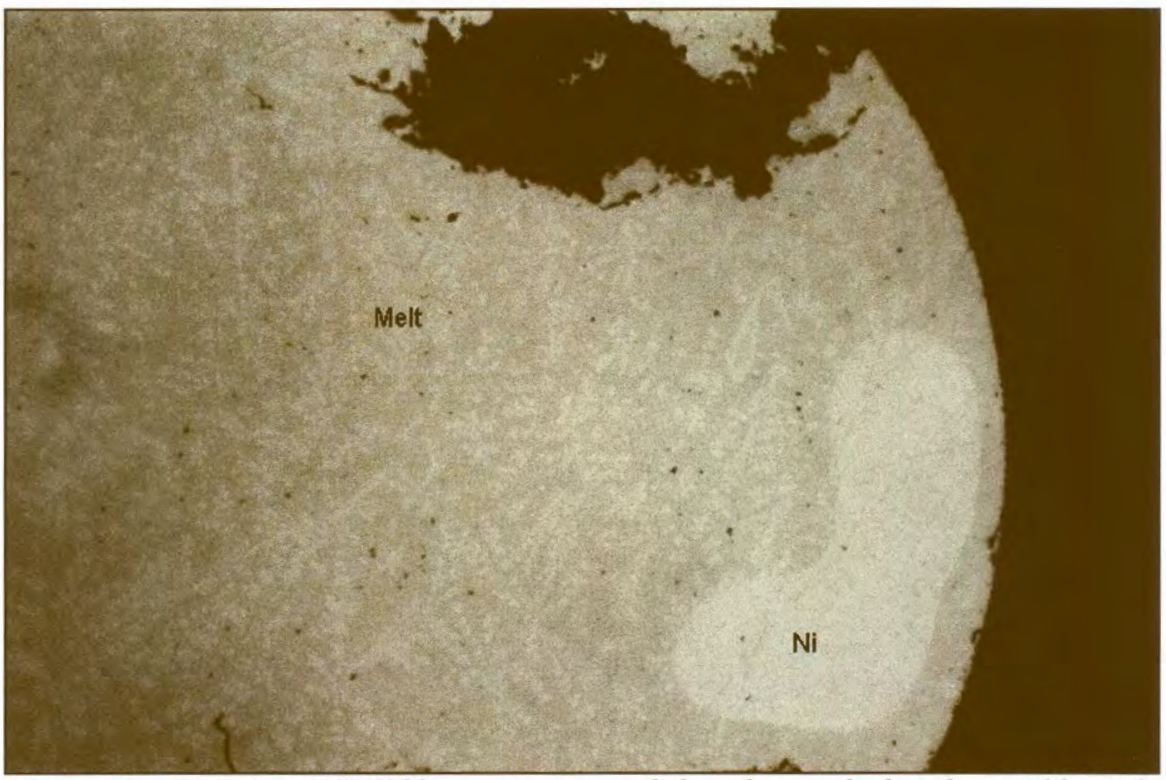

Figure 6. *Experiment HU393, co-existing nickel and quenched melt, equilibrated at 1000°C. Image was digitally enhanced. Field of view 4mm.*

3.1.2. Cu-S system

3.1.2.1. Copper

Bright, fresh pink, isotropic, tarnishes fast to reddish brown (Figure 7).

3.1.2.2. Digenite ($Cu_{2-x}S$)

Greyish blue, isotropic to weakly anisotropic. Twinning sometimes very pronounced, sometimes not visible. Shown in Figure 7 without twinning, and in Figure 8 with very clear twinning.

3.1.2.3. Cu-S melt

Three different melt compositions were investigated. The melt that co-exists with digenite has a similar colour (as well as similar composition) but is speckled with quench-phase alloys (Figure 8). The two immiscible melts investigated at 1200°C are similar in appearance to copper (the Cu-rich melt) and digenite (the S-rich melt), and are shown in Figure 9.

3.1.3. Fe-S system

3.1.3.1. Iron

Bright white, isotropic, tarnishes very quickly to grey-brown (Figure 10).

3.1.3.2. Troilite (FeS) and pyrrhotite (FeS_{1+x})

Both light yellow, strongly anisotropic, pyrrhotite weakly pleochroic (Figure 10, 26).

3.1.3.3. Fe-S melt

Creamy yellow colour, with quench-phase alloys visible, and sometimes a faint heterogeneous texture; anisotropic. Quench-phase alloy is visible in the melt shown in Figure 11.

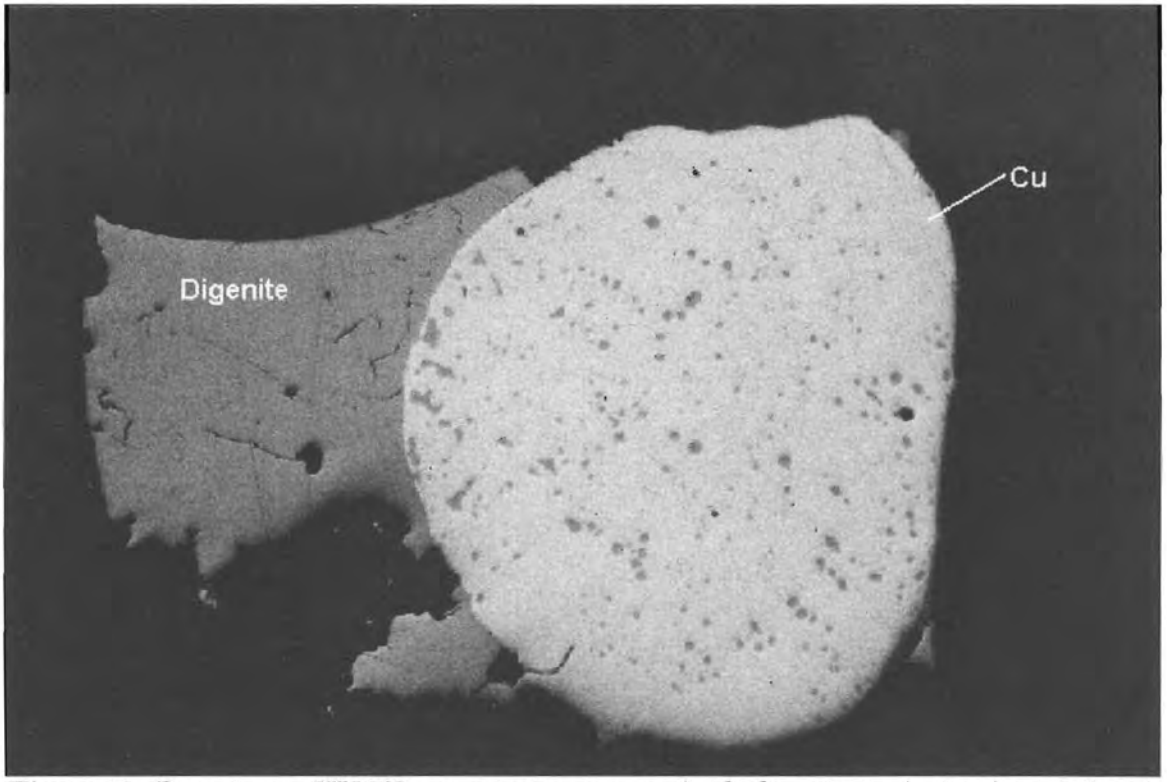

Figure 7. *Experiment HU465, co-existing copper (with digenite inclusions) and digenite, equilibrated at 1000°C. Field of view 4 mm long.*

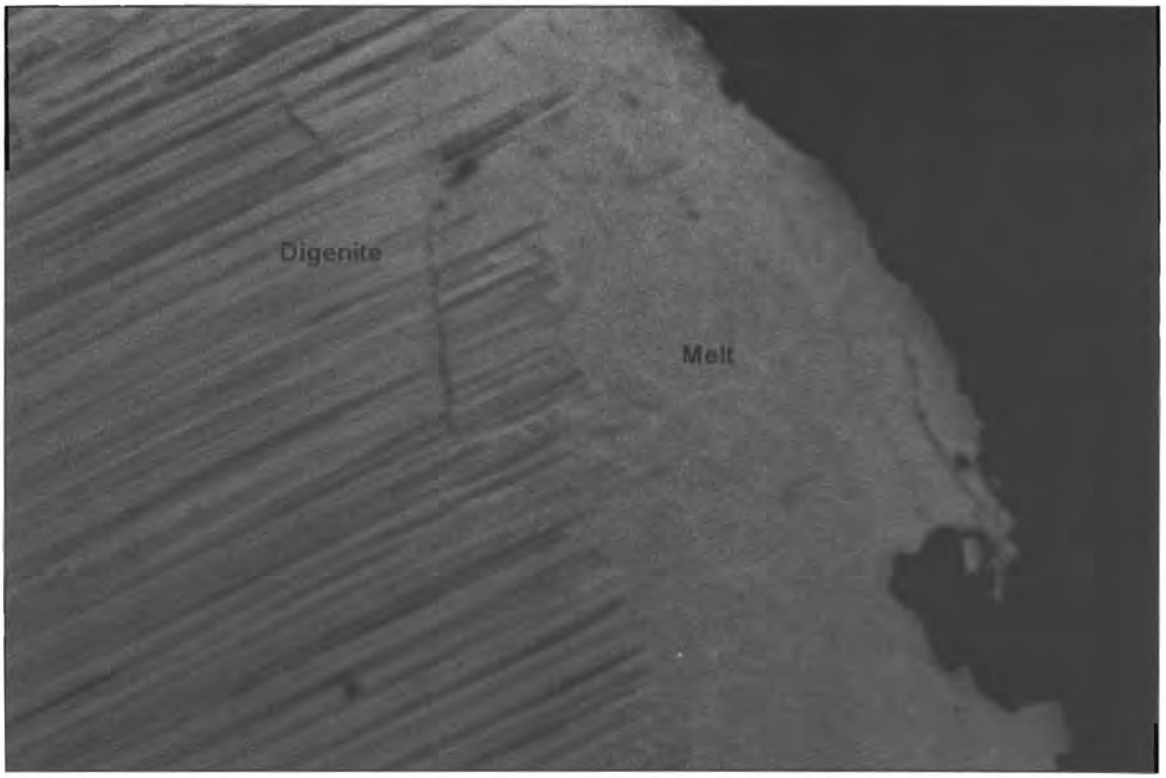

Figure 8. *Experiment HU420, co-existing digenite (twinned) and quenched melt, equilibrated at 1000°C. Image was digitally enhanced. Field of view2 mm.*

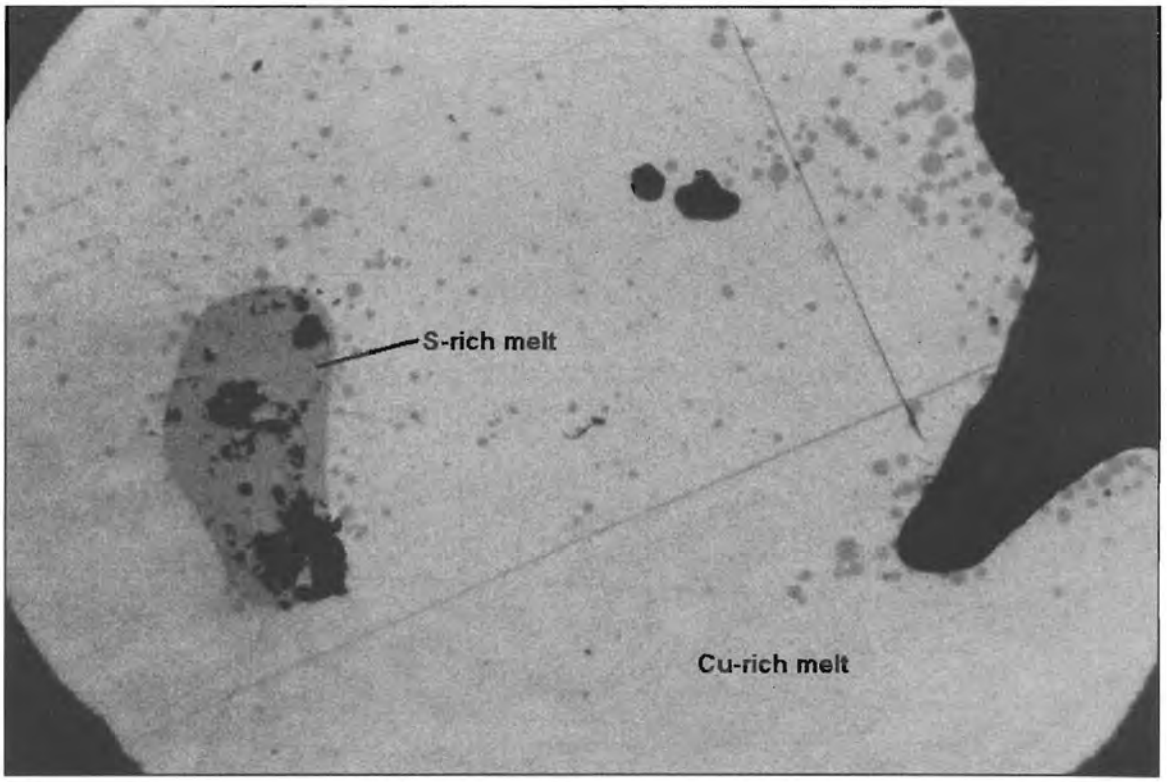

Figure 9. *Experiment HU442, co-existing immiscible Cu-rich melt and S-rich melt, equilibrated at 1200°C. Field of view 4 mm.*

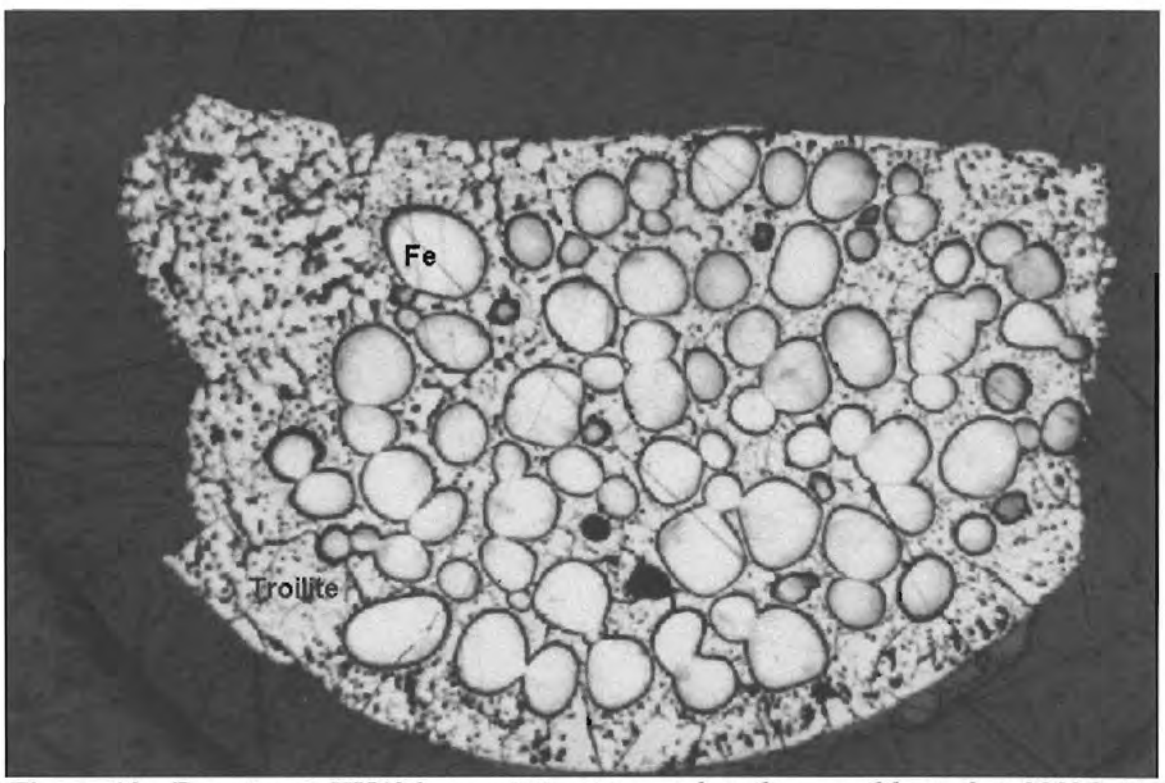

Figure 10. *Experiment HU436, co-existing iron and troilite, equilibrated at 900°C. Note the fast tarnishing of the iron to brownish colours. Field of view 4 mm.*

Figure 11. *Experiment HU736, Fe-S melt that co-exists with iron (not visible in this photograph), equilibrated at 1100°C. Image was digitally enhanced. Field of view 4 mm.*

3.2. Textures

3.2.1. Ni-S system

The phase diagram of the Ni-S system, after Sharma and Chang (1980) and Cemic and Kleppa (1986), is shown in Figure 12, where the initial bulk experiment compositions and expected equilibrated phase compositions in the present investigation are indicated. The assemblage investigated is described in Table 1.

3.2.1.1. Nickel - sulphide melt assemblage

The nickel globules mostly occur scattered evenly through the melt (Figure 13), but in some experiments they are concentrated in a specific sector of the melt (Figure 14), possibly as a result of gravity settling. Small bright specks of metal scattered through the heterogeneous sulphide melt (Figures 13 and 14) were formed during quenching, when the ability of the melt to contain Ni decreased during cooling. At equilibration temperature they were part of the melt phase, and were included during analyses of the melt. Fleet and Stone (1991) also reported quench-phase alloys, resulting from excess metal in their sulphide melt when it was quenched.

Table 1. *Assemblage of the Ni-S system that was investigated.*

Assemblage	Temp	Phase identification	Figures
Nickel - sulphide melt	1100 – 700°C	Nickel: bright white spherical globules. Sulphide melt: heterogeneous with quench-phase alloys.	13, 14

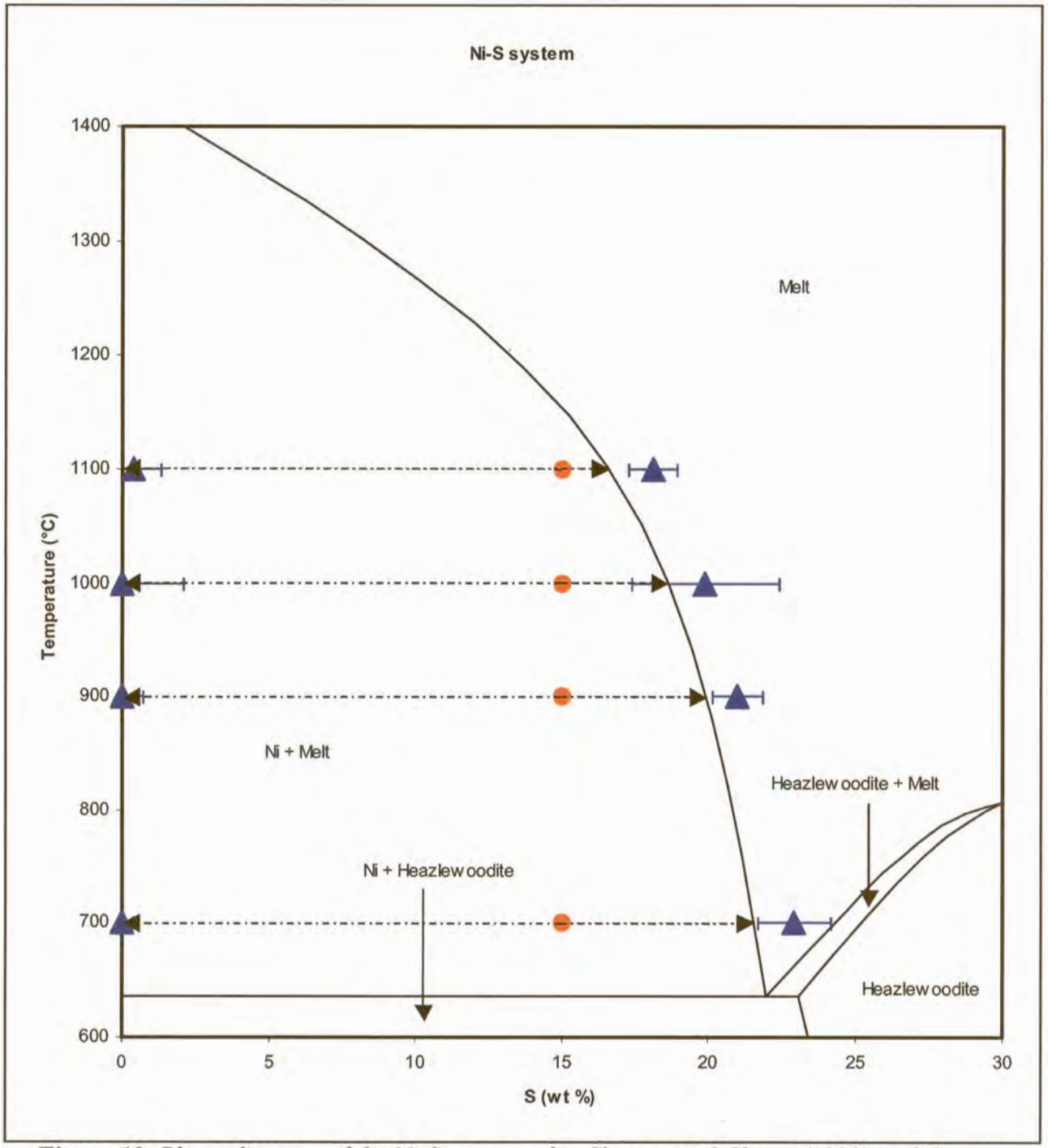

Figure 12. *Phase diagram of the Ni-S system, after Sharma and Chang (1980) and Cemic and Kleppa (1986). The red symbols indicate the bulk compositions of the experimental charges prepared to investigate the nickel - Ni-S melt assemblage, projected on the binary system. The expected compositions of the co-existing phases after equilibrium was achieved at the required temperatures are indicated by the tips of the arrows, and the average compositions of the equilibrated phases as determined by EPMA are indicated by the blue triangles, with error bars.*

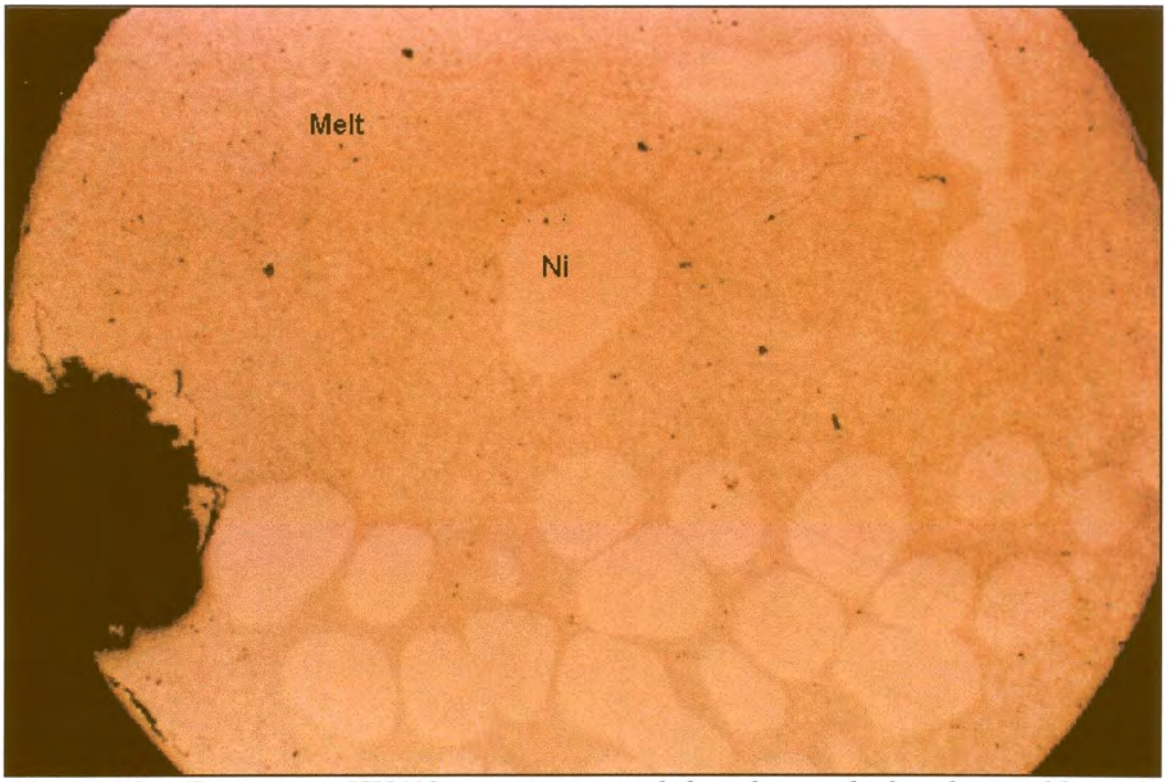

Figure 13. *Experiment HU412, co-existing nickel and quenched melt, equilibrated at 1000°C. Image was digitally enhanced. Field of view 4 mm.*

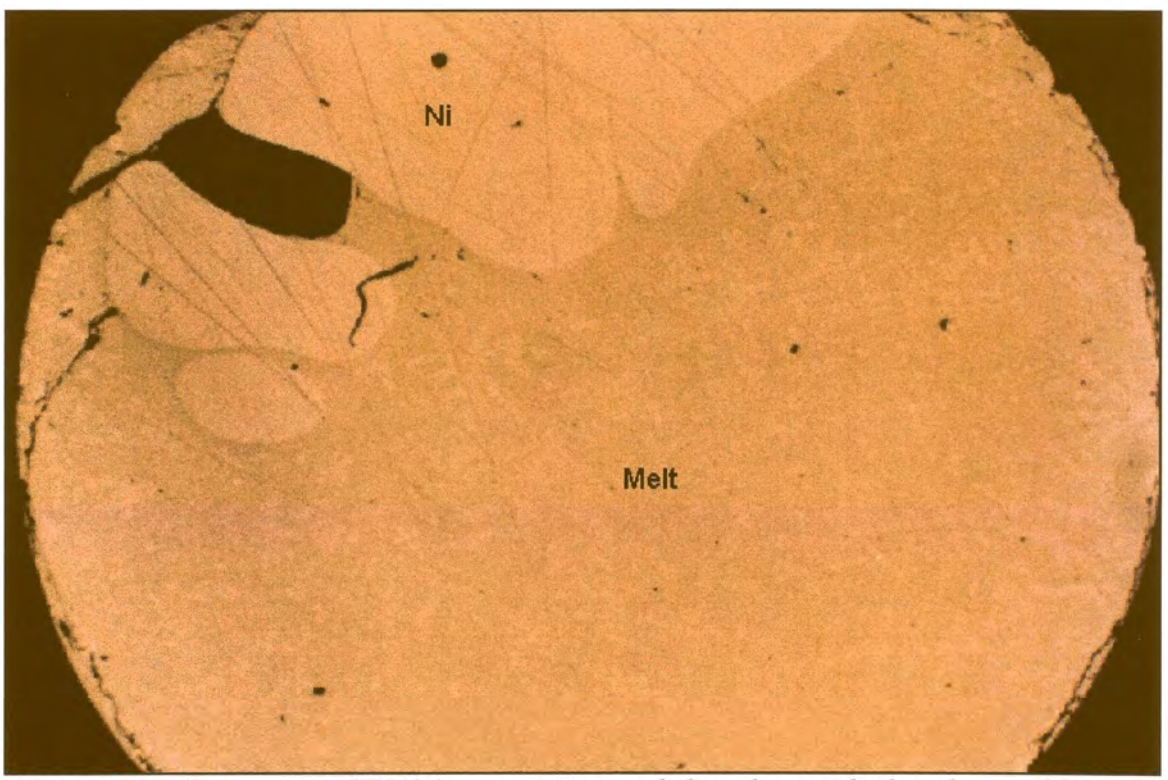

Figure 14. *Experiment HU426, co-existing nickel and quenched melt, equilibrated at 900°C. Image was digitally enhanced. Field of view 4 mm.*

3.2.2. Cu-S system

The phase diagram of the Cu-S system, after Chakrabarti and Laughlin (1986), is shown in Figures 15 and 16, where the initial bulk compositions and expected equilibration compositions of phases that were investigated are indicated. The assemblages that were investigated are discussed in Table 2.

Table 2. *Assemblages of the Cu-S system that were investigated.*

Assemblage	Temp	Phase identification	Figures
Copper - digenite	1000 – 700°C	Copper: viscous with high surface tension, commonly forms spherical drops in the centre of the experiments. Digenite: concentrated at the perimeter of the charge, forming a rim around the metal.	17, 18
Cu melt - digenite	1100°C	Cu melt: viscous, forms spherical drops in the centre of the experiments. Digenite: found along the perimeter of the experiment.	19, 20
Cu melt - sulphide melt	1200°C	Cu-rich melt: viscous, commonly forms spherical drops in the centre of the experiments, also scattered through sulphide melt as small spheres. Sulphide melt: mostly found along rim of experiment, but also dispersed as small and sometimes large spheres through Cu melt.	21, 22
Digenite - sulphide melt	1000°C	Digenite: occasionally shows clearly developed cleavage. Sulphide melt: slight heterogeneous appearance.	8, 23

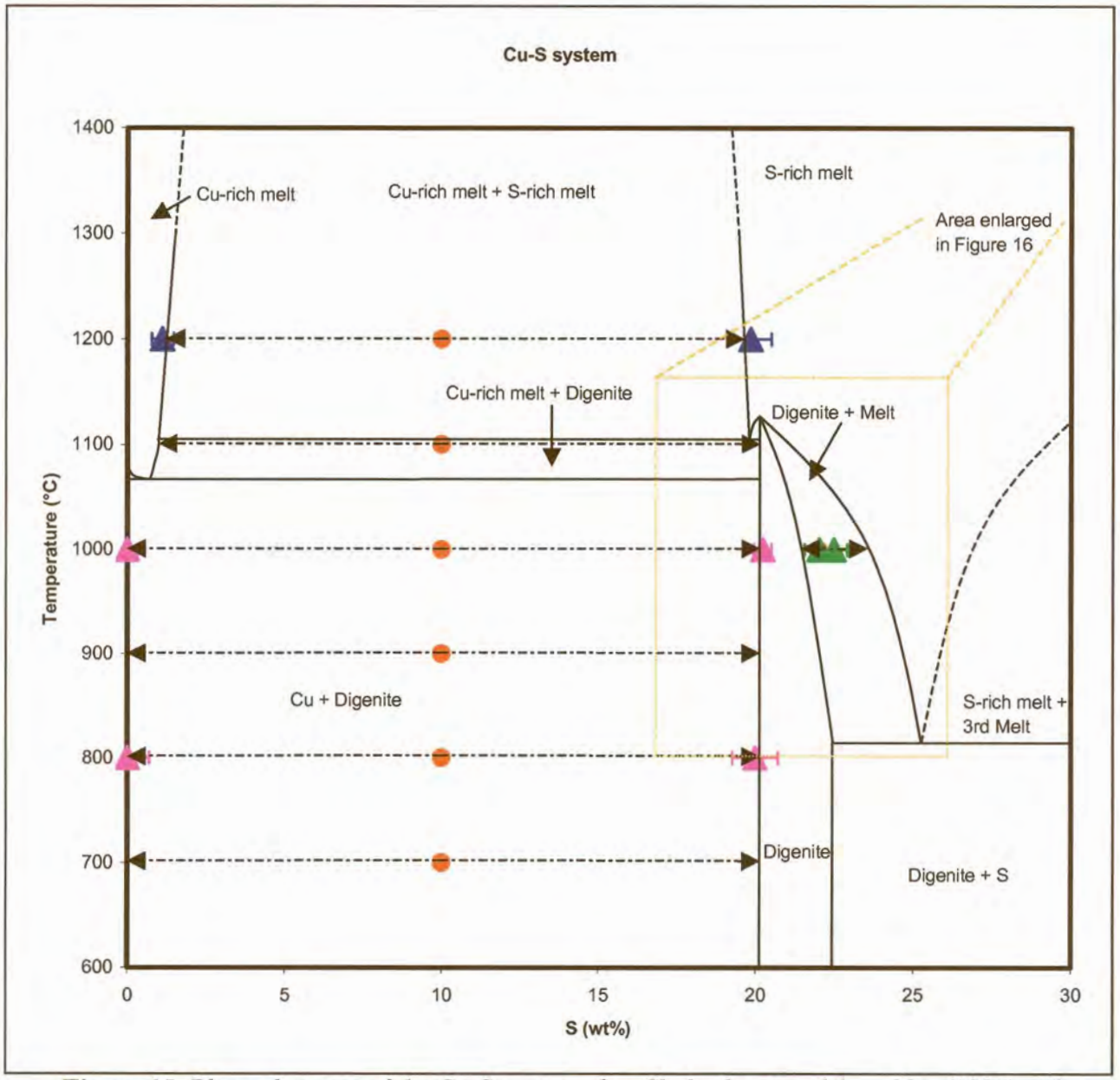

Figure 15. *Phase diagram of the Cu-S system after Chakrabarti and Laughlin (1986). The red symbols indicate the bulk compositions of the experimental charges prepared to investigate this system at various temperatures, projected on the binary Cu-S system, and the expected compositions of the resulting phases after equilibrium conditions were reached are indicated by the tips of the arrows. The blue triangles with error bars indicate the determined compositions of co-existing S-rich melt and Cu-rich melt at 1200°C, as determined by EPMA. The pink triangles indicate determined compositions of co-existing digenite and copper at 1000°C and 800°C, and the green triangles the determined compositions of co-existing digenite and melt at 1000°C. Experiments prepared to investigate co-existing Cu-rich melt and digenite at 1100°C and co-existing copper and digenite at 900°C and 700°C were too finely textured to analyse. These experiments will not be discussed further.*

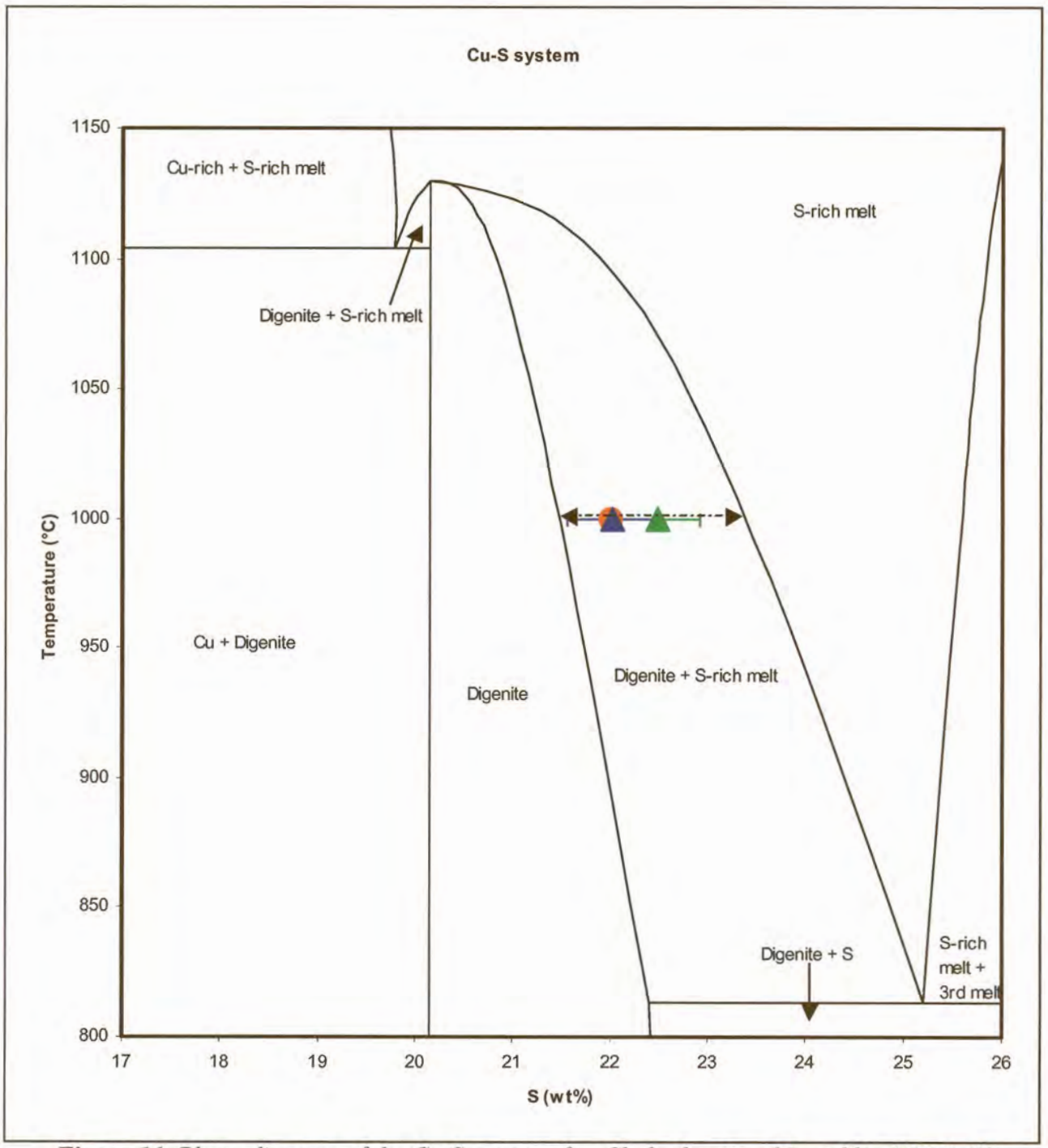

Figure 16. *Phase diagram of the Cu-S system after Chakrabarti and Laughlin (1986). The red symbols indicate the bulk compositions of the experimental charges prepared to investigate co-existing digenite and sulphide melt at 1000°C, projected on the binary Cu-S system, and the expected compositions of the resulting phases after equilibrium conditions were reached are indicated by the tips of the arrows. The blue triangle with error bars indicate the composition of the digenite, and the green triangle the composition of the melt, as determined by EPMA.*

3.2.2.1. Copper - digenite assemblage

The countless small drops of sulphide dispersed through the central copper core (Figure 18) could have formed on quenching, but they are less common in experiments that were equilibrated for longer periods. Despite leaving some experiments for long periods at high temperatures, small pieces of sulphide were still scattered through the copper. Experiment HU423 (Figure 18) was melted at 1100°C for 4 days, then equilibrated at 900°C for 51 days. Analyses of trace elements in the copper is complicated by the presence of these drops, as in-situ analytical methods also analyse in depth, where the presence of sulphides cannot be observed and avoided. If, however, the blebs are exsolutions that formed on quenching, their composition should be included with that of the metal. Practical difficulties were experienced during the mounting of these experiments. Because the sulphide is very porous and brittle, while the metal is malleable, the sulphide breaks away from the central copper core when the experiment is split open.

3.2.2.2. Cu melt - digenite assemblage

As in the copper - digenite assemblage (Section 3.2.2.1.), the sulphide crumbles away from the metal centre during mounting. Also, the Cu melt is speckled with sulphide (Figure 19), while the digenite is clear of Cu melt except for a few cracks (Figure 20). It was not possible to find areas of sufficient size clear of digenite for analysis of the melt, and this system was not analysed further.

3.2.2.3. Cu melt - sulphide melt assemblage

Of these two immiscible melts the Cu melt displays stronger surface tension, and generally forms a spherical blob in the centre of the charge surrounded by a rim of sulphide melt (see also Sections 3.2.2.1. and 3.2.2.2.). Both the Cu melt and the sulphide melt also occur as small droplets scattered throughout the other phase, in contrast to the previously discussed Cu-S assemblages (sections 3.2.2.1. and 3.2.2.2.) where only the sulphide melts show this behaviour.

3.2.2.4. Digenite - sulphide melt assemblage

The chemical compositions of the digenite and the sulphide melt and their optical characteristics are very similar. In some instances, the digenite is clearly twinned (Figure 8), but otherwise the only way to distinguish between the two phases is by the heterogeneous appearance of the melt (Figure 23).

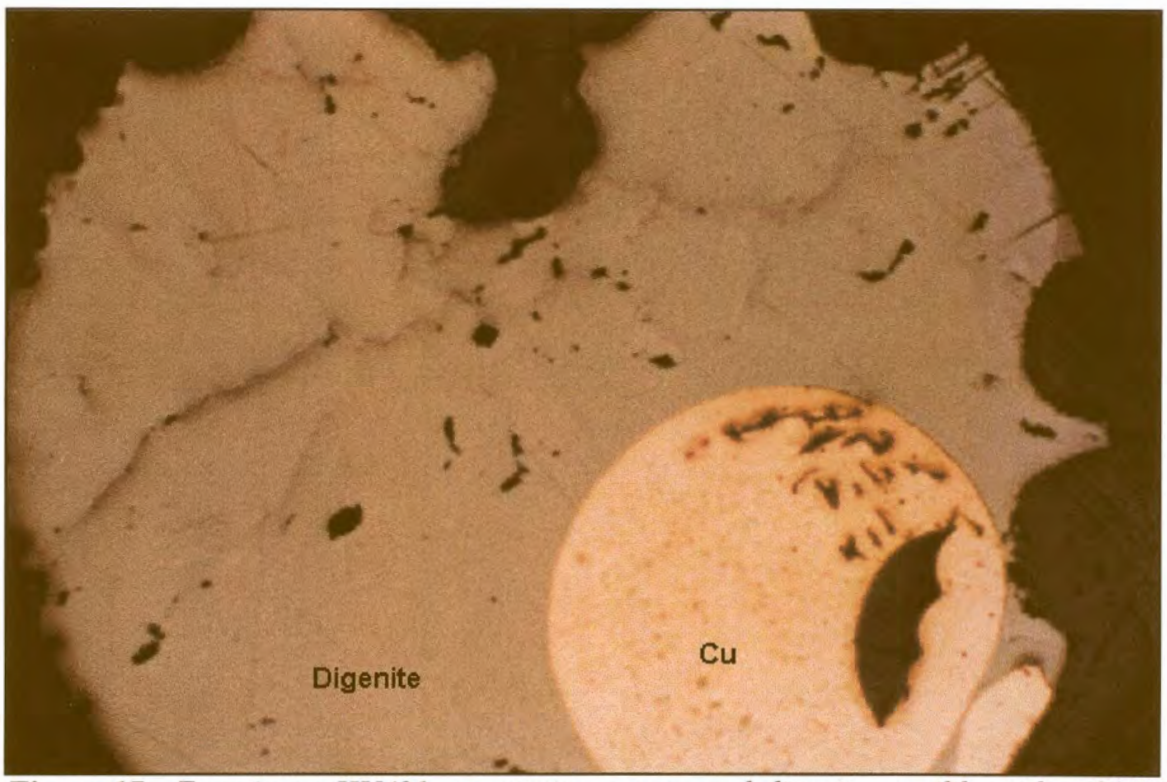

Figure 17. *Experiment HU421, co-existing copper and digenite, equilibrated at 900°C. Sulphide blebs scattered through the metal vary in size from extremely small to large. Field of view 4 mm.*

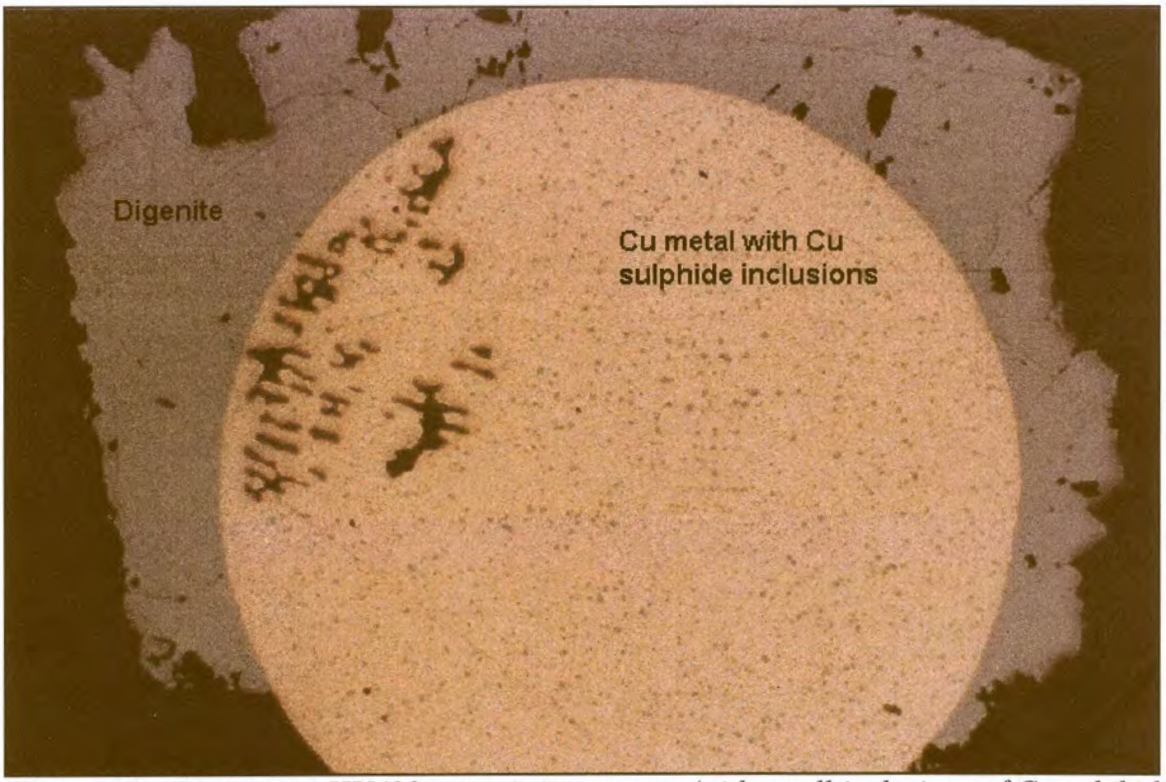

Figure 18. *Experiment HU423, co-existing copper (with small inclusions of Cu sulphide) and digenite, equilibrated at 900°C. Field of view 4 mm.*

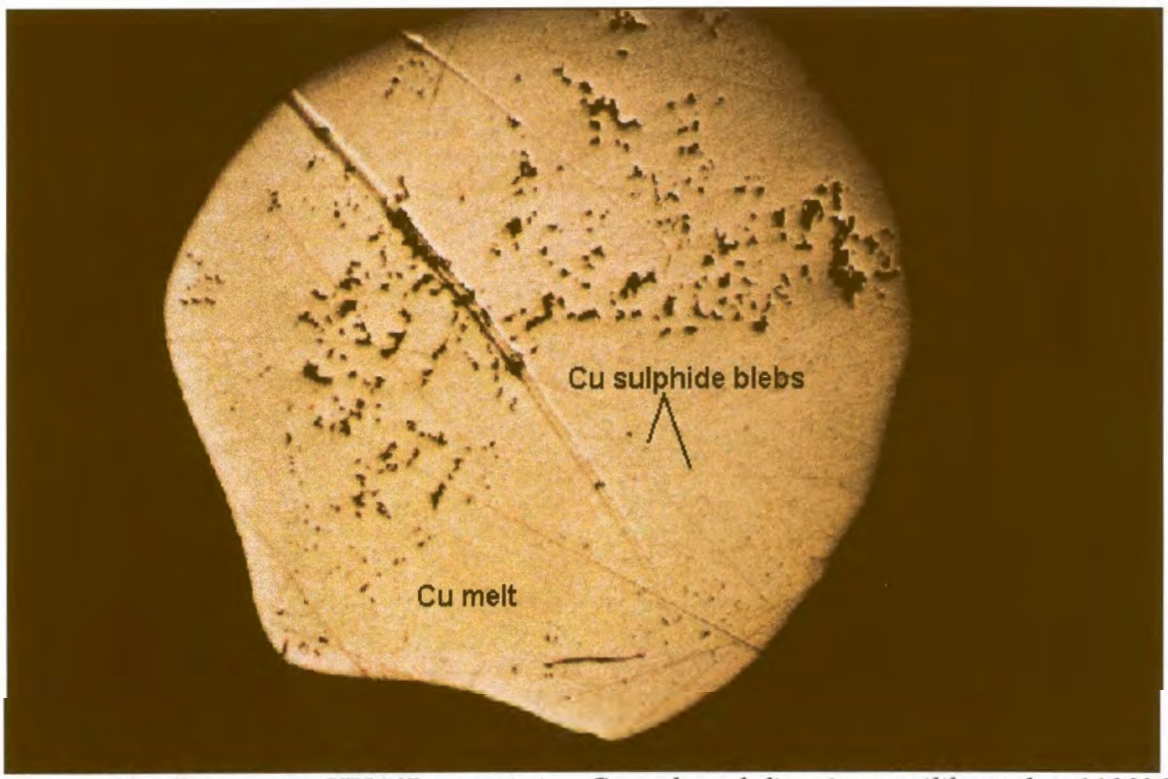

Figure 19. *Experiment HU467, co-existing Cu melt and digenite, equilibrated at 1100°C. The Cu melt contains small sulphide blebs. Image was digitally enhanced. Field of view 4 mm.*

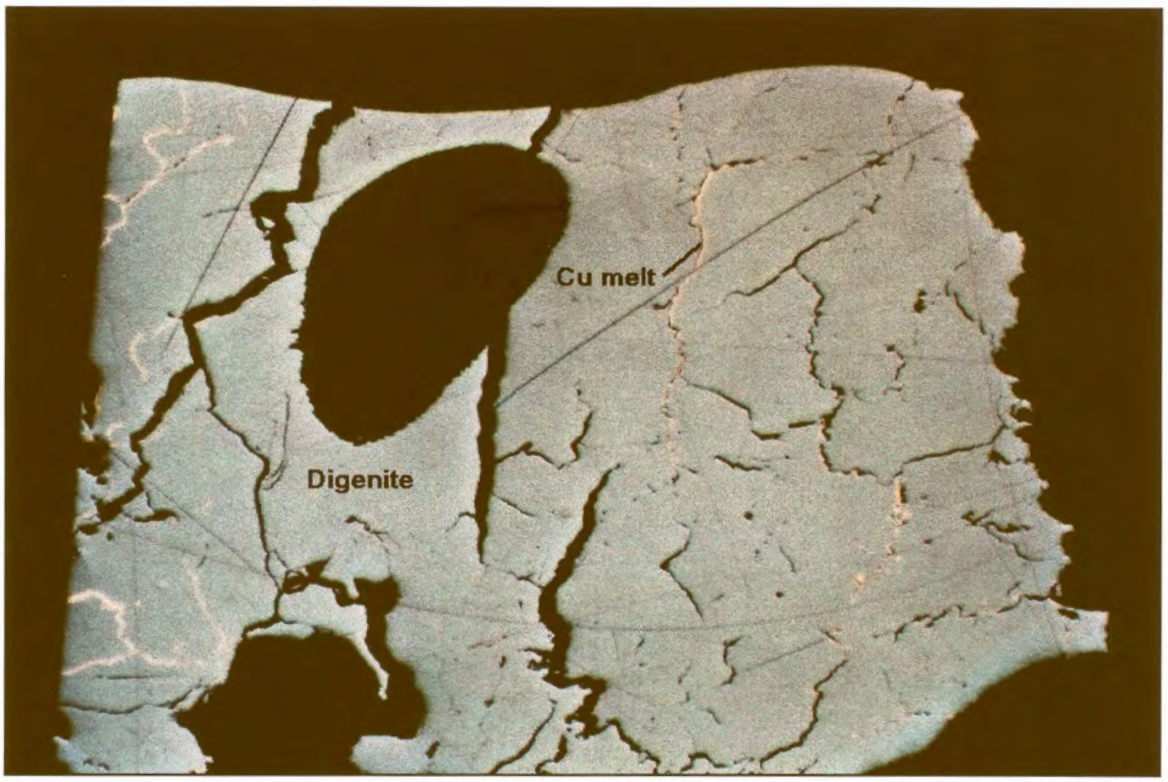

Figure 20. *Experiment HU467, digenite with quenched Cu melt filling the cracks, equilibrated at 1100°C. Image was digitally enhanced. Field of view 4 mm.*

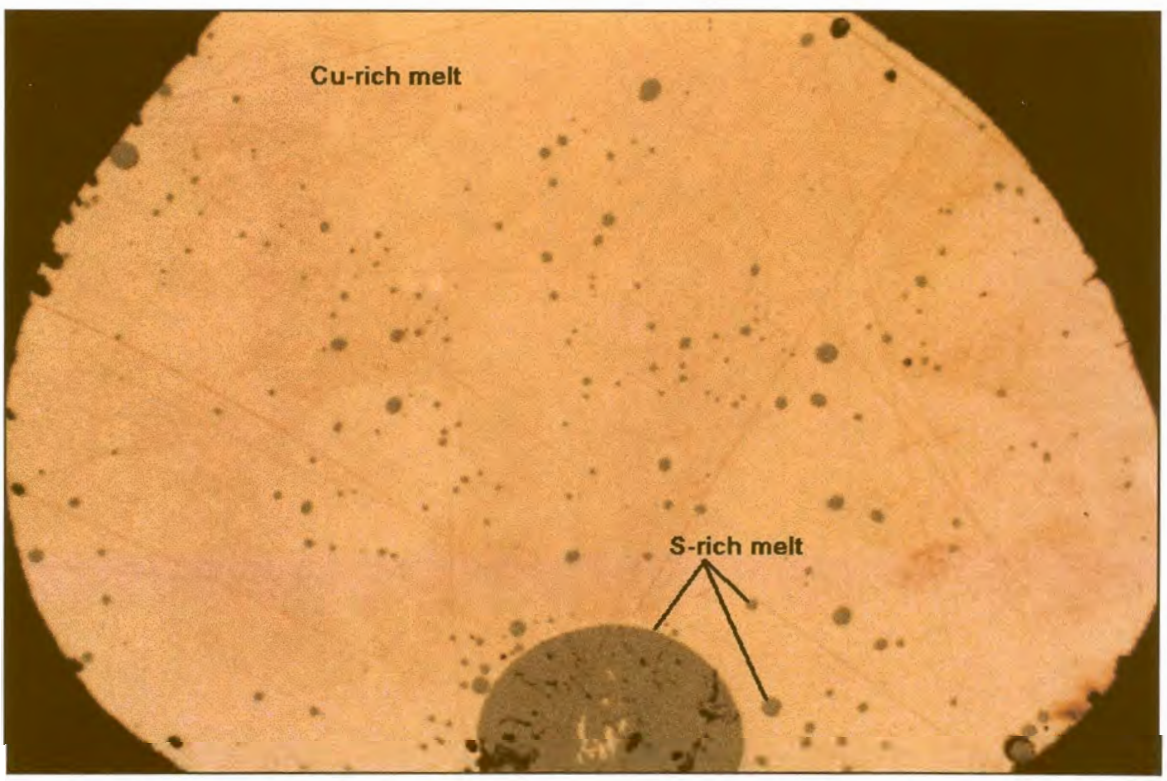

Figure 21. *Experiment HU445, co-existing immiscible Cu-rich and S-rich melts, equilibrated at 1200°C. The sulphide melt rim broke away from this central section during mounting, but sulphide melt is also observed as small and larger spheres dispersed through the Cu melt. Field of view 4 mm.*

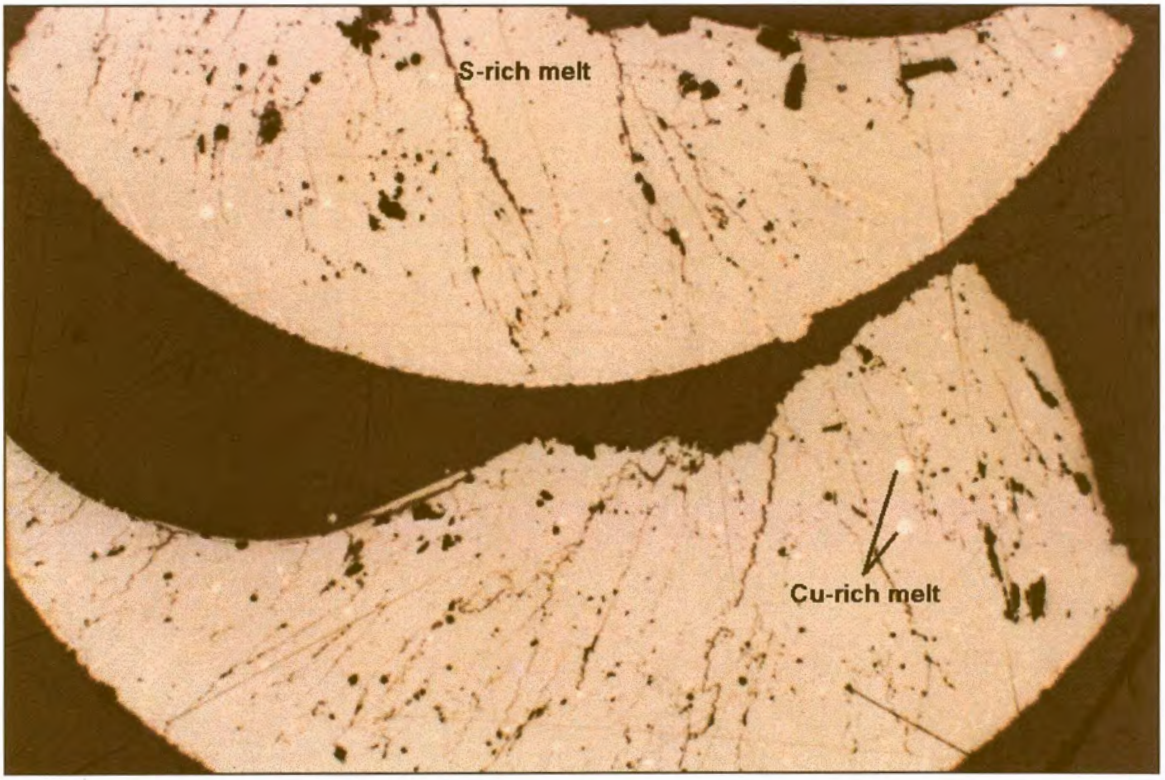

Figure 22. *Experiment HU445, equilibrated at 1200°C. S-rich melts as found around the rim of the experiment shown in Photograph 21, with Cu-rich melt present as small spheres scattered through the sulphide melt. Image was digitally enhanced. Field of view 4 mm.*

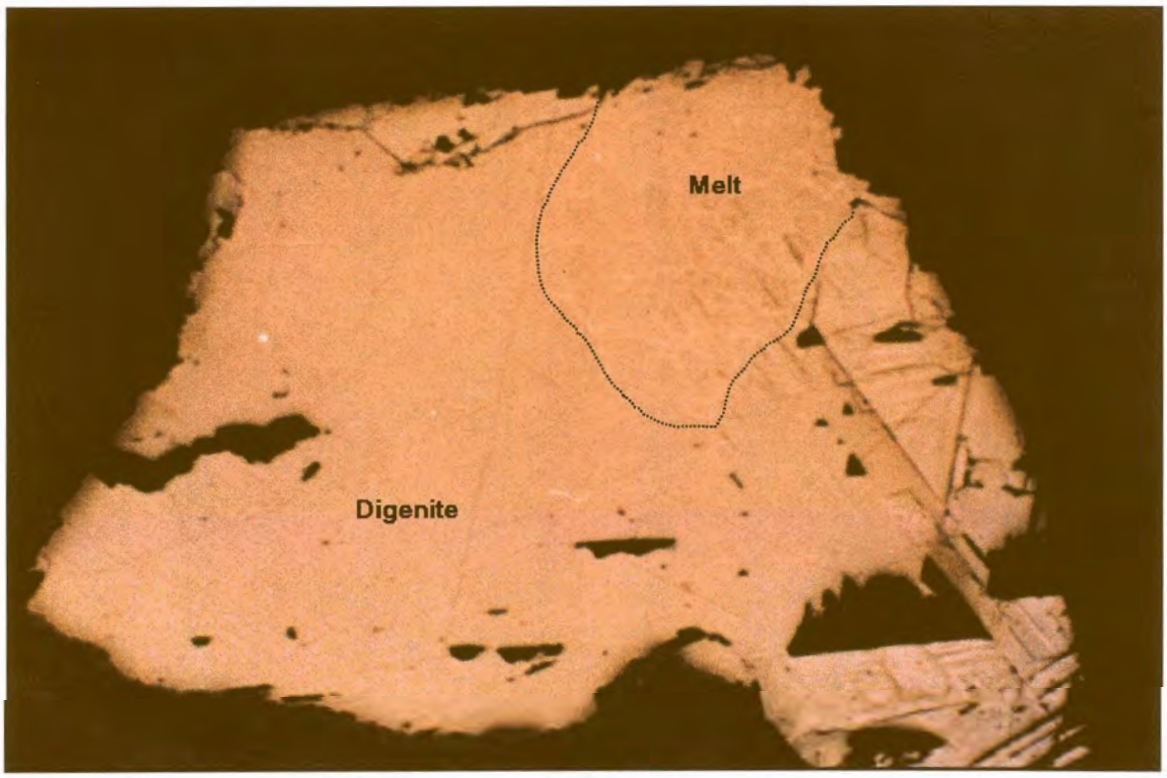

Figure 23. *Experiment HU418, co-existing digenite and quenched melt, equilibrated at 1000°C. Without visible twinning of the digenite, the melt phase can be identified by its heterogeneous appearance. Image was digitally enhanced. Field of view 4 mm.*

3.2.3. Fe-S system

The phase diagram of the Fe-S system, after Chuang *et al.* (1985), is shown in Figure 24, indicating the investigated assemblages which are described in Table 3.

***Table 3**. Assemblages of the Fe-S system that were investigated.*

Assemblage	Temp	Phase identification	Figures
Iron - sulphide melt	1200 – 1000°C	Iron: bright white with good polish. Sulphide melt: creamy yellow, lower reflectivity and hardness than metal.	25
Pyrrhotite - sulphide melt	1100°C	Both phases have a creamy yellow colour, similar reflectivity and hardness.	26
Iron - troilite	900°C	Iron: bright white with good polish. Troilite: dull yellow, very brittle with bad polish.	10, 27

3.2.3.1. Iron - sulphide melt assemblage

The iron occurs as roundish blebs dispersed through the sulphide melt matrix. Occasionally small exsolutions of iron, which form skeletal textures, occur scattered through the melt. These small pieces of metal were produced during quenching, and formed part of the melt at the equilibration temperatures.

3.2.3.2. Pyrrhotite - sulphide melt assemblage

There is not a clear optical distinction between the melt and the pyrrhotite, possibly due to the similarity in the compositions (phase diagram - Figure 24). The phases are intergrown with curving boundaries, but the melt is slightly heterogeneous with darker and lighter zones, which makes identification possible.

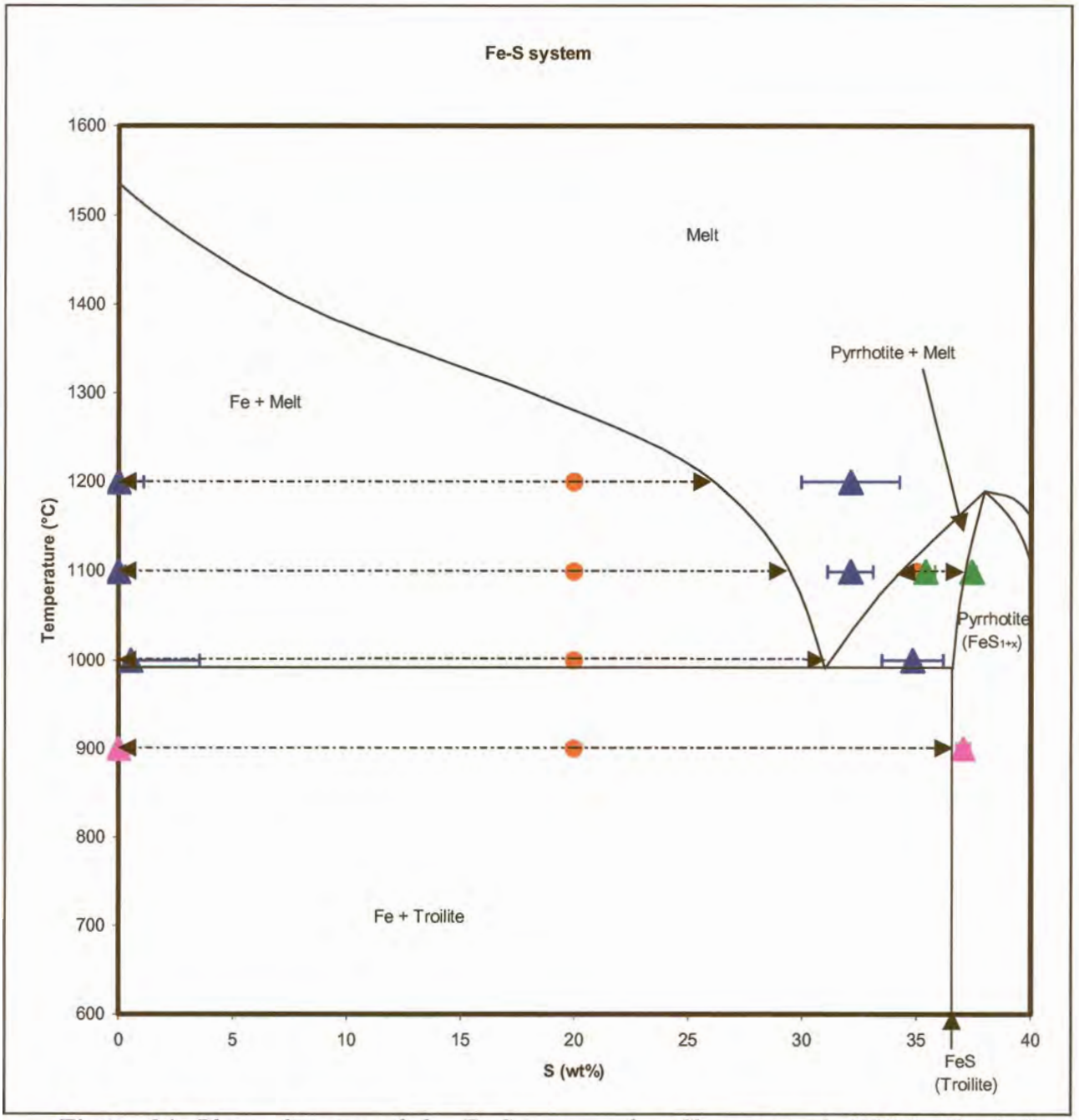

Figure 24. *Phase diagram of the Fe-S system after Chuang et al. (1985). The bulk compositions of the experimental charges are indicated by the red symbols, the expected compositions of the co-existing phases after equilibrium was reached by the tips of the arrows, and the true compositions of the co-existing phases as determined by EPMA are projected onto the diagram and indicated by the triangles. The blue triangles with error bars indicate the F:S ratio of co-existing iron and sulphide melt, the pink triangles the Fe:S ratio of co-existing iron and troilite, and the green triangles the Fe:S ratio of co-existing pyrrhotite and sulphide melt. Many of these experiments were oxidised.*

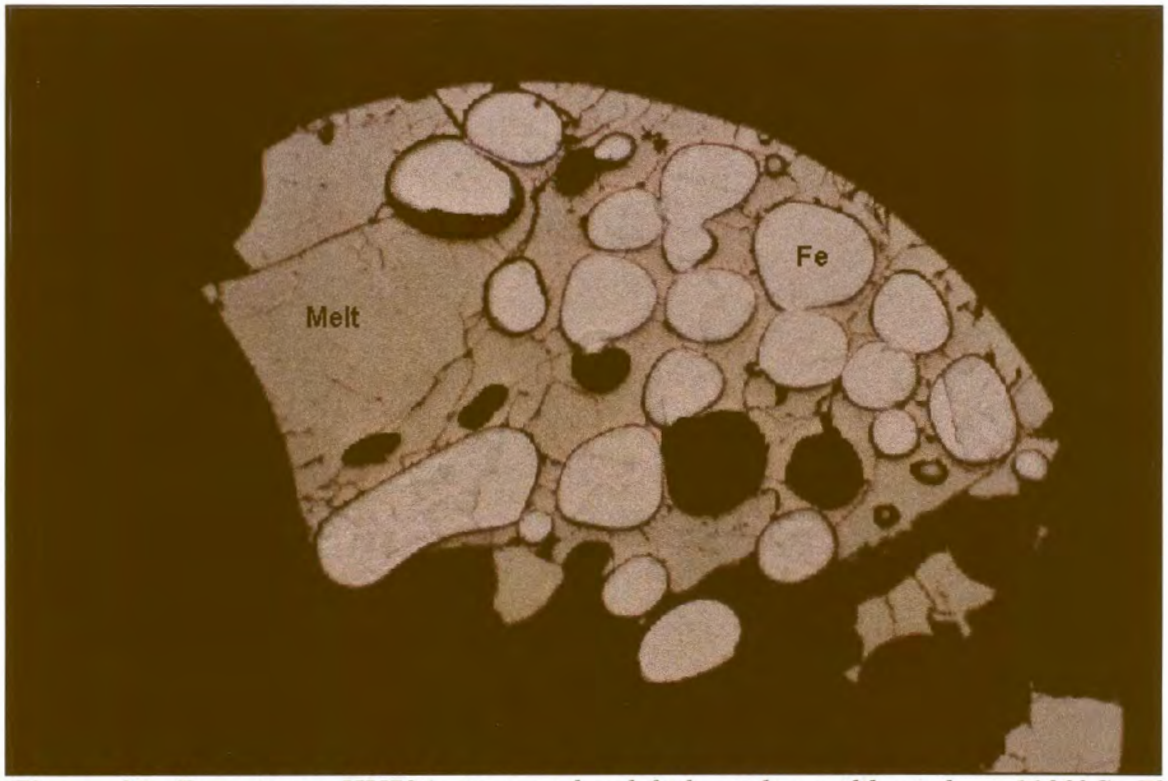

Figure 25. *Experiment HU734, iron and sulphide melt equilibrated at 1100°C. The sulphide melt appears homogeneous on this scale. Field of view 4 mm.*

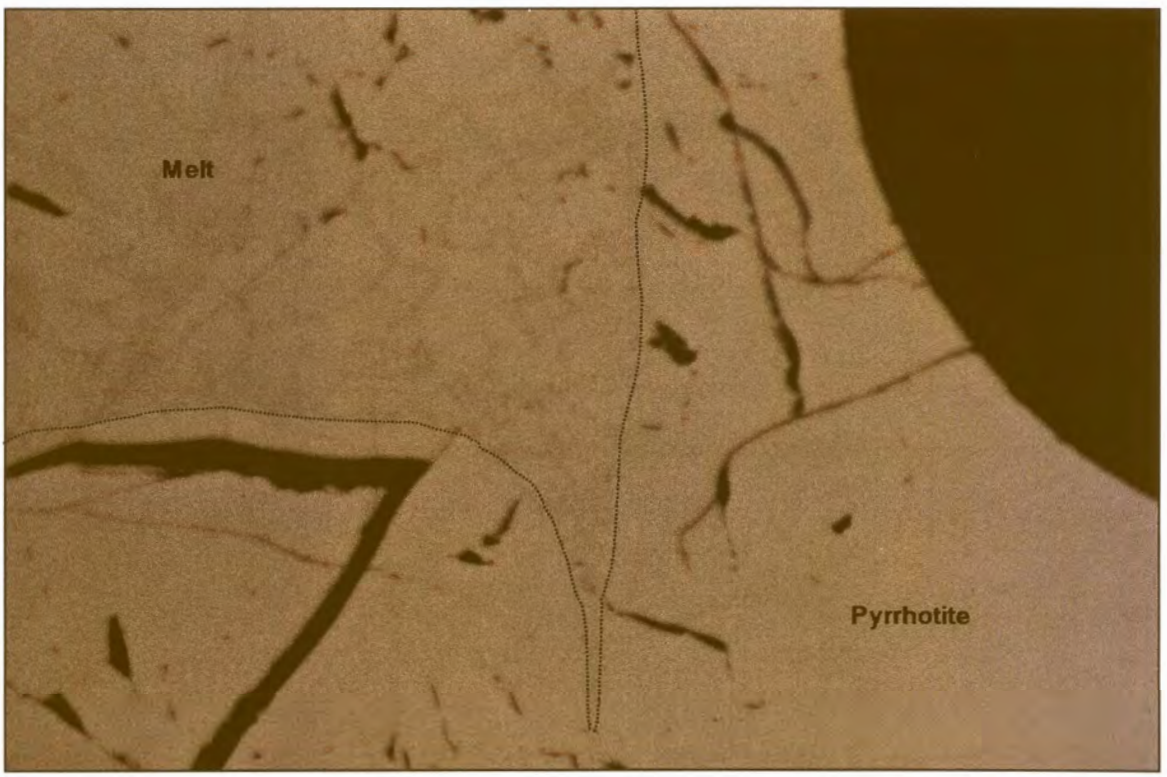

Figure 26. *Experiment HU739, co-existing pyrrhotite and quenched sulphide melt equilibrated at 1100°. The melt can be distinguished from the sulphide only by its heterogeneous appearance. Image was digitally enhanced. Field of view 1.4 mm.*

3.2.3.3. Iron - troilite assemblage

The iron occurs as round blebs scattered through the troilite, which forms the matrix.

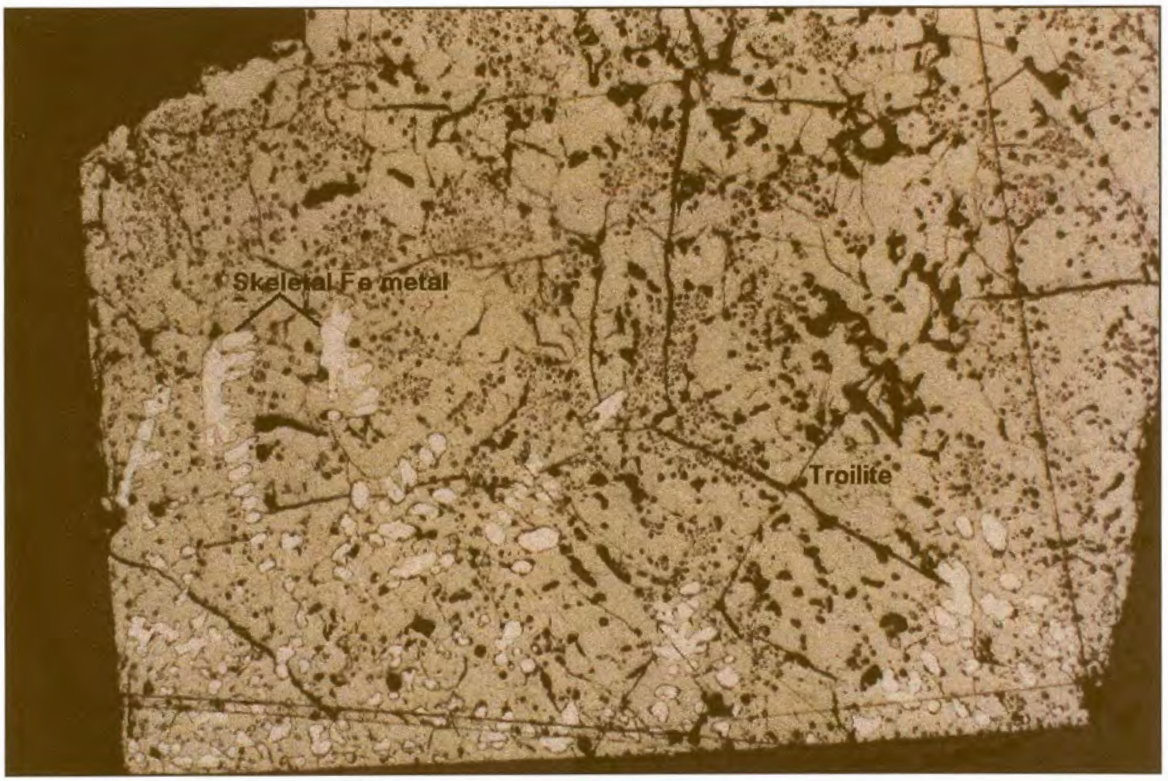

Figure 27. *Experiment HU436, containing troilite and dendritic iron, equilibrated at 900°C. Field of view 4 mm.*

4. Analytical Techniques

4.1. Electron Probe Micro Analysis (EPMA)

Areas of interest for microprobe analysis were selected by microscopic investigation. Reflected light photographs of these areas were used for reference and orientation during microprobe analysis. Polished sections were coated with a 20 to 25 nm conductive carbon layer.

A JEOL 733 Superprobe was used to analyse for the major element contents at an accelerating voltage of 20 KeV and a beam current of 20 nA, measured on a Faraday cup, in wavelength-dispersive (WD) mode. Counting times were 50 seconds on the peak and 25 seconds on the backgrounds. For the metals, pure Cu, Ni and Fe were used as standards. For the sulphides, millerite was used as a standard for nickel sulphides and chalcopyrite for copper and iron sulphides. Spot analyses, with a diameter of <2 μm, were made of the metals and sulphides. Standards were routinely measured before, during and after analysis to control instrumental drift.

To analyse the heterogeneously quenched Cu-S, Ni-S and Fe-S melts, representative areas of the melts were analysed in scanning mode. The sizes of the analysed areas were selected according to the size of the quench-phase alloys in the solidified melts as well as the areas of melt available between the crystals of the primary solid phase, but were generally about 200 μm^2. The heterogeneity of the quenched melt was compensated for in this way. For the Ni-S and Cu-S melts, two types of standards were tested: synthetically prepared quenched melt phases as well as the sulphides described above. No difference was found in the quality of the analyses. Heterogeneous textures containing quench-phase alloys have also been analysed by other authors (e.g. Fleet and Stone, 1991), who applied a defocussed electron beam to obtain bulk chemical analyses of quenched liquids. This method was also tested in the present investigation, but resulted in very large standard deviations, and the technique of scanning the beam over an area on the sample is preferred. The standard

deviations of quenched melt analyses reflect true compositional differences. If a very large number of 1 μm beam spots was used to analyse the same phase, it would result in similar element averages as the result of a few large area scans, but the standard deviations would be much larger. All EPMA results of quenched melts provided in this report were performed with area scans, except when specified otherwise.

Occasional EPMA analyses of PGE contents were performed with pure Rh, Pd and Pt as standards for the PGE, Cu-, Ni- and Fe sulphides for the melts and sulphides, and Cu, Ni and Fe for the metals.

The results of analyses of the Ni-S melt phases described in Section 5.1.1.1. were found to be consistently more S-rich than predicted by the phase diagram of the Ni-S system (Sharma and Chang, 1980) at all four temperatures investigated. Duplicate analyses were performed to confirm the quality of the results. Area scans of 200 μm^2, 40 μm diameter spot analyses as well as 600 1μm diameter spot analyses all resulted in similar average melt compositions, enriched in S compared to the phase diagram. Different sulphide standards were used with no difference in results. The analyses are consistent, and no analytical explanation for the deviation from the published phase diagram can be given.

Detection limits for PGE in metals and sulphides are 200 to 300 ppm with the EPMA, which is not sufficient to determine the low PGE contents of interest in this investigation. An additional analytical technique (PIXE) had to be considered, as discussed in the following section. Only the major elements (Ni, Cu, Fe and S) were routinely determined by EPMA. Trace PGE were ignored during EPMA analyses of major elements, as their effect on the correction factors would be smaller than the analytical uncertainty due to counting statistics.

4.2. Particle Induced X-ray Emission (PIXE) Analysis

PIXE is a non-destructive, in-situ multi-element analytical technique, capable of detection limits down to the ppm level (Halden *et al.*, 1995). The sample is bombarded with high

energy protons (or other particles) to generate characteristic X-rays from the sample. These protons are less easily scattered than electrons (Johansson, 1992). Czamanske *et al.* (1993) reported that the X-rays emitted by the sample after MeV energy proton bombardment to be quantitatively similar to those emitted by KeV energy electron bombardment. However, the bremsstrahlung background is much lower with PIXE, so that the ratio of characteristic X-rays to background is much higher (Cabri *et al.*, 1984a; Remond *et al.*, 1987; Sie *et al.*, 1989a; Johansson, 1992), which lowers detection limits considerably. The secondary bremsstrahlung emitted by electrons set in motion by the primary protons determines the limit of detection (Halden *et al.*, 1995). A focused beam of protons, or other particles, with a spot size of a few square microns or more can be used for point analysis, or the beam can be scanned over larger areas to provide a two-dimensional X-ray map of element distribution (Halden *et al.*, 1995). Cabri (1988) and Sie *et al.* (1989a) expanded on the practical aspects of combining EPMA and PIXE analysis applied to geological and mineralogical investigations. Both techniques use focused beams of charged particles to excite characteristic X-rays. EPMA can be utilised for major element determinations while PIXE is very successful for determining trace element concentrations, especially in simple matrixes (Campbell *et al.*, 1990), as demonstrated by Remond *et al.* (1987) on determination of trace concentrations of In, Se and Hg, undetectable with EPMA, with micro-PIXE.

Minimum detection limits of 1.2 to 3 ppm for Pd and Rh, and 50 to 60 ppm for Pt in sulphides were obtained by Cabri *et al.* (1984b). Cousens *et al.* (1989) and Paktunc *et al.* (1990) used the technique to investigate partitioning of PGE and other trace elements in sulphides from the Bushveld Complex. PIXE analyses for many elements, including PGE, were performed by Czamanske *et al.* (1992) on sulphide ores from the Norilsk-Talnakh district. Milli-PIXE analysis of platinum-group minerals from the Witwatersrand basin was employed by Merkle and Franklyn (1999) to determine trace element contents in an attempt to obtain information on the sources of the grains. Sie *et al.* (1989b) used PIXE in combination with fire-assay to determine PGE and Au at sub-ppm levels suitable for application in exploration.

There are some contradictions regarding analysis depth and surface effect of EPMA compared to PIXE. According to Campbell *et al.* (1990) a significant difference between EPMA and micro-PIXE is that the depth analysed with micro-PIXE is about 10 times greater. Remond *et al.* (1987) verified by calculation of X-ray yields that the accuracy of micro-PIXE measurements are less influenced by surface contamination than for EPMA. This statement is directly contradicted by Franklyn and Merkle (1999), but still requires quantification. Ryan *et al.* (1990) calculated that a typical PIXE beam spot of 20µm diameter at 10 nA excites X-rays from depths often greater than 40µm in the matrix. Variation of excitation depth for different elements in different matrixes, varying from Zr X-ray yields from a depth of 39.7 µm in a matrix with density 2.7 (feldspar), to an excitation depth as low as 10.1 µm for Ni in a matrix with density 5.5 (chromite), was reported by Cabri and Campbell (1998). The area analysed by EPMA is usually a few μm^2, while the area analysed by micro-PIXE is sometimes much larger. This problem was pointed out by Franklyn and Merkle (1999), who compared 1 µm diameter EPMA point analysis results with 100 µm diameter milli-PIXE analyses. It was more difficult to ensure that only one phase was analysed with a larger milli-PIXE beam spot. The penetration depth of the proton beam also has to be considered when choosing a position for analysis, and homogeneity at depth in a sample has to be established, as X-rays may be excited from beneath the phase under investigation (Halden *et al.*, 1995). The relatively large effective area of analysis of PIXE results in better averaging of the sample - larger beams obtain a better averaging effect (Sie *et al.*, 1989b; Franklyn and Merkle, 1999). Remond *et al.* (1987) reported that contamination or surface changes can be introduced during mechanical polishing or during electron or proton beam irradiation.

4.2.1. Milli-PIXE

The analyses were performed on the same PIXE beam line with the same set-up described by Franklyn and Merkle (1999). Quadrupole magnets are used to focus the 3 MeV H^+ beam from the Van De Graaff Accelerator to a 2 mm diameter beam spot, which is then collimated to 100 µm diameter with two 100 µm carbon collimators. The collimators are spaced 200 mm apart, with the last collimator 120 mm from the target position. The term

milli-PIXE is appropriate to describe this system with a beam diameter of 100 µm. X-rays emitted from a 50 µm thick W wire that was moved across the beam were used to determine the spatial distribution of the beam. A halo contribution of less than 0.5 % was observed at 0.2 mm from the beam centre. Beam currents of up to 1 nA were used on the targets. The polished epoxy mounts containing the samples were initially oriented at a 45° angle to the incoming beam, with the detector at 45° to the sample surface. This meant that the impact area on the sample surface was oval and the longest elongation greater than 100 µm (see Photograph 20). During later analyses, the samples were mounted perpendicular to the incoming beam, with the detector at a 45° angle to the sample. Energy-dispersive X-ray analysis was performed utilising a germanium detector, with FWHM resolution of 165 eV at 5.9 KeV, initially mounted at 90° to the beam direction, but later changed to 45°. The detector had a 25 µm thick Be window and the exit window of the PIXE chamber consisted of 23 µm of Mylar. Pile-up suppression in the X-ray spectra was obtained through dynamic beam pulsing, and electronic pile-up rejection was used to reduce doubling (Franklyn and Merkle, 1999).

The spectra were processed with the GUPIX software package developed at Guelph for PIXE analysis (Maxwell *et al.*, 1989, 1994, 1995). GUPIX was used by Campbell *et al.* (1996) in the analysis of silicate reference standards, and was also evaluated by Czamanske *et al.* (1993). A model spectrum containing all relevant X-ray lines is fitted to the measured spectrum by non-linear least squares, the background continuum being removed by digital filtering (Maxwell *et al.*, 1989). Relative intensities of element lines are adjusted to reflect matrix effects, absorber transmission and detector efficiency. The elemental concentrations for PIXE are obtained by reference to a single element in the same spectrum that can be analysed independently (Rogers *et al.*, 1987), and in the present investigation this was achieved by the EPMA analyses of major elements. According to Rogers *et al.* (1987), the disadvantage of internal normalisation, where relative intensities are calculated from theory and compilations of experimental data, is that the errors in the final values are difficult to determine. Calculation of the final uncertainty is further complicated by spectrum fitting errors and uncertainties in the filter absorption and the amplifier calibration. Fitting errors are believed to predominate over errors in relative intensity calculations.

Detection limits decrease in inverse proportion to the square root of the measurement duration (Czamanske *et al.*, 1993) or, as stated by Halden *et al.* (1995), detection limits depend on the total charge used during analysis and therefore on the total accumulated counts, which is increased by longer counting times. This implies that lower detection limits can be obtained by increasing analysis time. For each spectrum the principal peak for each element is evaluated with a 3σ standard deviation, which reflects both counting statistics and error from peak overlap, and a lower limit of detection. In the present investigation, the detection limit for each PGE, together with the error or standard deviation, is given for every individual analysis, but the lowest detection limits obtained in each analysed phase are summarised in Table 4. Traditionally EPMA analyses are described by, amongst other factors, the analysis time on the peaks and background. However, the milli-PIXE analyses were performed by considering the total number of counts detected during each analysis. These counts are provided along with the other information for each milli-PIXE analysis in this investigation.

Table 4. *Detection limits obtained for the PGE by milli-PIXE.*

Phase	Rh LLD (wt%)	Pd LLD (wt%)	Pt LLD (wt%)
Nickel	0.009	0.004	0.011
Ni-S-melt	0.013	0.014	0.020
Cu-rich melt	0.016	0.013	0.031
S-rich melt	0.011	0.014	0.031
Copper	0.025	0.021	0.024
Digenite	0.013	0.014	0.036
Iron	0.020	0.040	0.040
Fe-S-melt	0.020	0.030	0.030
Pyrrhotite	0.030	0.020	0.040
Troilite	0.040	0.040	0.050

The S-rich melt of experiment HU443 was analysed seven times, but it was suspected that one of these measurements was influenced by another phase and was ignored. In each of the six remaining analyses, shown in Table 5, the Pt content was below the detection limit. The

fourth analysis was left to collect 400000 counts - more than any of the other analyses - and the detection limit that was obtained was the lowest of all the analyses. In Figure 28 the detection limits obtained for each of the analyses are plotted against the number of counts collected, showing that increased count collection lowers the detection limit. The scatter in the points indicates that the detection limit is not only a function of the total counts collected. Other factors, such as the precise alignment of all the components in the PIXE line, and the fine-tuning of the electronics, both of which are dependent on temperature and pressure which change during long work sessions, also influence the LLD's. The GUPIX program does not have the option of combining results to obtain very low detection limits.

***Table 5**. Repeated measurement of the S-rich melt of experiment HU443, showing a relationship between total counts collected and detection limit.*

Exp	Pt wt% (± 3σ)	Pt LLD	Counts
HU443	*0.003* (0.026)	0.048	200000
HU443	bd	0.057	200000
HU443	*0.015* (0.018)	0.031	400000
HU443	*0.036* (0.032)	0.053	100000
HU443	*0.024* (0.030)	0.053	100000
HU443	*0.007* (0.037)	0.067	100000

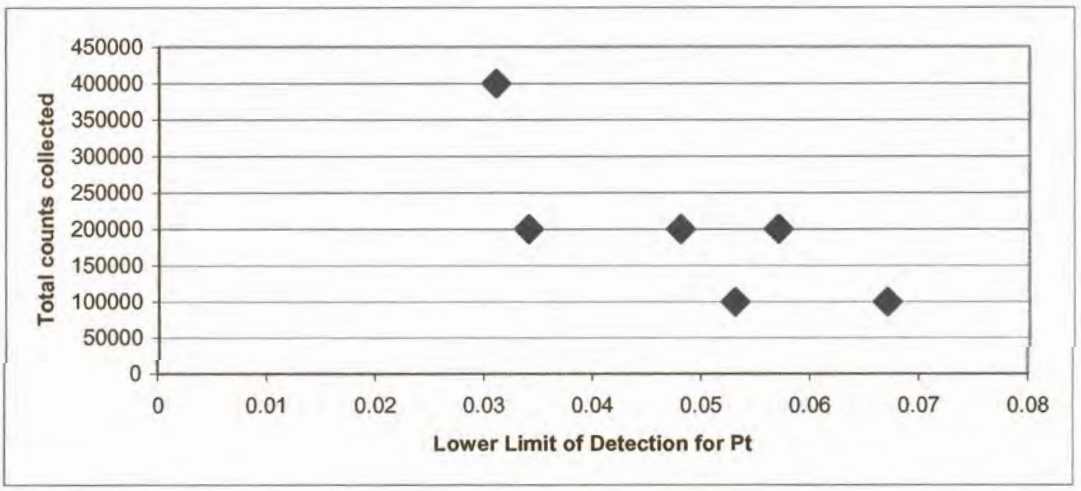

***Figure 28.** The influence of counts collected on the detection limit of Pt in the S-rich melt of experiment HU443.*

When an element could not be detected, it was assumed that the concentration of that element was lower than, or equal to, the detection limit, and the detection limit was used as the maximum content of that element for further calculations.

An advantage of PIXE is its independence of matrix matched external standards (Ryan *et al.*, 1990). The problem of non-availability of trace element standards, as well as the problem of heterogeneity of trace element standards on the micron scale, are eliminated. Standards of pure Rh, Pd and Pt as well as Cu, Ni and Fe were used to determine and correct for peak shift.

Similar to EPMA analyses, a thin conductive carbon coating on the sample surface is required for analysis. Areas to be analysed were identified prior to insertion of the sample into the PIXE chamber. No optical system was available to orient the sample once it was sealed inside the vacuum chamber, and positions were determined by monitoring X-ray spectra while moving the sample through the beam to determine its shape and precise orientation, and with the assistance of reflected light photographs of the grains, the required positions for analyses were determined. As far as possible, the same areas analysed by EPMA were analysed by PIXE.

4.2.1.1. Evaluation of analytical conditions

As the major element contents (Cu, Fe, Ni, S) in the experiments are much higher than the PGE contents, the X-rays from these elements are very pronounced, and together with the resulting background, normally overlap completely with the PGE peaks. Due to the presence of more than 20 wt% S in half of the analyses, an Al filter had to be used to absorb most of the low energy S X-rays. The use of thick filters in micro-PIXE has a major effect on the low energy portion of the ED spectrum. Remond *et al.* (1987) used a 750 µm thick Al filter, which made detection of Cu and Fe, known to be present in their samples, impossible. For the results reported here, experimentation with different filter thickness and even beam acceleration voltage was necessary to obtain the best possible conditions for PGE detection.

A spectrum acquired at 2.45 MeV on the Ni-S melt phase in experiment HU429 (Figure 29), which contains about 20 wt% S, 80 wt% Ni and traces of Pt, Pd and Rh, is shown in Figure 30. The white specks in Figure 30 indicate the number of counts detected in every energy channel, from low energy (left) to high energy (right) radiation, to form an X-ray spectrum of the analysed spot.

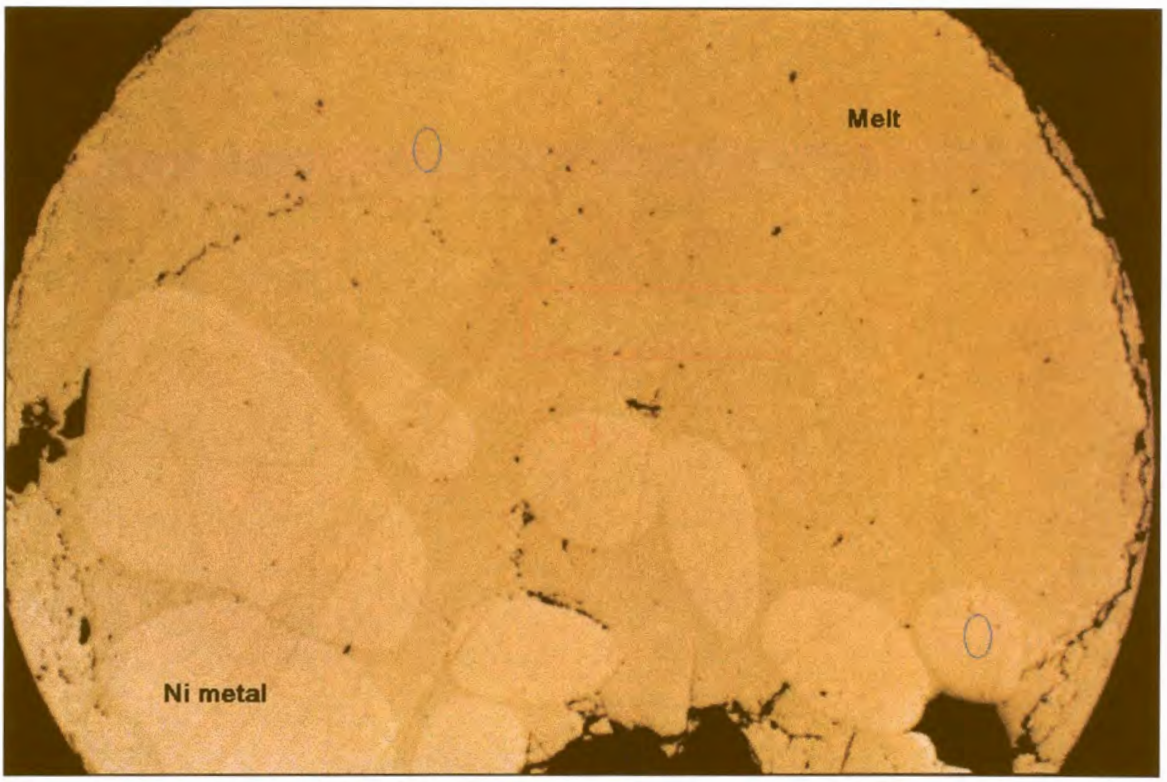

Figure 29. *Experiment HU429, co-existing nickel and quenched melt, equilibrated at 900°C. The red rectangles indicate the size and shapes of the areas analysed by micro-PIXE by moving the beam across the sample, and the blue ovals indicate the size and shape of the milli-PIXE spots, which are elongated to ovals due to the 45° angle of incidence with the incoming beam. Field of view 4 mm.*

In Figure 31 a calculated curve (yellow line) was fitted to the spectrum in Figure 30 with the GUPIX software, to quantify the elements. The background for the entire spectrum is very high, so that even the Ni and S peaks do not appear very clearly. If a huge amount of radiation of a certain energy reaches the detector, it is unable to handle the signal effectively and adds the signals so that a false peak at double the energy of the true peak is reported. This phenomena is called doubling and can be seen in Figure 30 for Ni and S. This same

effect described above also occurs at three or four times, or more, of the energy of the original peak, but with decreasing intensity. Two peaks – for example S and Ni – can also be added and a false peak created at the sum of their energies. This doubling or tripling also increases the background of the spectrum. The software package used to process the spectrum takes this effect into consideration. In Figure 31, the Pd and Rh-K peaks and the Pt L-peaks are mostly hidden by the high background, making accurate detection hidden by the S radiation. As Pt K radiation has a very high excitation energy, the L radiation has to be used for the analyses. impossible. The Rh and Pd L peaks are found close to the S K peaks, but are in this case

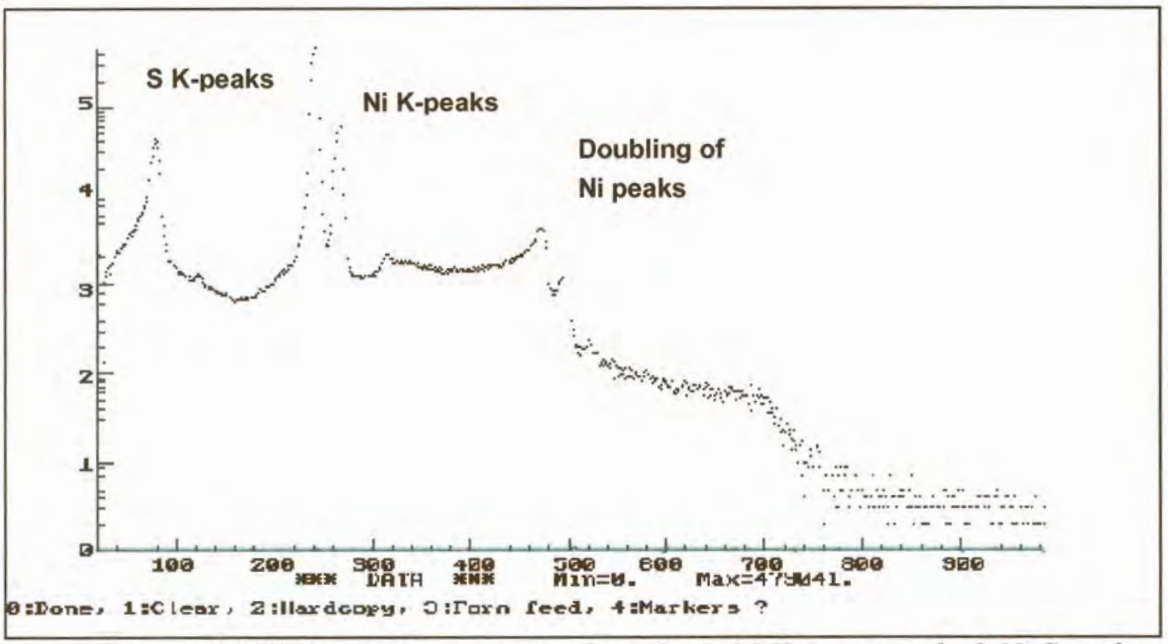

Figure 30. *Milli-PIXE spectrum acquired at 2.45 MeV on quenched Ni-S melt of experiment HU429, no filter. The vertical intensity scale is logarithmic. Doubling of the S peak, each Ni peak as well as the sum of the two Ni peaks and the sum of the Ni and the S peaks all increase the background.*

A spectrum acquired at the same spot as the spectrum shown in Figures 30 and 31, under the same conditions, but with a 125 µm thick Al filter inserted in front of the detector, is shown in Figure 32. The S peak visible in Figure 31 was completely removed from the spectrum, together with some of the Ni radiation. S is a light element and the Kα and Kβ peaks have low energies and are easily excitable, but are also easily absorbed. In this example, the background of the entire spectrum is lowered significantly, and the doubling

of the Ni peaks is also much reduced. This allows for accurate detection of the Pd and Rh K peaks by the software, although the Pd and Rh L peaks - located close to the S K peaks - were completely absorbed. The Pt L peaks remain difficult to detect, due to their position in the spectrum close to the Ni K peaks, where the background is very high. A thicker Al filter can be used to absorb higher energy radiation, and thereby to remove more of the Ni radiation from the spectrum and lower the background and Ni doubling further. However, a thicker filter would also absorb some of the Pt L radiation. The filter thickness has to be chosen to allow for optimum detection of the Pt peaks.

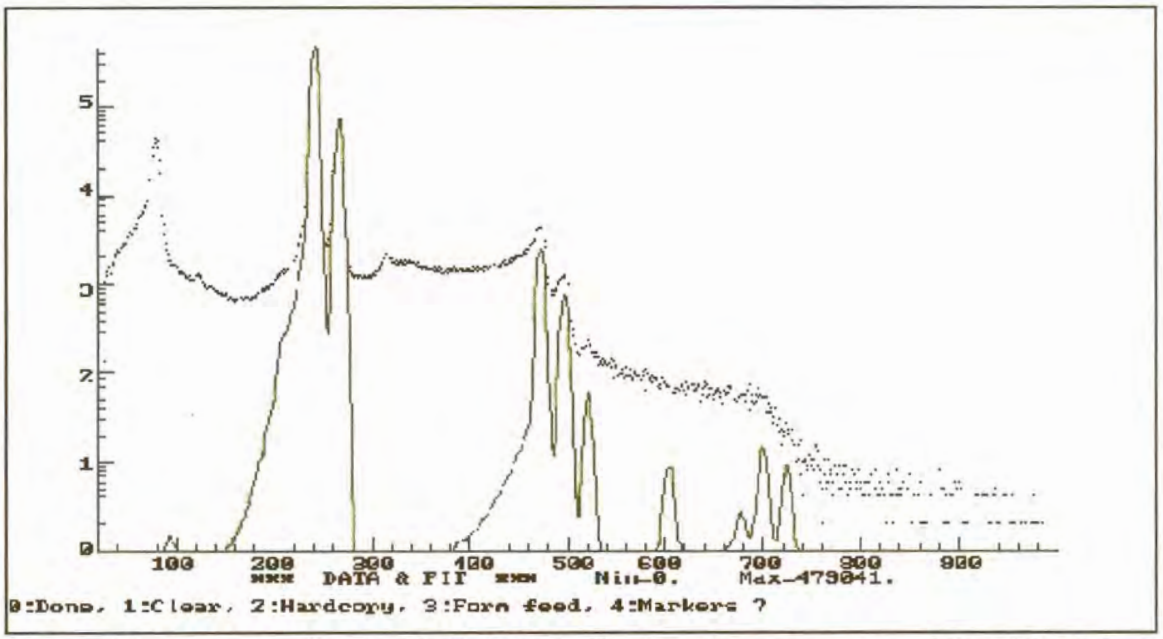

Figure 31. *Spectrum fitted with GUPIX (yellow) to determine composition. Fitted for Ni, Rh and Pd.*

The influence of the acceleration voltage was investigated by analysing the same spot on the Ni-S melt of experiment HU429, under the same conditions, first at 2.45 MeV and then at 3.00 MeV. The spectrum obtained at 3.00 MeV is shown in Figure 33 and can be compared with the 2.45 MeV spectrum in Figure 32. The peak to background ratio for the higher acceleration voltage is larger than for the lower acceleration voltage, making identification of Rh and Pd by the software possible, which was sufficient reason to perform further analyses at 3.000 MeV.

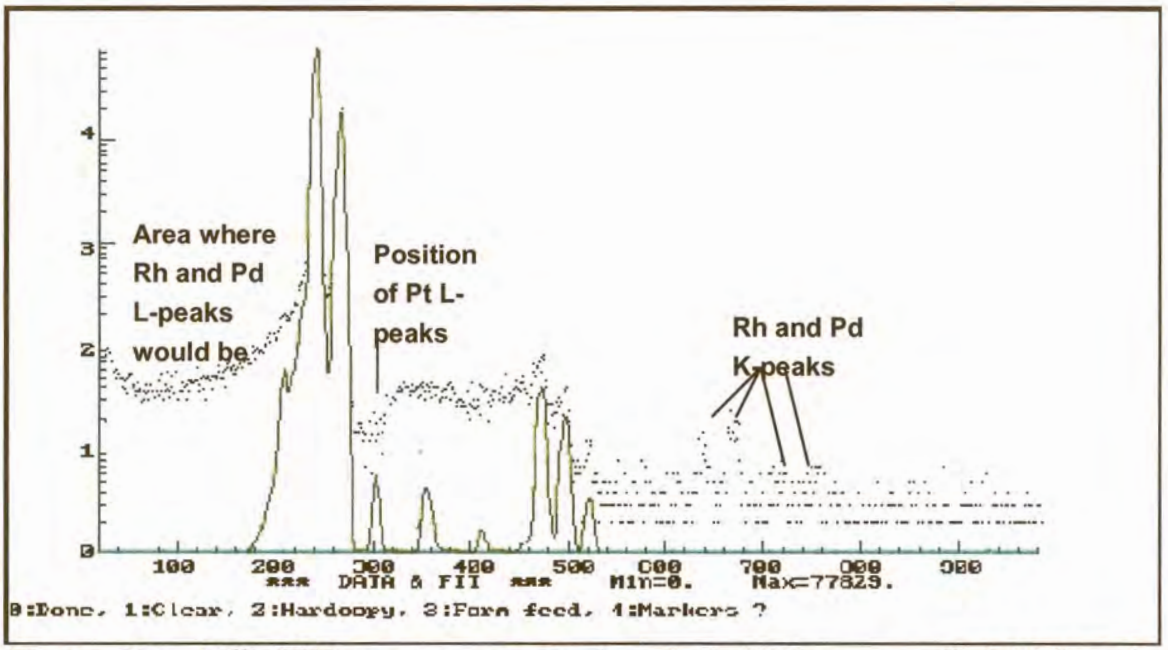

Figure 32. *Milli-PIXE spectrum acquired at 2.45 MeV on quenched Ni-S melt of experiment HU429, 125 μm Al filter.*

For the Ni-S system a 125 μm filter was used, and for the Fe-S and Cu-S systems a 200 μm thick filter was used (the Pt L peaks are even closer to the Cu and Fe K peaks than to the Ni K peaks) at an acceleration voltage of 3.00 MeV.

Analyses were generally left to collect $2x10^5$ counts on each spot. This took between one and three hours. Fewer counts did not provide spectra of the same clarity, and more counts usually did not improve the peak to background ratios significantly, due to an increase in the background. The beam current was generally between 0.2 and 0.7 nA, but was sometimes much lower due to technical difficulties. This did not have any effect on the quality of the spectra, only on the time it took to collect the spectra.

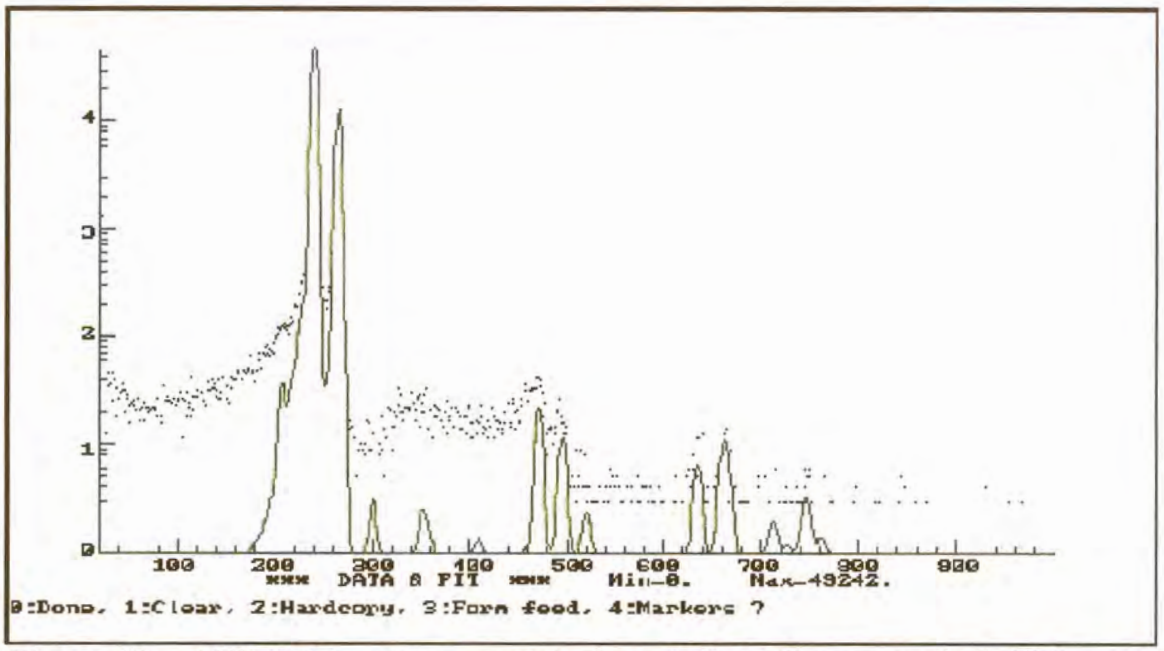

Figure 33. *Milli-PIXE spectrum acquired at 3.00 MeV on quenched Ni-S melt of experiment HU429, 125 μm Al filter.*

Table 6*. Evaluation of filter thickness and acceleration voltage.*

Acceleration voltage	Filter	Comment
2.45 MeV	None	Very high background - PGE below detection.
2.45 MeV	125 – 200 μm Al	Significant background reduction, almost complete removal of S radiation.
2.45 MeV	> 200 μm Al	Partial absorption of Pt L radiation.
3.00 MeV	125 – 200 μm Al	Slightly increased background, also increased peak to background ratio.

A spot that was analysed on Fe-S melt is shown in Figure 34. The carbon coating at the centre of the spot is discoloured. Analysis spots were always microscopically investigated to ensure that the correct positions were analysed. The size and shape of the milli-PIXE analyses are indicated in Figure 29, in comparison with the micro-PIXE analyses. Initially the spots were oval, but after the angle between the incoming beam and the sample surface was changed to 90°, the shape of the spot was round. The Fe-S analyses were performed with a round beam spot.

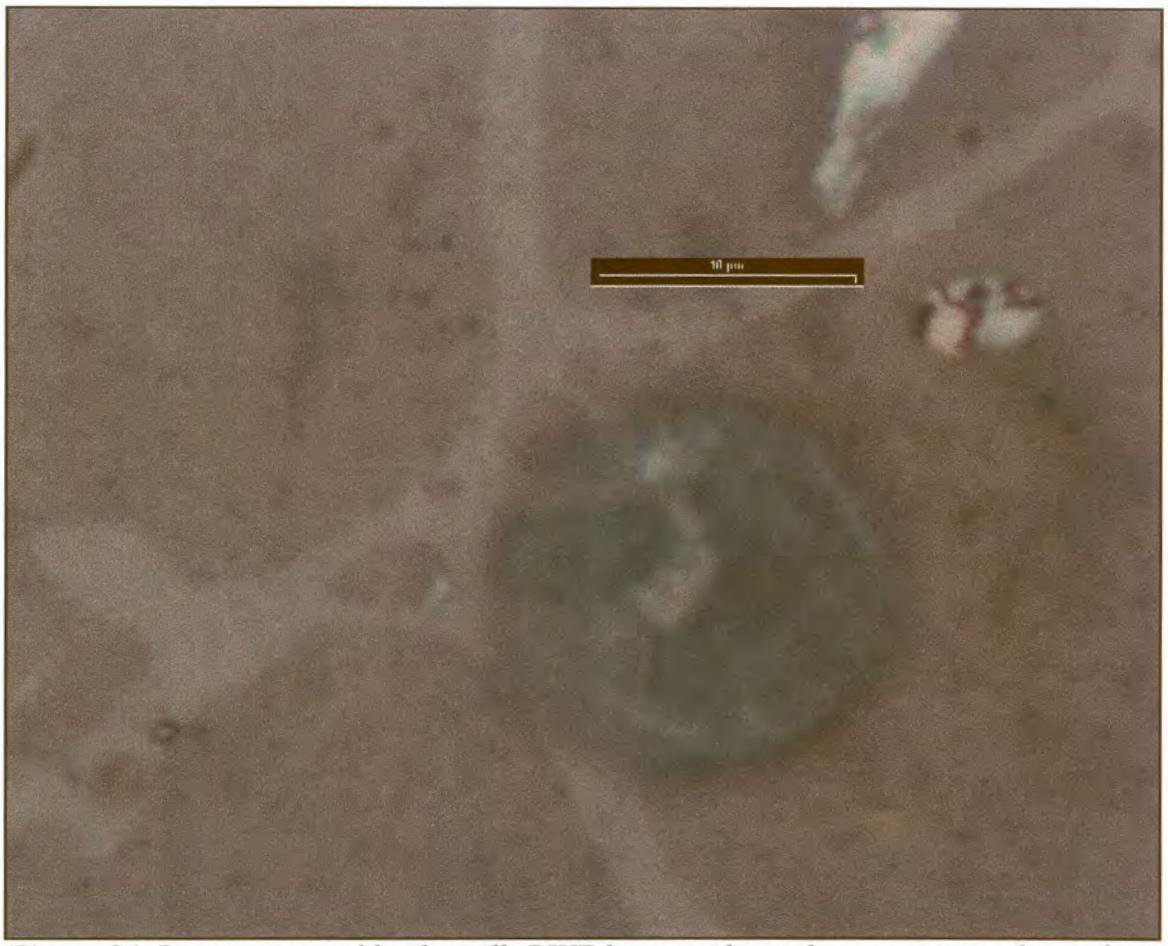

Figure 34. *Damage caused by the milli-PIXE beam in the carbon coating on the surface of Fe-S melt. The heterogeneous texture of the melt is visible. The scale bar is 10 µm. The diameter of the milli-PIXE beam is 100 µm. Only the central part of the beam caused damage.*

4.2.2. Micro-PIXE

At the National Accelerator Centre (NAC), a proton beam facility with a beam diameter of 2 µm is available, which allows PIXE analysis of microscopically small areas - called micro-PIXE. However, the quenched melts are heterogeneous, and larger areas were analysed to average out heterogeneities. This was achieved by rastering the beam over a rectangular surface on the sample while collecting the resulting X-rays. Typical areas analysed are indicated in Figure 29. A 125 µm Al filter was used to eliminate some of the major element radiation - mostly the S - to lower the overall background (as discussed for milli-PIXE, section 4.2.1.1.). A 3.00 MeV beam of H protons at a beam current of between 150 and 300 pA was used.

Whole spectra were collected until statistically acceptable peaks for the PGE were obtained, while noting the total counts. These were measured in nano-Coulombs (nC), and cannot be compared directly to the counts collected for the milli-PIXE analyses. Time varied from about 5 minutes to more than 10 hours per spectrum.

NAC data were processed with the GEOPIXE software described by Ryan *et al.* (1990). Yields and relative intensities are calculated, the X-ray spectrum is fitted by a least squares fitting routine and then combined with the yield calculations. EPMA major element analyses are incorporated with the PIXE data. Standard deviations and detection limits are determined individually for each element in each spectrum. The detection limits obtained for the PGE in each phase analysed are given in Table 7.

***Table** 7. Detection limits obtained for the PGE by micro-PIXE.*

Phase	Rh LLD (wt%)	Pd LLD (wt%)	Pt LLD (wt%)
Nickel	0.005	0.004	0.014
Ni-S-melt	0.0004	0.0005	0.001
Cu-S-melt	0.004	0.005	0.008
Digenite	0.0006	0.0007	0.002
Copper	0.009	0.011	0.032

4.3. Statistics

The averages (arithmetic means) and standard deviations were calculated from the EPMA analyses of each phase in the conventional way. Standard deviations are indications of the changes in instrumental conditions and heterogeneity of the analysed phases. Each individual PIXE analysis is supplied with an error calculated to reflect both counting statistics and peak overlap. As both EPMA and PIXE analyses values are accompanied by associated errors or standard deviations, these have to be considered when averages of the averages and ratios of the averages are determined. Resampling statistics were used in the

present investigation to make this possible, and to recalculate errors for the averages and ratios.

4.3.1. Resampling

Resampling is a Monte Carlo method that uses observed data to produce new hypothetical samples by randomly generating additional samples. Rather than using statistical formulae to describe a population, the technique simulates the underlying physical process. It is a useful tool for problems that require probabilistic and statistical analyses (Simon, 1997).

To determine the mean value of two or more means:
During the present investigation, mean compositions for phases had to be determined from EPMA analyses of several individual phases, each with its own mean and standard deviation (sections 5.1.1.1., 5.2.1.1., 5.2.2.1., 5.2.3.1., 5.3.1.1., 5.3.2.1., 5.3.3.1.). Several PIXE analyses of a specific phase, each with it's own associated error, were combined (sections 5.1.1.2., 5.2.1.2., 5.2.2.2., 5.2.3.2., 5.3.1.2., 5.3.2.2., 5.3.3.2.). This involves creating a normal distribution with a very large population according to the mean and standard deviation of each analysis. These populations are combined and a new mean and standard deviation obtained for the combined data. The larger the size of the recreated population, the more accurate the final values will be. The following routine was used.

MAXSIZE DEFAULT 15000	*Maximum sample size allowed.*
NORMAL 7500 (measured value1) (analytical uncertainty1) a	*Take 1 value from a simulated normal distribution with measured value 1 and analytical uncertainty1, and store in space "a". Repeat 7500 times.*
NORMAL 7500 (measured value2) (analytical uncertainty2) b	*Take 1 value from a simulated normal distribution with measured value 2 and analytical uncertainty 2, and store in space "b". Repeat 7500 times.*
CONCAT a b c	*Combine "a" and "b" and store in "c"*
MEAN c x	*Determine the arithmetic mean of "c", store in "x"*

STDEV c y	*Determine the standard deviation of "c", store in "y"*
PRINT x	*Print resampled mean*
PRINT y	*Print standard deviation*

To determine the mean of three or more values, values from simulated normal distributions of these values were also added to the resampled data, and included in the determination of the resampled average and standard deviation.

To determine the ratio of two means:

To determine partition coefficients, one population with a known mean and standard deviation was divided by a second population with known mean and standard deviation, to obtain a third population whose mean and standard deviation represents the ratio and its associated confidence interval (Section 6). The following routine was used.

MAXSIZE DEFAULT 15000	*Maximum sample size allowed.*
NORMAL 7500 (measured value1) (analytical uncertainty1) a	*Take 1 value from a simulated normal distribution with measured value 1 and analytical uncertainty1, and store in space "a". Repeat 7500 times.*
NORMAL 7500 (measured value2) (analytical uncertainty2) b	*Take 1 value from a simulated normal distribution with measured value 2 and analytical uncertainty 2, and store in space "b". Repeat 7500 times.*
DIVIDE a b m	*Divide population "a" by population "b" and store in "m".*
MEAN m x	*Store the arithmetic mean of "m" in "x".*
STDEV m y	*Store the standard deviation of "m" in "y".*
PRINT x	*Print the mean.*
PRINT y	*Print the standard deviation.*

5. Experimental Results

5.1. The Ni-S system

5.1.1. Nickel – Ni-S melt assemblage (1100°C - 700°C)

5.1.1.1. EPMA results

Major element compositions of co-existing nickel and Ni-S melt at 1100°C, 1000°C, 900°C and 700°C, as determined by EPMA, are given in Tables 8 to 11, with 3σ standard deviations. In addition to Ni and S, the total PGE content as determined by PIXE (Section 5.1.1.2.) is also given. The low calculated total for some metal phases (for example experiment HU441, Table 8, with a total of 98.21 wt%) does not take into account the PGE content, which, if considered, would bring the total elemental content close to 100 wt%.

EPMA determined Ni:S ratios were projected onto the Ni-S phase diagram (Figure 12 – blue triangles), ignoring the effect of PGE content, which is comparably very small. Average compositions of metals and melts were calculated with resampling statistics. The compositions can be compared to their expected compositions from the initial bulk compositions of the experimental charges. All the determined compositions of the melts were clearly more S-rich than predicted by the Ni-S phase diagram by Sharma and Chang (1980) and Cemic and Kleppa (1986).

Table 8. *Major element compositions, determined by EPMA, of co-existing nickel and quenched melt equilibrated at 1100°C.*

Exp	Phase	Ni wt% (± 3σ)	S wt% (± 3σ)	Total (wt%)	PGE# (wt%)	n
HU437	Nickel	99.83 (0.35)	0.04 (0.02)	99.87	~0.1	40
	Melt	81.49 (1.02)	18.53 (0.48)	100.02	~0.1	34
HU441	Nickel	98.21 (0.34)	bd	98.21	~1.8	22
	Melt	81.92 (1.03)	18.37 (0.51)	100.29	~0.4	24
HU731	Nickel	100.42 (0.43)	bd	100.42	~0.4	32
	Melt	81.84 (0.96)	18.03 (0.91)	99.87	~0.1	26
HU733	Nickel	100.06 (0.59)	bd	100.06	~0.3	26
	Melt	82.93 (1.28)	17.66 (0.92)	100.59	~0.2	26

Estimation of total PGE content as determined by PIXE, discussed in section 5.1.1.2.

5.1.1.1.1. Separated drops

A small drop separated from experiment HU441 (1100°C). EPMA analysis of the drop gave the Ni content at 78.84 wt% (1σ = 6.88 wt%), and the S content at 19.46 wt% (1σ = 6.19 wt%). Twenty spot analyses of 40 µm diameter were performed as the drop was too small to allow for area analyses, which accounts for the high standard deviations. PGE were below detection. The drop was also analysed separately during PIXE analyses, as discussed below. It is believed that the drop separated from the melt during quenching of the charge after equilibrium was established in the system, and has no influence on the results of the experiment.

A comparatively small drop found with experiment HU392 (1000°C) is shown in Figure 35. Investigation of the experimental charge revealed the absence of metal in the charge - despite three cross-sections cut through the charge none could be detected. The only detectable metal was found in the separated drop, which also contained melt. The drop separated from the bulk charge before equilibrium was reached, but equilibrium would have been achieved within this separated drop, considering its small size and an equilibration time of 35 days. The results of the melt analyses of experiment HU392, and the results of

the analyses on the separated drop, are shown in Table 9. The melt of the main charge was analysed in the same manner as the other melts in Table 9 (area analyses), but the separated drop was analysed with a 40 µm diameter spot (32 spot analyses), resulting in large standard deviations and uncertainty. Both the melt and metal in the separated drop were analysed for Rh, Pd and Pt. No PGE were detected in the melt, but in the metal 0.41 wt% Rh (1σ = 0.12 wt %) and 2.31 wt% Pt (1σ = 0.17 wt%) were. No Pd was detected in the metal. PIXE analyses were performed on all three phases (melt of the main experiment and metal and melt in the separated drop), and are discussed in the following section.

Table 9. *Major element compositions, determined by EPMA, of co-existing nickel and quenched melt equilibrated at 1000°C.*

Exp	Phase	Ni wt% (± 3σ)	S wt% (± 3σ)	Total (wt%)	PGE# (wt%)	n
HU381	Nickel	97.46 (0.67)	bd	97.46	~2.5	26
	Melt	80.56 (0.99)	19.25 (1.08)	99.81	~0.7	20
HU392	Melt	78.96 (0.49)	20.04 (0.33)	99.00	-	36
HU392	Nickel	96.54 (0.91)	bd	96.54	~2.2	32
(drop)	Melt	77.27 (5.43)	20.64 (5.93)	97.91	~0.1	30
HU393	Nickel	99.57 (0.02)	bd	99.57	~1.1	35
	Melt	80.92 (1.07)	19.19 (0.90)	100.11	~0.2	34
HU394	Nickel	92.95 (1.93)	bd	92.95	~6.6	128
	Melt	80.04 (1.45)	19.26 (1.16)	99.30	~1.4	62
HU395	Nickel	88.05 (4.43)	bd	88.05	~10.6	100
	Melt	79.33 (1.14)	20.21 (0.86)	99.54	~2.7	37
HU412	Nickel	89.44 (0.60)	bd	89.44	~8.1	28
	Melt	79.36 (1.10)	19.60 (0.95)	98.96	~1.9	61

Estimation of total PGE content as determined by PIXE, discussed in section 5.1.1.2.

***Table 10**. Major element compositions, determined by EPMA, of co-existing nickel and quenched melt equilibrated at 900°C.*

Exp	Phase	Ni wt% (± 3σ)	S wt% (± 3σ)	Total (wt%)	PGE[#] (wt%)	n
HU426	Nickel	98.43 (0.35)	bd	98.43	~0.4	18
	Melt	79.20 (0.83)	19.88 (0.78)	99.08	<0.1	53
HU427	Nickel	99.72 (0.95)	bd	99.72	~0.3	16
	Melt	78.69 (1.05)	21.14 (0.93)	99.83	~0.3	35
HU428	Nickel	99.74 (0.45)	bd	99.74	~0.6	34
	Melt	79.46 (0.73)	20.93 (0.72)	100.39	~0.1	42
HU429	Nickel	99.94 (0.62)	bd	99.94	~1.6	18
	Melt	78.38 (0.66)	21.36 (0.59)	99.74	~0.4	30
HU753	Nickel	99.23 (1.03)	bd	99.23	~0.8	46
	Melt	79.00 (0.73)	21.66 (0.34)	100.66	~0.2	30

Estimation of total PGE content as determined by PIXE, discussed in section 5.1.1.2.

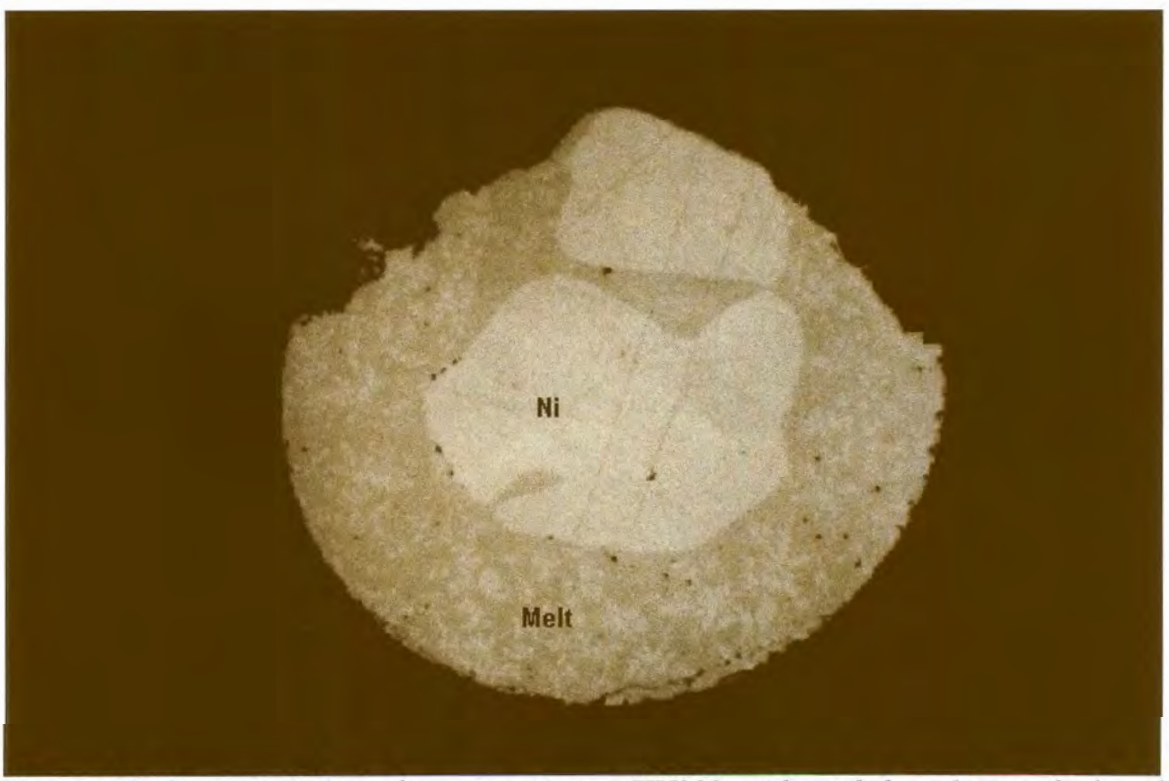

***Figure 35.** Separated drop from experiment HU392 with nickel and quenched melt equilibrated at 1000°C. Field of view 4 mm.*

Table 11. *Major element compositions, determined by EPMA, of co-existing nickel and quenched melt, equilibrated at 700°C.*

Exp	Phase	Ni wt% (± 3σ)	S wt% (± 3σ)	Total (wt%)	PGE# (wt%)	n
HU469	Nickel	99.45 (0.49)	bd	99.45	~0.3	30
	Melt	76.51 (0.65)	22.34 (0.47)	98.85	~0.1	54
HU471	Nickel	98.76 (0.40)	bd	98.76	~1.1	30
	Melt	75.12 (1.98)	23.95 (1.92)	99.07	<0.1	39
HU472	Nickel	99.48 (0.28)	bd	99.48	nd	26
	Melt	76.95 (0.72)	22.45 (0.19)	99.40	~0.4	82
HU473	Nickel	99.43 (0.29)	bd	99.43	~0.6	26
	Melt	77.60 (0.70)	22.48 (0.58)	100.08	~0.1	94

Estimation of total PGE content as determined by PIXE, discussed in section 5.1.1.2.

A separated drop was also found with experiment HU395. This drop consisted only of melt, and was analysed for Ni, S, Rh, Pd and Pt with a 40 µm diameter beam spot (28 spot analyses). The melt contained 75.16 wt% Ni (1σ = 4.43 wt%), 22.52 wt% S (1σ = 5.16 wt%), no detectable Rh, 1.29 wt% Pd (1σ = 0.53 wt%), and no detectable Pt. The drop was also analysed by PIXE, as discussed below (Section 5.1.1.2.).

A very small separated drop found with experiment HU427 (900°C) consisted only of quenched melt, and was analysed for Ni, S, Rh, Pd and Pt with a beam spot of 40 µm diameter. From 10 analyses, 77.17 wt% Ni (1σ = 0.94 wt%), 21.70 wt% S (1σ = 0.45 wt%), and no PGE were detected. The drop probably separated from the charge during quenching, but was also analysed separately by PIXE, as discussed in the following section.

5.1.1.2. PIXE results

5.1.1.2.1. Milli-PIXE

5.1.1.2.1.1. Results for equilibration at 1100°C

Heterogeneity of the melt of experiment HU733 for the PGE, is indicated by the significant variation between the two analyses (Table 13), which could not be corrected for by the large diameter of the beam spot (~ 0.1 mm; see Photograph 36 for the heterogeneous texture). The Rh and Pd results of these two analyses were combined with resampling statistics (Table 20). As the Pt content from the second analysis is below detection, the value from the first analysis was used for further calculations (Table 20). Two analyses were performed on the melt phase of experiment HU731, where only Pt was added to the experiment. Considering the standard deviations, there is no significant difference between the two analyses. The two analyses were combined with resampling statistics for further calculations (Table 20).

Table 12. *Milli-PIXE trace element spot analyses of nickel that co-exists with melt, equilibrated at 1100°C.*

Exp	Rh wt% (± 3σ)	Rh LLD	Pd wt% (± 3σ)	Pd LLD	Pt wt% (± 3σ)	Pt LLD	Counts
HU733	0.140 (0.014)	0.012	0.051 (0.014)	0.017	0.127 (0.020)	0.019	200000
HU731					0.387 (0.026)	0.011	200000

Table 13. *Milli-PIXE trace element spot analyses of the melt phase that co-exists with nickel, equilibrated at 1100°C. Values in italics are statistically unreliable.*

Exp	Rh wt% (± 3σ)	Rh LLD	Pd wt% (± 3σ)	Pd LLD	Pt wt% (± 3σ)	Pt LLD	Counts
HU733	0.107 (0.013)	0.017	0.082 (0.014)	0.013	0.032 (0.015)	0.024	200000
HU733	0.077 (0.013)	0.017	0.125 (0.016)	0.019	*0.011* (0.016)	0.028	200000
HU731					0.073 (0.016)	0.025	200000
HU731					0.090 (0.016)	0.023	200000

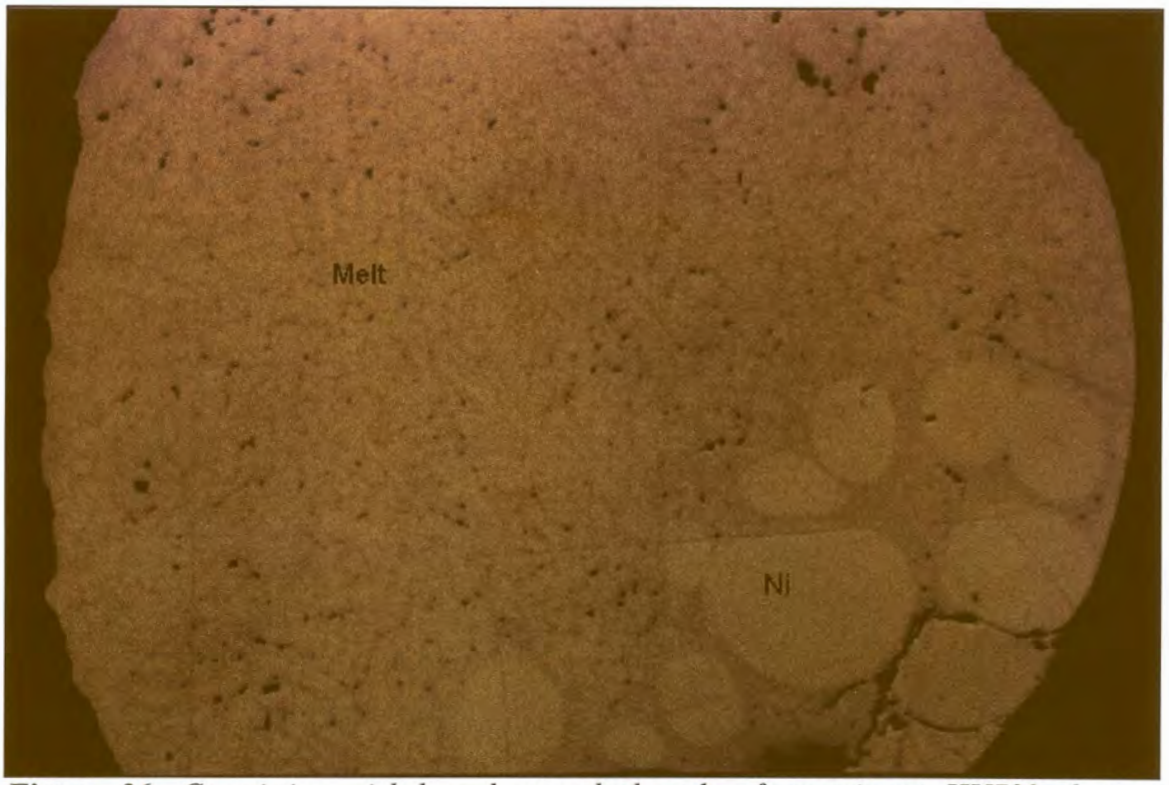

Figure 36. *Co-existing nickel and quenched melt of experiment HU733 that was equilibrated at 1100°C. The experiment contained a bulk of 500 ppm each of Rh, Pd and Pt (exact amounts in Table A2; Appendix A). Field of view 4 mm.*

5.1.1.2.1.2. Results for equilibration at 1000°C

Two analyses were performed on the nickel in experiment HU381, and the average was used in further discussions (Table 20). The Pt value obtained in the analysis of melt in experiment HU393 (Table 15) is only just above the detection limit. This value was used for further calculations. The two analyses of the melt phase of experiment HU381 compare well (between 10 and 15 % variation for the three PGE), considering the associated errors. They were combined with resampling statistics (Table 20).

Table 14. *Milli-PIXE trace element analyses of nickel that co-exists with melt, equilibrated at 1000°C.*

Exp	Rh wt% (± 3σ)	Rh LLD	Pd wt% (± 3σ)	Pd LLD	Pt wt% (± 3σ)	Pt LLD	Counts
HU393	0.391 (0.024)	0.020	0.111 (0.020)	0.031	0.555 (0.026)	0.017	200000
HU381	0.869 (0.037)	0.016	0.289 (0.025)	0.019	1.387 (0.042)	0.028	200000
HU381	0.907 (0.039)	0.028	0.291 (0.027)	0.026	1.322 (0.044)	0.026	200000

Table 15. *Milli-PIXE trace element analyses of the melt phases that co-exist with nickel, equilibrated at 1000°C.*

Exp	Rh wt% (± 3σ)	Rh LLD	Pd wt% (± 3σ)	Pd LLD	Pt wt% (± 3σ)	Pt LLD	Counts
HU393	0.141 (0.014)	0.017	0.184 (0.017)	0.014	0.025 (0.015)	0.023	200000
HU381	0.198 (0.021)	0.013	0.375 (0.030)	0.034	0.047 (0.017)	0.027	200000
HU381	0.249 (0.024)	0.035	0.435 (0.030)	0.024	0.058 (0.018)	0.028	200000

5.1.1.2.1.3. Results for equilibration at 900°C

Two analyses were performed on the melt phase of experiment HU753 (Table 17). The Rh and Pd contents from the two analyses compare well, and the two analyses were combined with resampling statistics (Table 20). The Pt contents in both analyses were below detection, and the lowest detection limit was used in further calculations. The melt phase of experiment HU429 (Table 17) was analysed twice, and the two analyses vary considerably. From all the melt analyses it becomes clear that Pd is slightly concentrated in the melt phase, as opposed to Pt and Rh, which are concentrated in the nickel. However, in the second melt analysis of experiment HU429, the Rh content is almost the same as the Pd content, and therefore higher than would be expected. The Pt content is much higher than in the previous analysis. The calculated detection limits of all the elements are lower for the second analysis - more typical of a nickel analysis. Therefore, it is believed that this melt analysis was at least in part influenced by a hidden nickel phase that was not visible on the surface of the melt (penetration depth is discussed in section 4.2.). The second melt analysis was ignored in further discussions, and only the first analysis was used. The Pt detection limit was used further on.

Table 16. *Milli-PIXE trace element analyses of nickel that co-exists with melt, equilibrated at 900°C.*

Exp	Rh wt% (± 3σ)	Rh LLD	Pd wt% (± 3σ)	Pd LLD	Pt wt% (± 3σ)	Pt LLD	Counts
HU753	0.374 (0.028)	0.009	0.077 (0.022)	0.021	0.332 (0.037)	0.013	200000
HU429	0.737 (0.032)	0.019	0.219 (0.023)	0.030	0.778 (0.029)	0.011	200000
HU427			0.304 (0.023)	0.025			200000

Table 17. *Milli-PIXE trace element analyses of the melt phases that co-exist with nickel equilibrated at 900°C. Values in italics are statistically unreliable.*

Exp	Rh wt% (± 3σ)	Rh LLD	Pd wt% (± 3σ)	Pd LLD	Pt wt% (± 3σ)	Pt LLD	Counts
HU753	0.081 (0.013)	0.019	0.105 (0.019)	0.018	nd	0.034	200000
HU753	0.102 (0.016)	0.015	0.094 (0.019)	0.032	*0.020* (0.015)	0.023	200000
HU429	0.134 (0.017)	0.026	0.344 (0.024)	0.024	*0.006* (0.016)	0.029	200000
HU429	0.236 (0.018)	0.008	0.254 (0.022)	0.018	0.038 (0.015)	0.020	200000
HU427			0.352 (0.026)	0.029			200000

5.1.1.2.1.4. Results for equilibration at 700°C

The melt phase of experiment HU471 was analysed twice, but Pt was below detection in both. For further calculations the lowest detection limit was used. The melt phase of experiment HU472 (Table 19) was analysed twice, but the second analysis was intended to be on the metal surface. After analysis of the sample the surface was microscopically investigated, and the analysis spots could be detected by the damage to the carbon coating of the sample. Both spots were found to be on the melt phase. The method used to orient the sample under the milli-PIXE beam was described in Section 4.2.1. and when the shape of a sample is not characteristic, it is difficult to find the intended position on the sample. Photograph 23 shows the position of the small nickel phase on the edge of the sample. The two melt analyses compare well, but due to the fact that no analysis was performed of the co-existing nickel in this experiment, it could not be used for further calculations.

All the milli-PIXE analyses that were used for further discussion are given in Table 20.

Table 18. *Milli-PIXE trace element analyses of nickel that co-exists with melt equilibrated at 700°C.*

Exp	Rh wt% (± 3σ)	Rh LLD	Pd wt% (± 3σ)	Pd LLD	Pt wt% (± 3σ)	Pt LLD	Counts
HU469	0.220 (0.022)	0.017	0.032 (0.014)	0.004	0.138 (0.023)	0.036	200000
HU471					1.133 (0.043)	0.024	200000
HU473	0.633 (0.043)	0.034					200000

Table 19. *Milli-PIXE trace element analyses of the melt phases of experiments equilibrated at 700°C. Values in italics are statistically unreliable.*

Exp	Rh wt% (± 3σ)	Rh LLD	Pd wt% (± 3σ)	Pd LLD	Pt wt% (± 3σ)	Pt LLD	Counts
HU469	0.040 (0.010)	0.013	0.062 (0.016)	0.019	*0.003* (0.016)	0.028	200000
HU471					*0.006* (0.024)	0.044	200000
HU471					nd	0.046	200000
HU472			0.408 (0.039)	0.045			200000
HU472			0.446 (0.035)	0.027			200000
HU473	0.065 (0.027)	0.046					200000

Table 20. *Milli-PIXE analyses of nickel and Ni-S melt in experiments of the Ni-S system. Values in italics are statistically unreliable.*

Exp	Temp (°C)	Nickel			Quenched melt		
		Rh (wt%)	Pd (wt%)	Pt (wt%)	Rh (wt%)	Pd (wt%)	Pt (wt%)
HU733	1100	0.140	0.051	0.127	0.092	0.104	0.032
HU731	1100			0.387			0.081
HU393	1000	0.391	0.111	0.555	0.141	0.184	0.025
HU381	1000	0.888	0.290	1.355	0.224	0.405	0.053
HU753	900	0.374	0.077	0.332	0.091	0.100	<0.023
HU429	900	0.737	0.219	0.778	0.134	0.344	<0.029
HU427	900		0.304			0.352	
HU469	700	0.220	0.032	0.138	0.040	0.062	<0.028
HU471	700			1.133			<0.044
HU473	700	0.633			0.065		

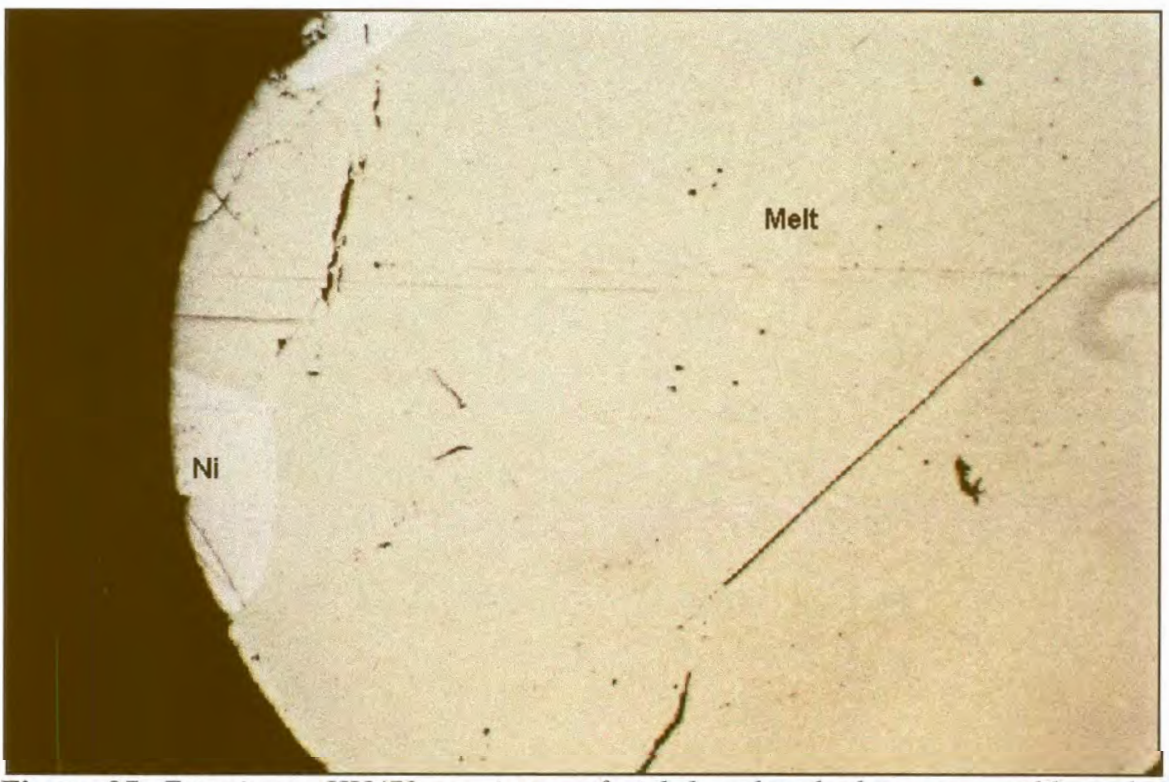

Figure 37. *Experiment HU472 consisting of nickel and melt that was equilibrated at 700°C. The small area of nickel was not found during milli-PIXE analysis. Field of view 4 mm.*

5.1.1.2.2. Micro-PIXE

5.1.1.2.2.1. Results for equilibration at 1100°C

The small separated drop of melt of experiment HU441 was analysed separately by both EPMA (Section 5.1.1.1.) and PIXE (Table 22). The PGE content of the drop is very similar to the PGE content of the melt phase (Table 22), which implies that it separated from the charge after equilibration, possibly during quenching, as was discussed in section 5.1.1.1. The analysis of the separated drop was ignored in further calculations.

Table 21. *Micro-PIXE trace element analyses of nickel that co-exists with melt equilibrated at 1100°C.*

Exp	Rh wt% (± 3σ)	Rh LLD	Pd wt% (± 3σ)	Pd LLD	Pt wt% (± 3σ)	Pt LLD	Charge (nC)
HU441	0.463 (0.020)	0.008	0.087 (0.008)	0.009	1.213 (0.029)	0.020	54
HU437			0.103 (0.010)	0.007			59

Table 22. *Micro-PIXE trace element analyses of the melt phases that co-exist with nickel, equilibrated at 1100°C.*

Exp	Rh wt% (± 3σ)	Rh LLD	Pd wt% (± 3σ)	Pd LLD	Pt wt% (± 3σ)	Pt LLD	Charge (nC)
HU441	0.169 (0.011)	0.004	0.183 (0.008)	0.005	0.061 (0.006)	0.010	106
HU441 drop	0.168 (0.008)	0.005	0.176 (0.011)	0.006	0.056 (0.006)	0.013	79
HU437			0.142 (0.010)	0.004			137

5.1.1.2.2.2. Results for equilibration at 1000°C

Experiment HU392 was analysed by EPMA (Table 9) and described in section 5.1.1.1. It contained a separated drop that consists of nickel and quenched melt, while only quenched melt was observed in the rest of the charge. The metal analysis of experiment HU392 in Table 23 was performed on the separated drop (as no metal could be found in the main charge). The melt phases of both the main charge and the drop were analysed and the results are given in Table 24. From the table it is clear that the contents of all three PGE in

the melt phase of the main charge are significantly lower than in the melt phase of the drop, implying that the drop was separated from the main charge before complete equilibrium was reached. The bulk composition of the drop can, therefore, only be roughly guessed by extrapolation from the compositions of the metal and melt. It is not directly related to the initial composition of the entire charge (provided in Appendix A). As no metal could be found in the main charge, the analyses of the drop will be used as "experiment HU392" for further discussions, even though the composition does not correspond to the planned composition of the experiment. It is believed that equilibrium was achieved within the drop itself. Two PIXE analyses were performed on the melt phase of the drop, as the PGE content was low. With the GEOPIXE software package it is possible to add the counts of two analyses and obtain a result for the added counts. This corresponds to an analysis taken for the total of the counts which would be more reliable than either of the two analyses would be on their own. In Table 24, this analysis is presented as HU392 (sum), which was used in further discussion.

Table 23. *Micro-PIXE trace element analyses of nickel that co-exists with melt, equilibrated at 1000°C.*

Exp	Rh wt% (± 3σ)	Rh LLD	Pd wt% (± 3σ)	Pd LLD	Pt wt% (± 3σ)	Pt LLD	Charge (nC)
HU393	0.349 (0.014)	0.008	0.096 (0.013)	0.009	0.737 (0.025)	0.019	54
HU394	2.148 (0.044)	0.014	0.493 (0.027)	0.016	4.460 (0.093)	0.029	30
HU395	3.197 (0.067)	0.013	1.116 (0.043)	0.015	6.351 (0.099)	0.024	54
HU412	2.707 (0.051)	0.009	0.761 (0.027)	0.012	4.784 (0.076)	0.022	60
HU392 drop	0.460 (0.016)	0.008	0.044 (0.009)	0.009	1.724 (0.034)	0.210	50

The melt phase of experiment HU393 was analysed twice in an attempt to determine the low Pt content (Table 24). For the second analysis, a large number of counts was collected, lowering the detection limit and the error significantly. The two analyses compare well, but the second analysis will be used for further calculations, due to its smaller error and lower detection limit (Table 27).

Slightly less PGE were detected in the drop that accompanied experiment HU395, which implies slight concentration of PGE in the charge (Table 24), suggesting that the drop was separated before equilibrium conditions were reached. However, considering the large size of the charge compared to the small drop, it is concluded that the PGE concentration effect is negligible. The drop was not considered in further discussions.

***Table 24**. Micro-PIXE trace element analyses of the melt phases that co-exist with nickel equilibrated at 1000°C. Values in italics are statistically unreliable.*

Exp	Rh wt% (± 3σ)	Rh LLD	Pd wt% (± 3σ)	Pd LLD	Pt wt% (± 3σ)	Pt LLD	Charge (nC)
HU393	0.081 (0.004)	0.002	0.136 (0.007)	0.003	0.017 (0.002)	0.007	300
HU393	0.075 (0.002)	0.0004	0.124 (0.003)	0.0005	0.015 (0.001)	0.001	9579*
HU394	0.489 (0.021)	0.011	0.790 (0.030)	0.013	0.098 (0.016)	0.021	30
HU395	0.826 (0.028)	0.007	1.760 (0.026)	0.008	0.113 (0.006)	0.012	89
HU395 drop	0.576 (0.014)	0.005	1.327 (0.028)	0.006	0.093 (0.005)	0.010	115
HU412	0.719 (0.027)	0.007	1.096 (0.027)	0.009	0.107 (0.008)	0.015	50
HU412 point	0.814 (0.020)	0.006	1.081 (0.025)	0.008	0.149 (0.007)	0.013	72
HU392 drop	0.066 (0.006)	0.004	0.042 (0.005)	0.005	*0.007* (0.004)	0.011	100
HU392 drop	0.064 (0.003)	0.003	0.050 (0.003)	0.003	*0.008* (0.004)	0.008	200
HU392 sum	0.065 (0.003)	0.002	0.048 (0.003)	0.003	0.008 (0.003)	0.006	300
HU392 main	0.005 (0.001)	0.002	0.003 (0.002)	0.002	*0.002* (0.002)	0.006	300

* ~10 hours

Two analyses were performed on the melt phase of experiment HU412 (Table 24). The first included an area on the melt (~ 100 x 100 μm), while the second was a point analysis on a spot with diameter of about 2 μm, ignoring the heterogeneity of the melt. The two analyses

do not differ much, possibly because the volume analysed by spot analysis is larger than the spot diameter itself. The area analysis was used for further discussion.

5.1.1.2.2.3. Results for equilibration at 900°C

Table 25. *Micro-PIXE trace element analyses of nickel that co-exists with melt, equilibrated at 900°C.*

Exp	Rh wt% (± 3σ)	Rh LLD	Pd wt% (± 3σ)	Pd LLD	Pt wt% (± 3σ)	Pt LLD	Charge (nC)
HU429	0.606 (0.020)	0.007	0.151 (0.009)	0.008	0.919 (0.020)	0.019	65
HU426					0.360 (0.013)	0.014	117
HU427			0.159 (0.008)	0.004			163
HU428	0.596 (0.027)	0.005					47

Table 26. *Micro-PIXE trace element analyses of the melt phases that co-exist with nickel equilibrated at 900°C. Values in italics are statistically unreliable.*

Exp	Rh wt% (± 3σ)	Rh LLD	Pd wt% (± 3σ)	Pd LLD	Pt wt% (± 3σ)	Pt LLD	Charge (nC)
HU429	0.115 (0.004)	0.002	0.225 (0.004)	0.002	0.011 (0.002)	0.005	510
HU426					*0.004* (0.002)	0.004	607
HU427			0.215 (0.008)	0.003			181
HU427 drop			*0.001* (0.002)	0.004			99
HU428	0.110 (0.004)	0.003					173

All the PGE contents determined by micro-PIXE analysis that were used for further discussion are presented in Table 27. Values in italics indicate analyses where errors and background were very high compared to the PGE content.

Table 27. *Results of micro-PIXE analyses of nickel and Ni-S-melt in experiments of the Ni-S system. Values in italics are statistically unreliable.*

Exp	Temp (°C)	Nickel			Quenched melt		
		Rh (wt%)	Pd (wt%)	Pt (wt%)	Rh (wt%)	Pd (wt%)	Pt (wt%)
HU441	1100	0.463	0.087	1.213	0.169	0.183	0.061
HU437	1100		0.103			0.142	
HU393	1000	0.349	0.096	0.737	0.075	0.124	0.015
HU394	1000	2.148	0.493	4.460	0.489	0.790	0.098
HU395	1000	3.197	1.116	6.351	0.826	1.760	0.113
HU412	1000	2.707	0.761	4.784	0.719	1.096	0.107
HU392	1000	0.460	0.044	1.724	0.065	0.048	0.008
HU429	900	0.606	0.151	0.919	0.115	0.225	0.011
HU426	900			0.360			*0.004*
HU427	900		0.159			0.215	
HU428	900	0.596			0.110		

5.2. The Cu-S system

5.2.1. Cu-rich melt - S-rich melt assemblage (1200°C)

5.2.1.1. EPMA results

The major element compositions of the quenched Cu-rich and S-rich melts determined by EPMA are given in Table 28, and projected onto the phase diagram of the Cu-S system (after Chakrabarti and Laughlin, 1986) at 1200°C (Figure 15 – blue triangles). These compositions compare favourably with the expected compositions.

***Table 28**. Major element compositions, determined by EPMA, of co-existing Cu-rich melt and S-rich melt equilibrated at 1200°C.*

Exp	Phase	Cu wt% (± 3σ)	S wt% (± 3σ)	Total (wt%)	PGE# (wt%)	n
HU442	Cu-rich melt	97.63 (0.36)	1.03 (0.26)	98.66	~0.8	39
	S-rich melt	80.21 (0.90)	19.84 (0.69)	100.05	<0.1	30
HU443	Cu-rich melt	97.92 (0.50)	1.04 (0.37)	98.96	~0.3	30
	S-rich melt	79.24 (0.89)	20.03 (0.25)	99.27	<0.1	16
HU444	Cu-rich melt	98.34 (0.80)	1.08 (0.35)	99.42	~0.4	29
	S-rich melt	80.10 (0.50)	19.43 (0.45)	99.53	~0.05	52
HU445	Cu-rich melt	99.05 (0.51)	1.16 (0.33)	100.21	~0.4	38
	S-rich melt	80.22 (0.89)	19.52 (1.00)	99.74	<0.01	38
HU450	Cu-rich melt	97.30 (0.45)	1.17 (0.40)	98.47	~0.8	35
	S-rich melt	79.33 (0.46)	19.97 (0.38)	99.30	<0.1	38

= Estimation of total PGE content as determined by PIXE, discussed in section 5.2.1.2.

5.2.1.2. PIXE results

5.2.1.2.1. Milli-PIXE

5.2.1.2.1.1. Results for equilibration at 1200°C

Very low detection limits were obtained for all three PGE in the Cu-rich melt of experiment HU442, because three times the normal number of counts were collected. The detection limits for the other experiments are much higher. The Cu-rich melt in experiment HU443 was analysed twice, the two results compare well, and were combined with resampling statistics (Table 31). In experiment HU444 two analyses were combined with resampling statistics.

Table 29. *Milli-PIXE trace element analyses of the Cu-rich melt phase co-existing with the S-rich melt phase equilibrated at 1200°C.*

Exp	Rh wt% (± 3σ)	Rh LLD	Pd wt% (± 3σ)	Pd LLD	Pt wt% (± 3σ)	Pt LLD	Counts
HU442	0.238 (0.013)	0.016	0.324 (0.016)	0.013	0.265 (0.022)	0.031	600000
HU443					0.359 (0.036)	0.053	200000
HU443					0.330 (0.037)	0.055	200000
HU444			0.366 (0.028)	0.032			200000
HU444			0.428 (0.028)	0.021			200000
HU445	0.384 (0.026)	0.025					200000
HU450	0.364 (0.025)	0.022	0.241 (0.021)	0.021	0.173 (0.032)	0.044	200000

The S-rich melt of experiment HU442 was analysed twice. In both cases the Rh and Pt contents were below the detection limits, and the lowest detection limits were used in further calculations. Pd could be detected in both analyses, because the detection limits at the Pd peak positions were much lower than for Rh and Pt. Resampling statistics was used to combine the analyses. Out of the seven analyses on the S-rich melt of experiment HU443, Pt was detected only during the second. This higher than expected Pt peak could indicate interference from the Cu-rich melt, or heterogeneity of the melt. Whatever the reason, this result is inconsistent with the other analyses, and will therefore be ignored. The fourth analysis was left to collect more counts than any of the other analyses, and obtained the lowest detection limit, which was used in further calculations. The S-rich melt of experiment HU444 was analysed three times. The analysis for which most counts was collected (200000) was the only one where Pd could be detected, and this was used for further calculations. The S-rich melt of experiment HU445 was analysed twice, and the second time twice as many counts were collected, resulting in a lower detection limit, which was used for further calculations. The peaks of all three PGE were found to be below detection in the S-rich melt of experiment HU450.

Table 30. *Milli-PIXE trace element analyses of the S-rich melt phases co-existing with Cu-rich melt phases, equilibrated at 1200°C. Values in italics are statistically unreliable.*

Exp	Rh wt% (± 3σ)	Rh LLD	Pd wt% (± 3σ)	Pd LLD	Pt wt% (± 3σ)	Pt LLD	Counts
HU442	bd	0.026	0.022 (0.009)	0.017	*0.021* (0.026)	0.044	200000
HU442	bd	0.029	0.026 (0.011)	0.014	bd	0.052	200000
HU443					*0.003* (0.026)	0.048	200000
HU443					0.063 (0.024)	0.034	200000
HU443					bd	0.057	200000
HU443					*0.015* (0.018)	0.031	400000
HU443					*0.036* (0.032)	0.053	100000
HU443					*0.024* (0.030)	0.053	100000
HU443					*0.007* (0.037)	0.067	100000
HU444			bd	0.122			100000
HU444			0.053 (0.015)	0.018			200000
HU444			bd	0.026			170000
HU445	bd	0.024					200000
HU445	*0.009* (0.007)	0.011					400000
HU450	*0.011* (0.009)	0.017	bd	0.038	bd	0.053	200000

Table 31. *Results of milli-PIXE analyses of Cu-rich melt and S-rich melt in experiments of the Cu-S system.*

Exp	Temp (°C)	Cu-rich melt			S-rich melt		
		Rh (wt%)	Pd (wt%)	Pt (wt%)	Rh (wt%)	Pd (wt%)	Pt (wt%)
HU442	1200	0.238	0.324	0.265	<0.026	0.024	<0.044
HU443	1200			0.345			<0.031
HU444	1200		0.397			0.053	
HU445	1200	0.384			<0.011		
HU450	1200	0.364	0.241	0.173	<0.017	<0.038	<0.053

5.2.2. Copper - digenite assemblage (1000°C and 800°C)

5.2.2.1. EPMA results

Tables 32 and 33 contain the major element compositions as determined by EPMA of the co-existing copper and digenite equilibrated at 1000°C and 800°C. These compositions are also shown on the phase diagram of the Cu-S system (Figure 15 – pink triangles), where the determined compositions are projected on the Cu-S phase diagram, and can be compared to the expected compositions of the phases according to Chakrabarti and Laughlin (1986).

5.2.2.2. PIXE results

5.2.2.2.1. Milli-PIXE

5.2.2.2.1.1. Results for equilibration at 1000°C

The copper of experiment HU384 was analysed twice, and the analyses were combined with resampling statistics. The copper phase of experiment HU385 was analysed three times, but more counts were collected for the last two, with resulting lower detection limits. The last two analyses were combined with resampling statistics and are used for further discussion. The low Pt content detected in the metal of experiment HU387 and the low Pd content in the metal of experiment HU417 are unusual in comparison with the analyses of the other experiments. The reason for this is unknown.

The lowest detection limit for Pt in digenite of experiment HU382, Rh in digenite of experiment HU384, and Rh, Pd and Pt in digenite of experiment HU385, were used for further discussion. Two analyses were performed on the digenite of experiment HU387, and although the analytical conditions were exactly the same during both analyses, lower detection were obtained from the second analysis, which was used for further discussion. Only a detection limit could be obtained for the Pd in the digenite of experiment HU417, and as only a detection limit is available for Pd in the co-existing metal in this experiment as

well, the results cannot be used for further calculations. The second analysis of the digenite of experiment HU465 was used.

Table 32. *Major element compositions, determined by EPMA, of co-existing copper and digenite equilibrated at 1000°C.*

Exp	Phase	Cu wt% (± 3σ)	S wt% (± 3σ)	Total (wt%)	PGE# (wt%)	n
HU382	Copper	98.63 (0.31)	bd	98.63	~0.7	28
	Digenite	79.25 (0.43)	19.90 (0.16)	99.15	~0.05	30
HU384	Copper	98.52 (0.29)	bd	98.52	~0.9	25
	Digenite	79.38 (0.39)	19.82 (0.19)	99.20	<0.1	34
HU385	Copper	97.79 (0.18)	bd	97.79	~1.7	39
	Digenite	79.35 (0.38)	20.11 (0.18)	99.46	<0.1	38
HU387	Copper	99.55 (0.50)	0.05 (0.06)	99.55	~0.9	22
	Digenite	79.97 (0.30)	20.19 (0.18)	100.16	<0.1	30
HU417	Copper	98.66 (0.26)	bd	98.66	bd	20
	Digenite	78.91 (0.47)	20.34 (0.19)	99.25	bd	22
HU465	Copper	93.63 (0.27)	bd	93.63	~7.9	30
	Digenite	79.53 (0.55)	20.47 (0.31)	100.00	<0.1	35

= Estimation of total PGE content as determined by PIXE, discussed in section 5.2.2.2.

Table 33. *Major element compositions, determined by EPMA, of co-existing copper and digenite equilibrated at 800°C.*

Exp	Phase	Cu wt% (± 3σ)	S wt% (± 3σ)	Total (wt%)	PGE# (wt%)	n
HU482	Copper	99.10 (0.50)	bd	99.10	3.4	24
	Digenite	80.18 (1.17)	19.97 (0.81)	100.15	<0.1	48
HU483	Copper	99.12 (0.70)	bd	99.12	nd	35
	Digenite	79.05 (0.43)	20.35 (0.19)	99.40	nd	38
HU484	Copper	99.98 (0.61)	bd	99.98	nd	63
	Digenite	80.09 (0.69)	20.09 (0.27)	100.18	nd	53
HU485	Copper	99.91 (0.89)	bd	99.91	nd	30
	Digenite	80.08 (0.84)	19.46 (0.95)	99.54	nd	52

= Estimation of total PGE content as determined by PIXE, discussed in section 5.2.2.2.

Table 34. *Milli-PIXE trace element analyses of copper that co-exists with digenite, equilibrated at 1000°C. Values in italics are statistically unreliable.*

Exp	Rh wt% (± 3σ)	Rh LLD	Pd wt% (± 3σ)	Pd LLD	Pt wt% (± 3σ)	Pt LLD	Counts
HU382					0.704 (0.044)	0.024	140000
HU384	0.972 (0.058)	0.053					100000
HU384	0.905 (0.056)	0.057					100000
HU385	0.386 (0.040)	0.048	1.054 (0.063)	0.048	0.590 (0.056)	0.060	100000
HU385	0.465 (0.030)	0.026	0.896 (0.040)	0.040	0.584 (0.042)	0.058	200000
HU385	0.395 (0.027)	0.029	0.741 (0.037)	0.038	0.443 (0.037)	0.041	200000
HU387	0.376 (0.027)	0.025	0.487 (0.031)	0.021	*0.060* (0.036)	0.061	200000
HU417			*0.005* (0.012)	0.023			200000
HU417			bd	0.041			200000
HU465	2.177 (0.070)	0.058	3.691 (0.084)	0.065	2.002 (0.068)	0.064	200000

Table 35. *Milli-PIXE trace element analyses of digenite that co-exists with copper, equilibrated at 1000°C. Values in italics are statistically unreliable.*

Exp	Rh wt% (± 3σ)	Rh LLD	Pd wt% (± 3σ)	Pd LLD	Pt wt% (± 3σ)	Pt LLD	Counts
HU382					bd	0.087	100000
HU382					bd	0.047	200000
HU384	bd	0.028					200000
HU384	bd	0.047					200000
HU384	*0.007* (0.009)	0.016					200000
HU385	*0.014* (0.009)	0.016	bd	0.032	bd	0.052	200000
HU385	bd	0.018	bd	0.028	bd	0.038	300000
HU387	bd	0.023	bd	0.035	bd	0.052	200000
HU387	bd	0.025	0.022 (0.011)	0.016	*0.003* (0.027)	0.049	200000
HU417			*0.012* (0.016)	0.032			200000
HU465	bd	0.026	0.040 (0.011)	0.019	*0.020* (0.022)	0.038	200000
HU465	*0.006* (0.007)	0.013	0.037 (0.009)	0.014	*0.022* (0.021)	0.036	400000

5.2.2.2.1.2. Results for equilibration at 800°C

The second of the two analyses on the digenite of experiment HU482 was used in further calculations.

Table 36. *Milli-PIXE trace element analysis of copper that co-exists with digenite, equilibrated at 800°C.*

Exp	Rh wt% (± 3σ)	Rh LLD	Pd wt% (± 3σ)	Pd LLD	Pt wt% (± 3σ)	Pt LLD	Counts
HU482	1.131 (0.045)	0.038	1.171 (0.047)	0.026	1.143 (0.055)	0.045	200000

Table 37. *Milli-PIXE trace element analyses of the digenite that co-exists with copper, equilibrated at 800°C.*

Exp	Rh wt% (± 3σ)	Rh LLD	Pd wt% (± 3σ)	Pd LLD	Pt wt% (± 3σ)	Pt LLD	Counts
HU482	bd	0.031	bd	0.034	bd	0.048	200000
HU482	0.025 (0.010)	0.013	bd	0.027	bd	0.053	200000

Table 38. *Results of milli-PIXE analyses of the copper - digenite assemblage in experiments of the Cu-S system.*

Exp	Temp (°C)	Copper			Digenite		
		Rh (wt%)	Pd (wt%)	Pt (wt%)	Rh (wt%)	Pd (wt%)	Pt (wt%)
HU382	1000			0.704			<0.047
HU384	1000	0.939			<0.016		
HU385	1000	0.430	0.819	0.514	<0.018	<0.028	<0.038
HU387	1000	0.376	0.487	<0.061	<0.025	0.022	<0.049
HU465	1000	2.177	3.691	2.002	<0.013	0.037	<0.036
HU482	800	1.131	1.171	1.143	0.025	<0.027	<0.053

5.2.2.2.2. Micro-PIXE

5.2.2.2.2.1. Results for equilibration at 1000°C

Table 39. *Micro-PIXE trace element analysis of copper that co-exists with digenite, equilibrated at 1000°C.*

Exp	Rh wt% (± 3σ)	Rh LLD	Pd wt% (± 3σ)	Pd LLD	Pt wt% (± 3σ)	Pt LLD	Charge (nC)
HU385	0.353 (0.014)	0.009	0.600 (0.027)	0.011	0.543 (0.020)	0.032	54

The PGE content in the digenite is so low that no peaks could be detected during a first analysis. The second analysis of this phase was left to collect much more charge, but the Rh peak was still lower than the detection limit. The Pd and Pt peaks were above the detection limits, and will be used for further calculations.

Table 40. *Micro-PIXE trace element analyses of digenite that co-exists with copper, equilibrated at 1000°C. Values in italics are statistically unreliable.*

Exp	Rh wt% (± 3σ)	Rh LLD	Pd wt% (± 3σ)	Pd LLD	Pt wt% (± 3σ)	Pt LLD	Charge (nC)
HU385	bd	bd	*0.001* (0.002)	0.004	bd	bd	165
HU385	*0.0004* (0.0002)	0.0006	0.0009 (0.0003)	0.0007	0.0026 (0.0055)	0.0021	5097

Table 41. *Results of micro-PIXE analyses of the copper - digenite assemblage in experiments of the Cu-S system.*

Exp	Temp (°C)	Copper			Digenite		
		Rh (wt%)	Pd (wt%)	Pt (wt%)	Rh (wt%)	Pd (wt%)	Pt (wt%)
HU385	1000	0.353	0.600	0.543	<0.0006	0.0009	0.0026

5.2.3. Digenite – Cu-S melt assemblage (1000°C)

5.2.3.1. EPMA results

Table 42 presents the major element compositions of co-existing digenite and melt that were equilibrated at 1000°C. The compositions are projected onto the Cu-S phase diagram at 1000°C, and can be compared to the compositions expected from published phase diagrams (Figure 15 – green triangles; Figure 16 – blue and green triangles). The determined compositions of both digenite and melt are very similar, with overlapping error bars as shown on the phase diagram. It is possible that the two phases, which are optically very similar, are closely inter-grown, and that the analysed areas frequently consisted of not only the intended phase but rather a mixture of both phases.

Table 42. *Major element compositions, determined by EPMA, of co-existing melt and digenite equilibrated at 1000°C.*

Exp	Phase	Cu wt% (± 3σ)	S wt% (± 3σ)	Total (wt%)	PGE# (wt%)	n
HU397	Melt	77.34 (0.33)	22.16 (0.14)	99.50	~2.3	19
	Digenite	78.18 (0.44)	22.06 (0.39)	100.24	~0.4	32
HU398	Melt	76.91 (0.38)	21.64 (0.13)	98.55	~4.4	16
	Digenite	78.80 (0.60)	21.54 (0.57)	100.34	~0.8	34
HU411	Melt	76.49 (0.71)	22.95 (0.15)	99.44	~3.5	22
	Digenite	78.24 (0.49)	22.17 (0.40)	100.41	~0.2	54
HU413	Melt	77.86 (0.31)	22.96 (0.12)	100.82	~1.7	7
	Digenite	78.56 (0.32)	22.39 (0.27)	100.95	~0.1	25
HU418	Melt	77.59 (0.50)	22.23 (0.27)	99.82	~0.5	27
	Digenite	78.08 (0.25)	22.53 (0.20)	100.61	<0.1	22
HU420	Melt	77.39 (0.47)	22.64 (0.29)	100.03	~0.2	48
	Digenite	78.23 (0.36)	22.04 (0.32)	100.27	<0.1	26

Estimation of total PGE content as determined by PIXE, discussed in section 5.2.3.2.

5.2.3.1.1. Separated drop

A separated drop, consisting of bright subhedral crystals in a heterogeneous matrix of lower reflectivity, was found with experiment HU397. The longest axis of the drop, shown in Figure 38, is about 3 mm. Experiment HU397, shown in Figure 39, consists of digenite and melt equilibrated at 1000°C. The separated drop differs significantly from the main charge. EPMA analyses (20 spot analyses) were performed on the two phases in the drop to determine the Cu, S, Rh, Pd and Pt contents. Accordingly, the bright crystals contain 13.95 wt% Cu ($1\sigma = 0.16$ wt%), 28.67 wt% S ($1\sigma = 0.30$ wt%), 28.85 wt% Rh ($1\sigma = 0.29$ wt%), and 28.87 wt% Pt ($1\sigma = 0.25$ wt%). This corresponds to 14.24 at% Cu, 57.99 at% S, 18.18 at% Rh and 9.60 at% Pt, with a proposed empirical formula of $Cu(Rh,Pt)_2S_4$. The formula lies between those of malanite ($CuPt_2S_4$) and cuprorhodsite ($CuRh_2S_4$), but due to the Rh:Pt atomic ratio of close to 2:1, would be classified as cuprorhodsite (Rudashevskiy *et al.* 1984; Rudashevskiy *et al.* 1985; Kolonin *et al.*, 1997). The atomic ratio of 2:1 of Rh to Pt corresponds to the ratio in which these elements were added to the experiment. No Pd could be detected in the crystals. The matrix was analysed with 40 µm diameter beam spots in order to compensate for the uneven texture, but the phase is very heterogeneous. According to ten analyses, it consists of 2.67 wt% Pt ($1\sigma = 0.52$ wt%), 15.10 wt% Rh ($1\sigma = 5.41$ wt%), 5.51 wt% Pd ($1\sigma = 1.05$ wt%), 52.22 wt% Cu ($1\sigma = 7.56$ wt%) and 22.47 wt% S ($1\sigma = 0.38$ wt%). If equilibrium was obtained in the drop, this implies that Pt, followed by Rh, and to a lesser extent S, were concentrated in the crystals, while Cu and Pd preferentially remained in the melt.

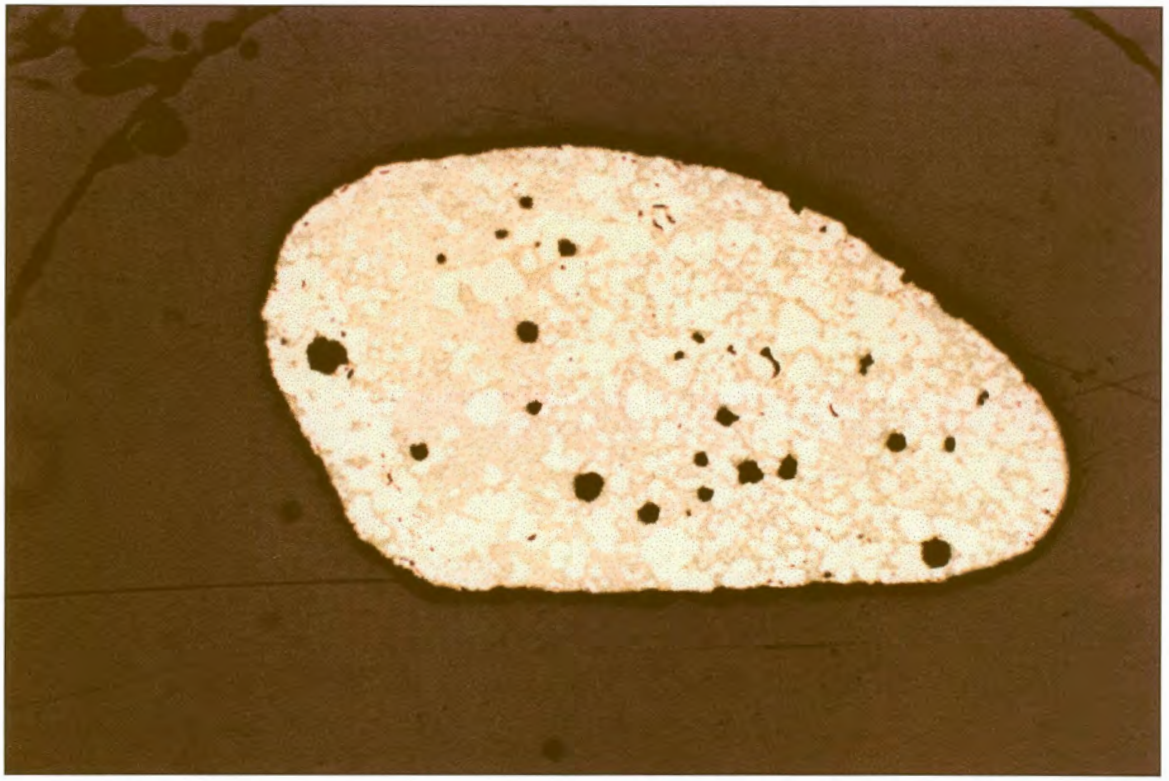

Figure 38. *The separated drop from experiment HU397. Bright subhedral crystals (Cu, S, Rh, Pt) and a highly heterogeneous matrix can be distinguished. Image was digitally enhanced. Field of view 4 mm.*

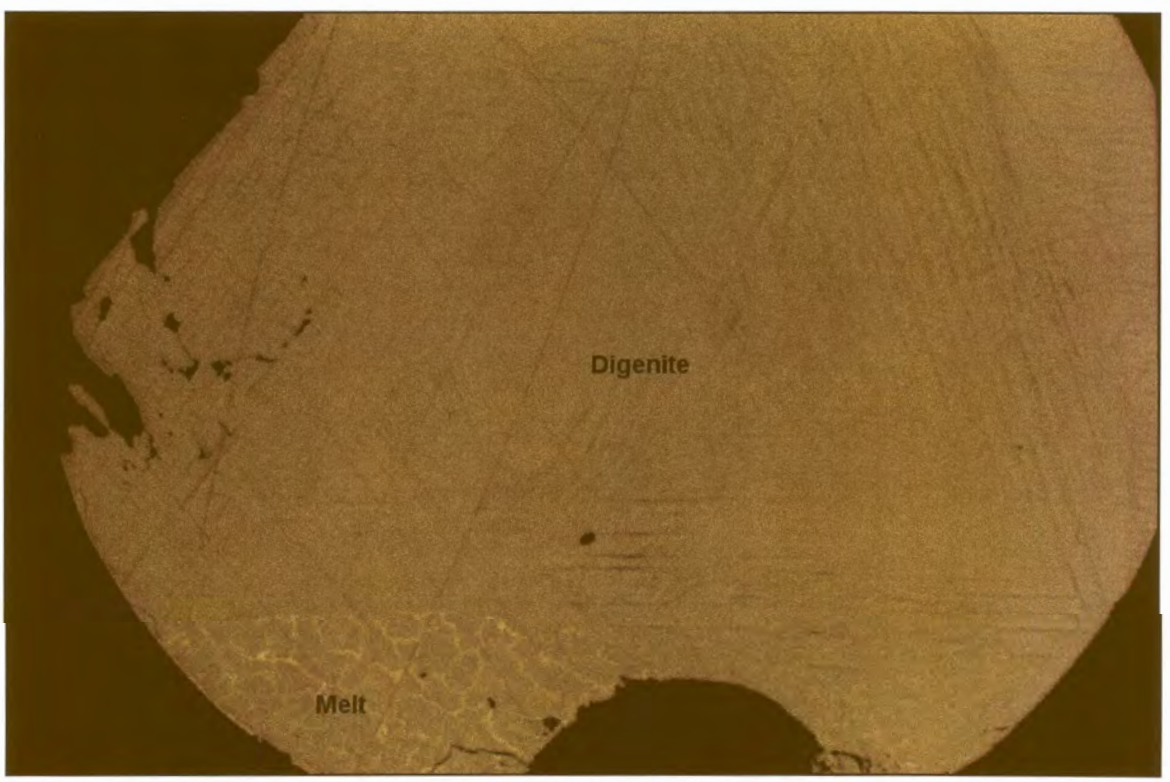

Figure 39. *Experiment HU397 that consists of co-existing digenite and melt. The experiment was equilibrated at 1000°C. Image was digitally enhanced. Field of view 4 mm.*

5.2.3.2. PIXE results

5.2.3.2.1. Micro-PIXE

5.2.3.2.1.1. Results for equilibration at 1000°C

The Rh contents of experiment HU397 in both the digenite and the melt are very low, and Rh was probably concentrated in the separated drop (EPMA results section 5.2.3.1. and Figure 38). Similarly, for experiment HU398, the Rh content in both the digenite and the melt is very low, but no separated drop or separated alloy was found in the experiment.

Table 43. *Micro-PIXE trace element analyses of digenite co-existing with melt, equilibrated at 1000°C.*

Exp	Rh wt% (± 3σ)	Rh LLD	Pd wt% (± 3σ)	Pd LLD	Pt wt% (± 3σ)	Pt LLD	Charge (nC)
HU397	0.004 (0.002)	0.003	0.397 (0.010)	0.004	0.023 (0.008)	0.013	165
HU398	0.015 (0.003)	0.005	0.668 (0.015)	0.006	0.148 (0.016)	0.016	102
HU398	0.014 (0.003)	0.005	0.659 (0.023)	0.006	0.127 (0.008)	0.019	85
HU411	0.051 (0.002)	0.002	0.136 (0.005)	0.003	0.033 (0.005)	0.008	414
HU413	0.021 (0.001)	0.002	0.055 (0.003)	0.002	0.014 (0.005)	0.007	503
HU418					0.043 (0.005)	0.009	307
HU420	0.024 (0.003)	0.003					164

Table 44. *Micro-PIXE trace element analyses of melt co-existing with digenite, equilibrated at 1000°C.*

Exp	Rh wt% (± 3σ)	Rh LLD	Pd wt% (± 3σ)	Pd LLD	Pt wt% (± 3σ)	Pt LLD	Charge (nC)
HU397	0.014 (0.003)	0.005	1.890 (0.020)	0.006	0.393 (0.013)	0.013	150
HU397 (drop)	1.232 (0.018)	0.004	0.145 (0.008)	0.005	1.408 (0.029)	0.008	101
HU398	0.091 (0.008)	0.009	2.645 (0.075)	0.011	1.743 (0.049)	0.025	50
HU411	2.199 (0.034)	0.009	0.548 (0.024)	0.011	0.777 (0.018)	0.020	74
HU413	1.317 (0.034)	0.008	0.159 (0.009)	0.009	0.199 (0.009)	0.019	70
HU418					0.546 (0.014)	0.018	87
HU420	0.234 (0.011)	0.004					108

***Table 45**. Results of micro-PIXE analyses of the digenite - melt assemblage in experiments of the Cu-S system.*

Exp	Temp	Digenite			Melt		
	(°C)	Rh (wt%)	Pd (wt%)	Pt (wt%)	Rh (wt%)	Pd (wt%)	Pt (wt%)
HU397	1000	0.004	0.397	0.023	0.014	1.890	0.393
HU398	1000	0.015	0.664	0.138	0.091	2.645	1.743
HU411	1000	0.051	0.136	0.033	2.199	0.548	0.777
HU413	1000	0.021	0.055	0.014	1.317	0.159	0.199
HU418	1000			0.043			0.546
HU420	1000	0.024			0.234		

5.3 The Fe-S (±O) system

The majority of the quartz tubes containing the Fe-S experiments cracked during heating which led to the frequent oxidation of experiments. This was probably due to poor quality of the quartz glass tubes. Where oxygen was present during equilibration, the system concerned is no longer the Fe-S system but the Fe-S-O system. Oxygen could not be measured with the available EPMA or PIXE instrumentation. Except for a few qualitative SEM analyses, oxygen was not determined. Some of the experiments were severely contaminated with oxygen (mostly those containing the metal-melt assemblage), others contained less oxygen (the pyrrhotite-melt assemblages), while some appeared not to have been contaminated (metal-troilite assemblages). Oxygen was present in the form of oxides in the experiments. The state of oxidation of individual experiments will be discussed.

A number of precautions were taken to prevent oxidation of the experiments. Longer reduction time of the metallic Fe at a variety of temperatures and H_2 pressures before weighing-in showed no decrease in failure rate. Experiments were also pre-reacted at lower temperatures for longer than normal, and the period of equilibration at high temperatures was limited. Resealing of experiments in new tubes as soon as signs of weakening of the glass, with subsequent cracking, became apparent, also did not help. Due to these technical

problems, the Fe-S system could not be investigated comprehensively. Only a few exploratory investigations are reported on.

5.3.1. Iron – Fe-S melt assemblage (1200°C to 1000°C)

5.3.1.1. EPMA results

The major element compositions of the co-existing iron and melt, as determined by EPMA, for the experiments at 1200°C, 1100°C and 1000°C are given in Tables 46 to 48.

Table 46. *Major element compositions, determined by EPMA, of co-existing iron and quenched melt (containing O) equilibrated at 1200°C.*

Exp	Phase	Fe wt% (± 3σ)	S wt% (± 3σ)	Total (wt%)	PGE# (wt%)	n
HU825	Iron	91.92 (1.78)	bd	**91.92	~14.1	30
	Melt	62.05 (1.10)	29.43 (1.41)	*91.48	~0.05	24
HU826	Iron	99.77 (0.36)	bd	99.77	~0.2	20
	Melt	66.21 (2.35)	28.68 (1.89)	*94.89	~0.3	20
HU827	Iron	99.44 (0.30)	bd	99.44	~0.5	20
	Melt	62.55 (0.97)	32.18 (1.03)	*94.73	~0.1	20

\# estimation of total PGE content as determined by PIXE, discussed in section 5.3.1.2.

* very low melt totals indicate presence of oxygen – see text for discussion

** low total due to large Pt content, as analysed by PIXE – see text for discussion

The melt analysis totals in Table 46 are very low. The surfaces of these melts appear tarnished or very badly polished, as is shown for experiment HU825 in Figures 40 and 41, but are not tarnished. Analysis by SEM confirmed that the dull grey material is Fe-oxide. As it was not possible to determine the oxygen content in the melts, it is assumed that the missing weight from the analytical totals is due to the presence of oxygen.

The low Fe total in the metal of experiment HU825 is due to a high Pt content. The large standard deviation of the Fe in the metal indicate that this phase is heterogeneous. EPMA

spot-analyses for Fe and Pt on the metal (14 points) showed that the metal consists of 8.41 wt% Pt (1σ = 1.69) and 87.02 wt% Fe (1σ = 1.73). The metal was also analysed by PIXE (Table 46), and is discussed in the following section. There is a significant difference between the Pt content determined in the metal by EPMA (8.41 wt%) and by PIXE (14.1 wt%). A beam spot with 100 µm diameter was used during PIXE analyses, while a beam spot with 1 µm diameter was used during EPMA analyses (as discussed in Section 4). During EPMA analysis spots were carefully chosen so as to exclude areas which appeared oxidised, while during PIXE analysis this was not possible, and oxidised areas were also analysed. It is possible that the Pt content in these bulk areas is higher than in the oxygen-free areas. The PIXE analyses provide a better estimation of the average PGE content in the metal phase than the EPMA analyses.

Table 47. *Major element compositions, determined by EPMA, of co-existing iron and quenched melt (possibly coexisting with oxides), equilibrated at 1100°C.*

Exp	Phase	Fe wt% (± 3σ)	S wt% (± 3σ)	Total (wt%)	PGE# (wt%)	n
HU734	Iron	100.34 (0.27)	bd	100.34	~0.2	18
	Melt	68.07 (0.95)	31.66 (0.74)	*99.73	bd	22
HU735	Iron	100.15 (0.33)	bd	100.15	~0.1	18
	Melt	65.80 (0.68)	32.46 (0.45)	*98.26	~0.2	20
HU736	Iron	100.10 (0.19)	bd	100.10	~0.1	20
	Melt	68.19 (1.12)	31.46 (0.99)	*99.65	~0.1	26

estimation of total PGE content as determined by PIXE, discussed in section 5.3.1.2.

* low melt totals indicate presence of oxygen – see text for discussion

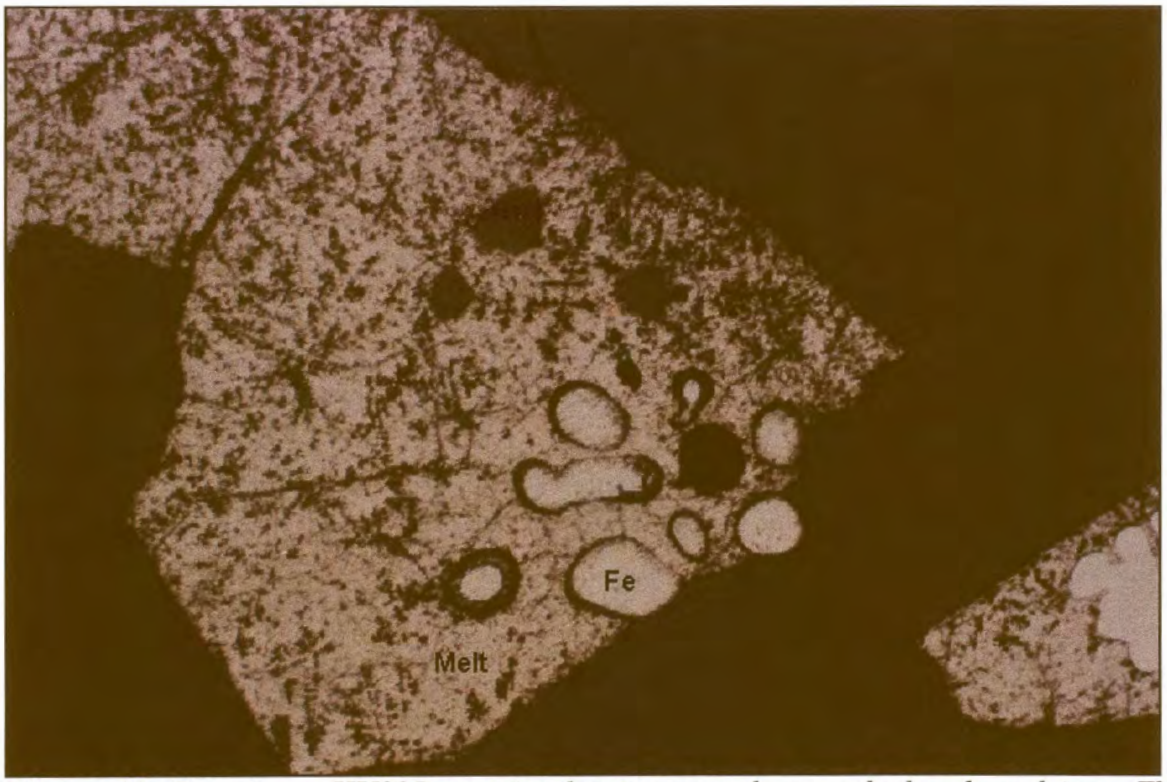

Figure 40. *Experiment HU825 contains heterogeneously quenched melt and iron. The appearance of the melt is unusual. The long side of the photograph is 4 mm long.*

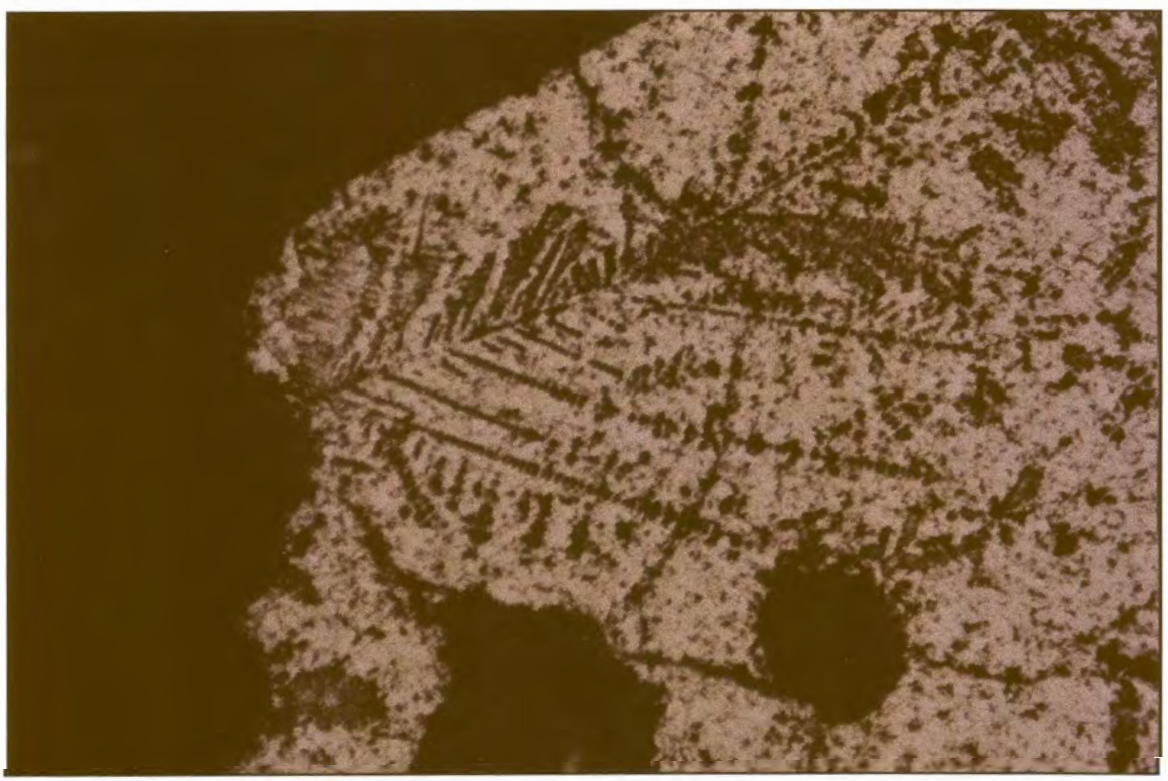

Figure 41. *Enlargement of the dendrites of experiment HU825, shown in Figure 40. The dull grey dendrites were determined by electron microscopy to have high contents of Fe-oxide along with Fe. Field of view 1.4 mm.*

The melt phases of the 1100°C experiments (Table 47 - experiments HU734, HU735 and HU736) apparently contain small amounts of oxygen, but the metals appear to be free of oxygen.

All five of the experiments for which data is presented in Table 41 were exposed to oxygen to some degree. The metal phases of experiments HU843 and HU845, and especially HU844, all contain oxides as inclusions (see Figures 42, 43, 44 and 45). These were avoided during EPMA analyses, and therefore are not clearly reflected in the totals of experiments HU843 and HU845. The metal phases of experiment HU844 (Figures 44 and 45) are so diluted by oxides that it was very difficult to find positions for analysis that did not contain oxides. The low total of the metal in experiment HU844 reflects the interference from oxide. The metals of experiments HU849 and HU850 were analysed separately by EPMA for PGE. The metal of experiment HU849 was found to contain 6.30 wt% Pt (1σ = 1.56 wt%), 3.82 wt% Rh (1σ = 0.59 wt%) and no detectable Pd. During PIXE analysis, the oxides in the metal could not be avoided, and much lower PGE contents were determined. The Pt and Rh could be more concentrated in the oxide-free areas of the metal. The metal of experiment HU850 contains about 0.13 wt% Pt (1σ = 0.06 wt%), 1.11 wt% Rh (1σ = 0.09 wt%) and no detectable Pd. Apparently the oxygen formed separate Fe oxides in the metal phase, but it is unclear whether Fe oxides were formed in the melt, or if the oxygen was incorporated into the structure of the sulphide melt.

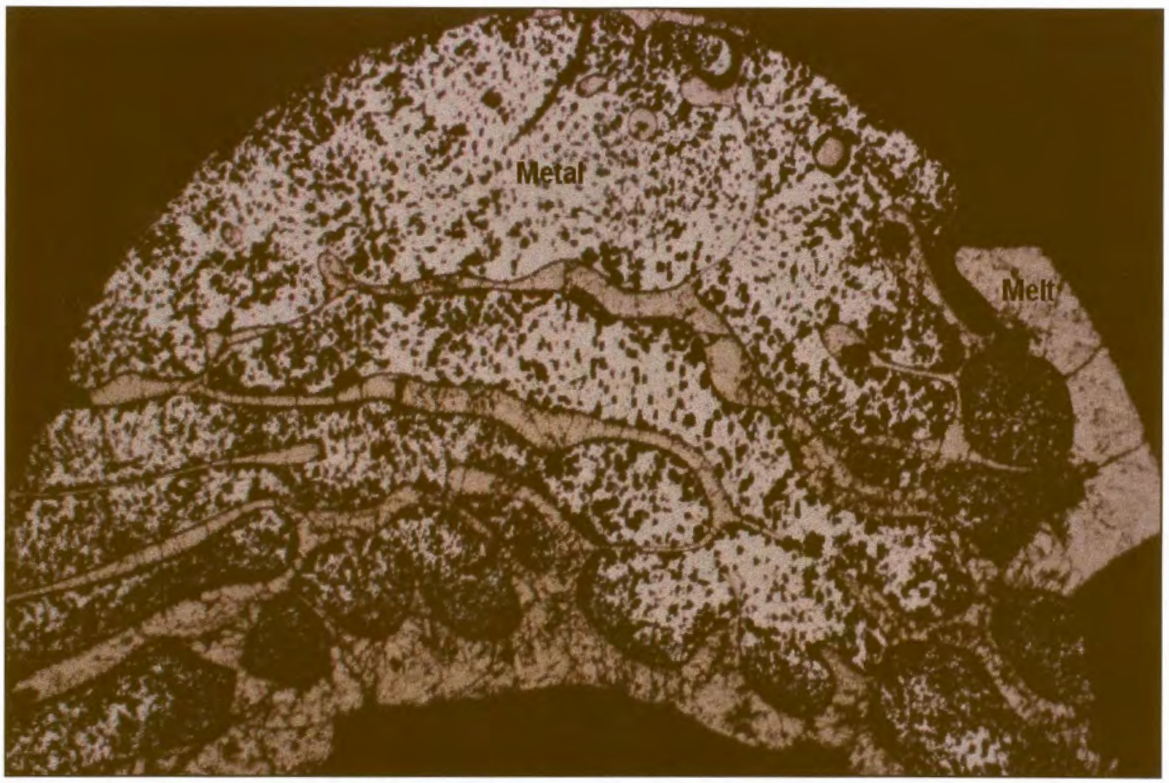

Figure 42. *Experiment HU845 contains metal and melt that were equilibrated at 1000°C. Both phases contain Fe oxides (grey inclusions). Field of view 4 mm.*

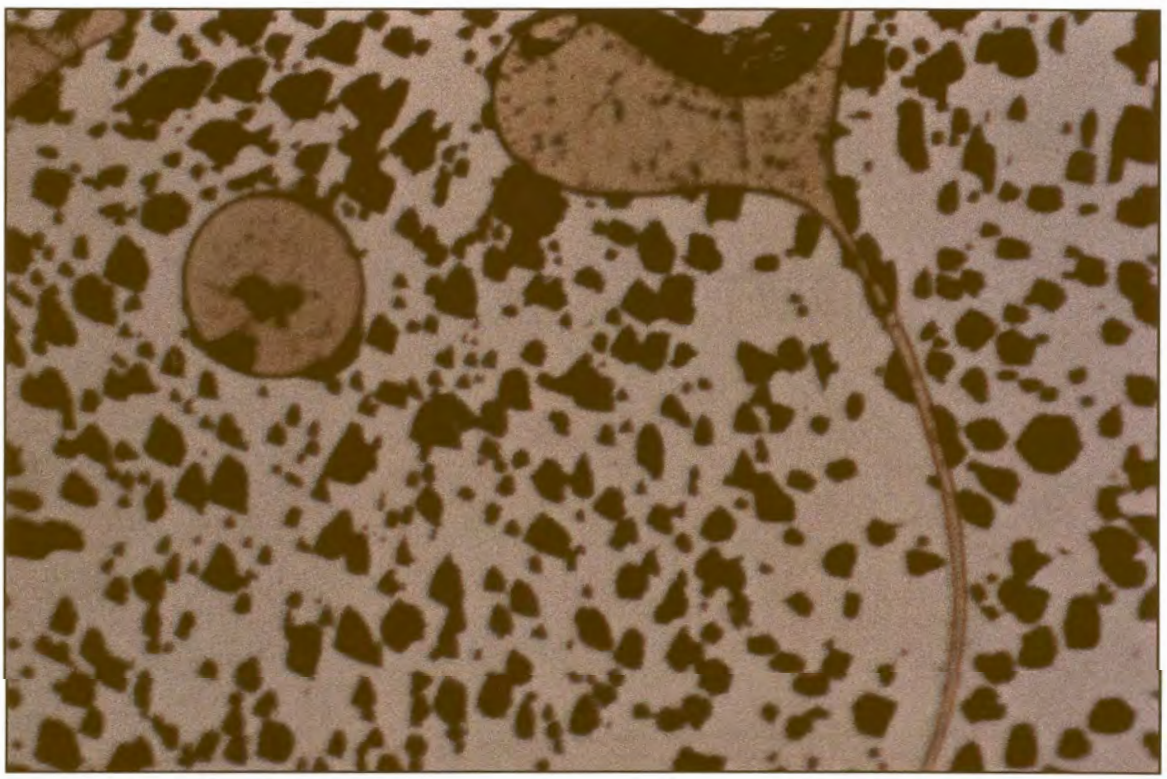

Figure 43. *Enlargement of the metal and melt phases of experiment HU845 shown in Figure 42. The grey oxides are scattered through the metal. Field of view 0.6 mm.*

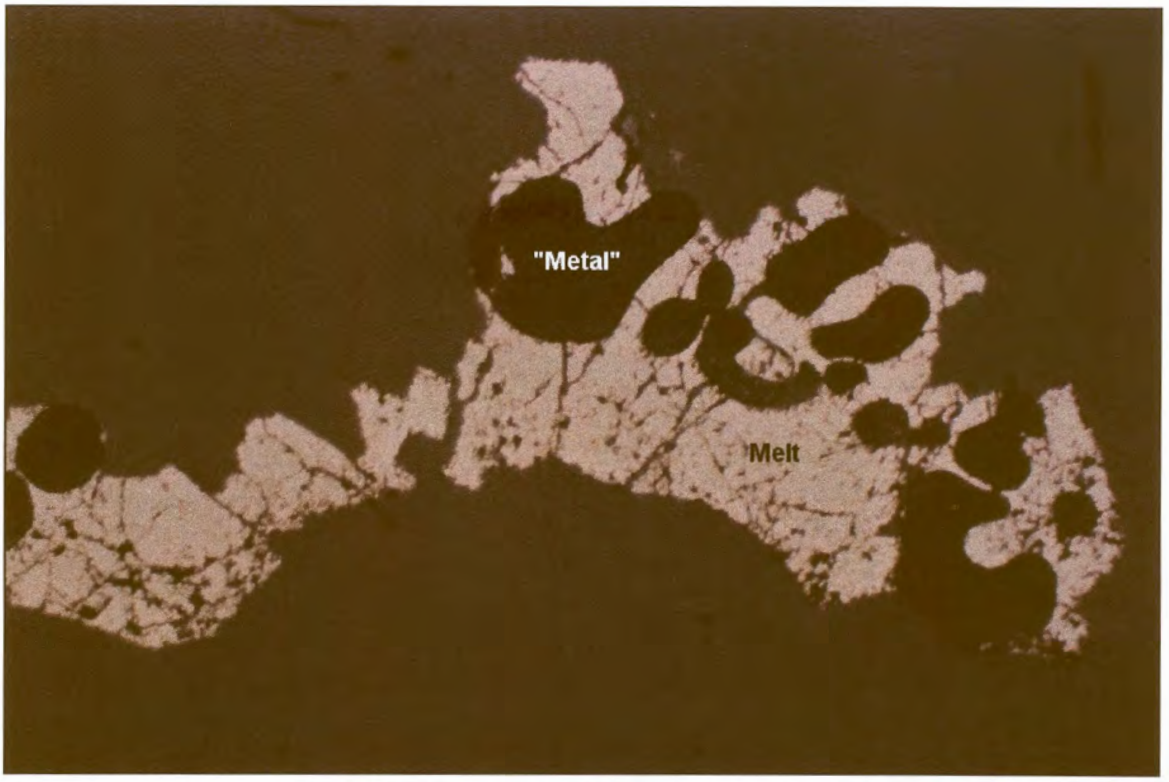

Figure 44. *Experiment HU844 should have contained metal and melt that were equilibrated at 1000°C. The "metal" phase is unrecognisable due to the low reflectivity oxides scattered all through it. Field of view 4 mm.*

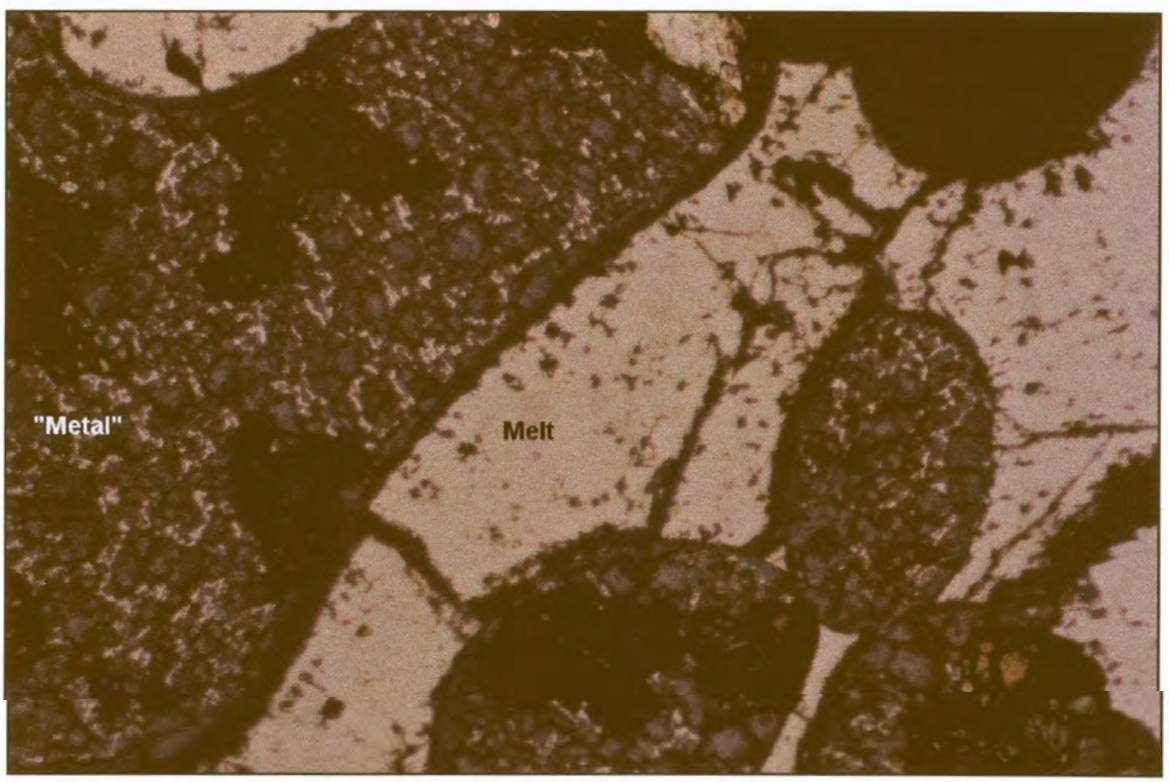

Figure 45. *Higher magnification of the "metal" phase of experiment HU844, in Figure 44. Large Fe-oxide crystals imply late stage oxidation. Field of view 0.6 mm.*

Table 48. *Major element compositions, determined by EPMA, of co-existing iron and quenched melt equilibrated at 1000°C. Some of the metal contains oxides, and some of the sulphide melts oxygen, which influenced the analyses.*

Exp	Phase	Fe wt% (± 3σ)	S wt% (± 3σ)	Total (wt%)	PGE# (wt%)	n
HU843	Iron	99.72 (0.32)	bd	99.72	~0.4	20
	Melt	63.09 (0.70)	35.42 (0.83)	*98.51	~0.3	20
HU844	Iron	60.47 (5.97)	1.71 (0.64)	*62.18	~0.1	30
	Melt	63.08 (0.56)	34.19 (1.01)	*97.27	<0.06	48
HU845	Iron	99.47 (0.34)	bd	99.47	~0.3	20
	Melt	62.81 (0.38)	34.05 (1.09)	*96.86	~0.1	40
HU849	Iron	89.29 (1.64)	bd	*89.29	~0.1	20
	Melt	63.90 (0.34)	33.50 (0.64)	*97.40	<0.1	25
HU850	Iron	97.78 (0.53)	bd	*97.78	~1.2	26
	Melt	65.23 (1.01)	33.00 (1.46)	*98.23	~0.3	26

\# estimation of total PGE content as determined by PIXE, discussed in section 5.3.1.2.

* low totals indicate presence of oxygen – see text for discussion

The compositions of all the experiments that contained the iron – melt assemblage were projected onto the Fe-S phase diagram (after Chuang *et al.*, 1985), ignoring the presence of oxygen and PGE (Figure 24 – blue triangles). From this projection it is clear that the experiments cannot be projected onto the binary phase diagram and contain significant amounts of at least one additional element.

5.3.1.2. PIXE results

5.3.1.2.1. Milli-PIXE

5.3.1.2.1.1. Results for equilibration at 1200°C

Two analyses were performed on the "iron" of experiment HU825, and the average as determined with resampling was used in further discussion (Table 55). The second analysis of the iron of experiment HU826 was used.

Table 49. *Milli-PIXE trace element analyses of the metal that co-exists with melt in the Fe – S ± O system, equilibrated at 1200°C.*

Exp	Rh wt% (± 3σ)	Rh LLD	Pd wt% (± 3σ)	Pd LLD	Pt wt% (± 3σ)	Pt LLD	Counts
HU825					13.49 (0.19)	0.12	500000
HU825					14.70 (0.24)	0.12	500000
HU826			bd	0.20			500000
HU826			0.22 (0.07)	0.10			500000
HU827	0.47 (0.09)	0.10					500000

Pt was detected in the second analysis of the melt of experiment HU825. The average Pd content as determined with resampling statistics from two analyses performed on the melt of experiment HU826 was used, and similarly the average Rh content of the two analyses on the melt of experiment HU827 (Table 55).

Table 50. *Milli-PIXE trace element analyses of the melt that co-exists with metal in the Fe – S ±O system, equilibrated at 1200°C.*

Exp	Rh wt% (± 3σ)	Rh LLD	Pd wt% (± 3σ)	Pd LLD	Pt wt% (± 3σ)	Pt LLD	Counts
HU825					*0.04* (0.03)	0.05	500000
HU825					0.06 (0.03)	0.05	500000
HU826			0.21(0.05)	0.06			500000
HU826			0.28 (0.07)	0.10			500000
HU827	0.09 (0.05)	0.07					500000
HU827	0.14 (0.06)	0.10					500000

5.3.1.2.1.2. Results for equilibration at 1100°C

In both analyses of the metal of experiment HU734 Pt was below detection, and the lowest detection limit was used. The Pd content of the first analysis on the metal of experiment HU735 was below detection, and the second analysis was used.

Table 51. *Milli-PIXE trace element analyses of the metal that co-exists with melt in the Fe – S ± O system, equilibrated at 1100°C.*

Exp	Rh wt% (± 3σ)	Rh LLD	Pd wt% (± 3σ)	Pd LLD	Pt wt% (± 3σ)	Pt LLD	Counts
HU734					bd	0.15	500000
HU734					bd	0.30	500000
HU735			*0.04* (0.05)	0.09			500000
HU735			0.16 (0.06)	0.11			500000
HU736	0.12 (0.05)	0.08					500000

The Pt content in the melt of experiment HU734 was below the detection limit. The first analysis on the melt of experiment HU736 could not detect any Rh and therefore the second analysis is used (Table 55).

Table 52. *Milli-PIXE trace element analyses of the melt that co-exists with metal in the Fe - S ± O system, equilibrated at 1100°C.*

Exp	Rh wt% (± 3σ)	Rh LLD	Pd wt% (± 3σ)	Pd LLD	Pt wt% (± 3σ)	Pt LLD	Counts
HU734					0.04 (0.03)	0.05	500000
HU735			0.21 (0.07)	0.12			500000
HU736	0.05 (0.04)	0.07					500000
HU736	0.13 (0.06)	0.10					500000

5.3.1.2.1.3. Results for equilibration at 1000°C

The average Pd content of the two analyses on the metal of experiment HU843, and the average Rh content of two analyses on the metal of experiment HU844, were determined with resampling statistics. The average Rh content and the average Pd content of the two analyses on the metal of experiment HU845 were determined with resampling statistics, and the lowest detection limit for Pt was used. Of the three analyses performed on the metal of experiment HU849, the average Rh content of the first two was determined with resampling statistics, the lowest Pd detection limit was used, and the Pt content in the second analysis

was used. For the melt of experiment HU850, the average Rh and Pd contents were determined. The average of the Pt analyses was also determined, although the first analysis is statistically unreliable. Values used for further calculations are provided in Table 55.

***Table 53**. Milli-PIXE trace element analyses of the metal that co-exists with melt in the Fe-S (±O) system, equilibrated at 1000°C.*

Exp	Rh wt% (± 3σ)	Rh LLD	Pd wt% (± 3σ)	Pd LLD	Pt wt% (± 3σ)	Pt LLD	Counts
HU843			0.57 (0.10)	0.07			500000
HU843			0.30 (0.07)	0.09			500000
HU844	0.13 (0.05)	0.07					500000
HU844	0.10 (0.03)	0.03					500000
HU845	0.21 (0.05)	0.06	0.10 (0.04)	0.06	*0.02* (0.04)	0.07	500000
HU845	0.17 (0.05)	0.07	0.19 (0.06)	0.10	*0.02* (0.04)	0.08	500000
HU849	0.09 (0.02)	0.02	*0.01* (0.02)	0.04	*0.06* (0.04)	0.08	500000
HU849	0.13 (0.04)	0.05	*0.06* (0.04)	0.07	0.09 (0.04)	0.07	500000
HU849	bd	0.16	bd	0.10	*0.06* (0.05)	0.08	500000
HU850	0.73 (0.09)	0.11	0.53 (0.09)	0.14	*0.08* (0.05)	0.08	500000
HU850	0.84 (0.12)	0.13	0.21 (0.09)	0.14	0.14 (0.06)	0.09	500000

The Pd content of the two analyses on the melt of experiment HU843 was averaged. In all three of the analyses on the melt of experiment HU844, Rh was below detection. All PGE were below detection in the melt of experiment HU845. Similarly, no PGE could be detected during the two analyses on the melt of experiment HU849. Of the two analyses on the melt of experiment HU850, the values for Rh and Pd from the second analysis was used. Pt was only observed above the detection limit in the first analysis, and this value will be used.

Table 54. *Milli-PIXE trace element analyses of the melt that co-exists with metal in the Fe-S (±O) system, equilibrated at 1000°C.*

Exp	Rh wt% (± 3σ)	Rh LLD	Pd wt% (± 3σ)	Pd LLD	Pt wt% (± 3σ)	Pt LLD	Counts
HU843			0.22 (0.07)	0.07			500000
HU843			0.31(0.09)	0.10			500000
HU844	*0.02* (0.03)	0.06					500000
HU844	*0.03* (0.04)	0.07					500000
HU844	bd	0.07					500000
HU845	bd	0.12	*0.07* (0.07)	0.13	*0.03* (0.04)	0.07	500000
HU845	bd	0.09	*0.09* (0.07)	0.13	*0.03* (0.03)	0.05	500000
HU849	*0.04* (0.03)	0.05	bd	0.13	bd	0.08	500000
HU849	bd	0.12	*0.08* (0.07)	0.12	bd	0.08	500000
HU850	bd	0.13	0.14 (0.07)	0.10	0.08 (0.03)	0.05	500000
HU850	0.12 (0.05)	0.06	0.24 (0.08)	0.13	*0.04* (0.04)	0.06	500000

Table 55. *Results of milli-PIXE analyses of the iron - sulphide melt assemblage in experiments of the Fe - S system.*

Exp	Temp (°C)	Iron			Sulphide melt		
		Rh (wt%)	Pd (wt%)	Pt (wt%)	Rh (wt%)	Pd (wt%)	Pt (wt%)
HU825	1200			14.10			0.06
HU826	1200		0.22			0.25	
HU827	1200	0.47			0.11		
HU734	1100			<0.15			<0.05
HU735	1100		0.16			0.21	
HU736	1100	0.12			0.13		
HU843	1000		0.44			0.27	
HU844	1000	0.12			<0.06		
HU845	1000	0.19	0.15	<0.07	<0.09	<0.13	<0.05
HU849	1000	0.11	<0.04	0.09	<0.05	<0.12	<0.08
HU850	1000	0.78	0.37	0.11	0.12	0.24	0.08

5.3.2. Pyrrhotite – Fe-S melt assemblage (1100°C)

5.3.2.1. EPMA results

The major element compositions of the co-existing pyrrhotite and melt in the experiments equilibrated at 1100°C, determined by EPMA, are given in Table 56. These compositions are also indicated on the Fe-S phase diagram (Figure 24 – green triangles). The compositions of the melt and pyrrhotite determined by EPMA do not plot at opposite sides of the original bulk experimental composition (Figure 24). This indicates that at least one more element influences the major elemnt compositions, possibly oxygen, even though the material does not look oxidised, and the totals from the EPMA analyses approach 100 %.

Table 56. *Major element compositions, determined by EPMA, of co-existing pyrrhotite and quenched melt equilibrated at 1100°C.*

Exp	Phase	Fe wt% (± 3σ)	S wt% (± 3σ)	Total (wt%)	PGE# (wt%)	n
HU737	Melt	64.06 (0.34)	35.38 (0.41)	99.44	~0.2	14
	Pyrrhotite	62.87 (0.11)	37.77 (0.12)	100.64	<0.04	18
HU738	Melt	63.95 (0.38)	34.81 (0.25)	98.76	~0.2	30
	Pyrrhotite	62.79 (0.11)	37.65 (0.17)	100.44	<0.02	20
HU739	Melt	64.54 (0.34)	35.33 (0.41)	99.87	~0.1	22
	Pyrrhotite	62.69 (0.13)	37.26 (0.18)	99.95	<0.03	19

estimation of total PGE content as determined by PIXE, discussed in section 5.3.2.2.

5.3.2.2. PIXE results

5.3.2.2.1. Milli-PIXE

Two analyses were performed on each of the melt phases, and the averages were determined with resampling statistics. Pt was below detection for both analyses of the pyrrhotite of experiment HU737 (Table 58), Pd was below detection in both analyses of the

pyrrhotite of experiment HU738, and the Rh content in both analyses of the pyrrhotite of experiment HU739 was below detection limits.

Table 57. *Milli-PIXE trace element analyses of the melt that co-exists with pyrrhotite in the Fe-S system, equilibrated at 1100°C.*

Exp	Rh wt% (± 3σ)	Rh LLD	Pd wt% (± 3σ)	Pd LLD	Pt wt% (± 3σ)	Pt LLD	Counts
HU737					0.14 (0.02)	0.03	500000
HU737					0.15 (0.02)	0.03	500000
HU738			0.21 (0.03)	0.03			500000
HU738			0.21 (0.03)	0.03			500000
HU739	0.13 (0.03)	0.04					500000
HU739	0.09 (0.02)	0.03					500000

Table 58. *Milli-PIXE trace element analyses of the pyrrhotite that co-exists with melt in the Fe-S system, equilibrated at 1100°C.*

Exp	Rh wt% (± 3σ)	Rh LLD	Pd wt% (± 3σ)	Pd LLD	Pt wt% (± 3σ)	Pt LLD	Counts
HU737					0.02 (0.02)	0.04	500000
HU737					bd	0.04	500000
HU738			0.02 (0.02)	0.03			500000
HU738			0.01 (0.01)	0.02			500000
HU739	0.01 (0.01)	0.03					500000
HU739	0.01 (0.02)	0.03					500000

Table 59. *Results of milli-PIXE analyses of the melt-pyrrhotite assemblage in experiments of the Fe-S system.*

Exp	Temp (°C)	Melt			Pyrrhotite		
		Rh (wt%)	Pd (wt%)	Pt (wt%)	Rh (wt%)	Pd (wt%)	Pt (wt%)
HU737	1100			0.15			<0.04
HU738	1100		0.21			<0.02	
HU739	1100	0.11			<0.03		

5.3.3. Iron - troilite assemblage (900°C)

5.3.3.1. EPMA results

The major element compositions of co-existing iron and troilite in experiments equilibrated at 900°C, determined by EPMA, are given in Table 60. The compositions are also shown on the phase diagram of the Fe-S system (Figure 24 – pink triangles). There is no evidence that these experiments were contaminated by oxygen.

Table 60. *Major element compositions, determined by EPMA, of co-existing iron and troilite equilibrated at 900°C.*

Exp	Phase	Fe wt% (± 3σ)	S wt% (± 3σ)	Total (wt%)	PGE# (wt%)	n
HU434	Iron	99.53 (0.44)	-	99.53	~0.1	26
	Troilite	63.03 (0.45)	37.09 (0.20)	100.12	<0.05	30
HU435	Iron	99.89 (0.52)	-	99.89	<0.28	25
	Troilite	62.84 (0.25)	36.74 (0.33)	99.58	<0.89	28
HU436	Iron	99.60 (0.66)	-	99.60	~0.2	28
	Troilite	62.62 (0.37)	37.11 (0.30)	99.73	<0.08	28
HU756	Iron	100.50 (0.27)	-	100.50	~0.3	30
	Troilite	63.10 (0.17)	37.07 (0.17)	100.17	~0.1	30

Estimation of total PGE content as determined by PIXE, discussed in section 5.3.3.2.

5.3.3.2. PIXE results

5.3.3.2.1. Milli-PIXE

5.3.3.2.1.1. Results for equilibration at 900°C

In the three analyses of the iron of experiment HU756, Rh was detected in the first two, and the average as determined with resampling statistics was used. Pd could also be detected in two of the analyses, and although the two results vary a lot, the average determined with

resampling statistics was used. The detection limit for Pt was low enough in only the last analysis to allow observation of Pt.

Table 61. *Milli-PIXE trace element analyses of iron that co-exists with troilite in the Fe-S system, equilibrated at 900°C.*

Exp	Rh wt% (± 3σ)	Rh LLD	Pd wt% (± 3σ)	Pd LLD	Pt wt% (± 3σ)	Pt LLD	Counts
HU434					bd	0.09	500000
HU434					0.14 (0.04)	0.06	500000
HU435			bd	0.28			500000
HU435			bd	1.54			500000
HU436	0.17 (0.06)	0.11					500000
HU436	*0.02* (0.05)	0.10					500000
HU756	0.13 (0.04)	0.06	*0.05* (0.04)	0.08	*0.05* (0.05)	0.08	500000
HU756	0.14 (0.04)	0.06	0.21 (0.06)	0.11	*0.01* (0.05)	0.09	500000
HU756	bd	0.07	0.10 (0.04)	0.04	0.08 (0.02)	0.04	500000

Table 62. *Milli-PIXE trace element analyses of the troilite that co-exists with metal in the Fe-S system, equilibrated at 900°C.*

Exp	Rh wt% (± 3σ)	Rh LLD	Pd wt% (± 3σ)	Pd LLD	Pt wt% (± 3σ)	Pt LLD	Counts
HU434					bd	0.05	500000
HU434					bd	0.05	500000
HU435			0.72 (0.53)	0.89			500000
HU435			1.95 (1.34)	2.27			500000
HU436	bd	0.08					500000
HU436	bd	0.10					500000
HU756	bd	0.04	0.04 (0.04)	0.07	bd	0.05	500000
HU756	bd	0.04	0.14 (0.03)	0.04	bd	0.05	500000

No Pt was detected in the two analyses of the troilite of experiment HU434 (Table 62), and the detection limit was used. The detection limits during both analyses of the troilite of

experiment HU435 were very high, and no Pd could be detected. The lowest Rh detection limit from the two analyses of the troilite of experiment HU436 was used. Two analyses were performed of the troilite of experiment HU756, and in both cases Rh was below detection limits. Pd was detected in the second analysis, but Pt could not be detected in either analyses. Values used in further calculations are shown in Table 63.

Table 63. *Results of milli-PIXE analyses of the iron-troilite assemblage in experiments of the Fe-S system.*

Exp	Temp	Iron			Troilite		
	(°C)	Rh (wt%)	Pd (wt%)	Pt (wt%)	Rh (wt%)	Pd (wt%)	Pt (wt%)
HU434	900			0.14			<0.05
HU435	900		<0.28			<0.89	
HU436	900	0.17			<0.08		
HU756	900	0.14	0.16	0.08	<0.04	0.14	<0.05

6. Discussion

It is obvious from the information obtained from EPMA, milli-PIXE, and micro-PIXE analyses (Section 5) that different analytical methods and different instruments show different concentrations for the same element in a phase. This problem was addressed by Franklyn and Merkle (1999) and Merkle *et al.* (in print). However, if the same element is successively analysed in two co-existing phases utilising the same instrument, and the ratio of these results is calculated, the instrumental influence on these results should be cancelled out or limited. In the present investigation, the partitioning of the three PGE Rh, Pd and Pt is examined between phases in the three systems Ni-S, Cu-S and Fe-S(±O), using Nernst partition coefficients (D).

6.1. The Ni-S system

6.1.1. Nickel – Ni-S melt assemblage (1100°C - 700°C)

Nernst partition coefficient: D = (PGE content in metal) / (PGE content in melt).

D were calculated from the micro-PIXE and milli-PIXE analyses discussed in section 5.1.1.2. (Tables 20 and 27). The ratios were obtained with resampling statistics (as discussed in section 4.3.), which made it possible to determine confidence intervals for the ratios. Tables 64 and 65 contain the D calculated separately for milli-PIXE and micro-PIXE results. These values vary a lot for the three elements between the two Tables (or two PIXE instruments), and also vary according to equilibration temperatures, PGE contents, and possibly the presence or absence of other PGE in the systems. The influence of these factors on the partition coefficients will be discussed below.

Table 64. *D (metal/melt) for the PGE determined for Ni metal and melt assemblages from the milli-PIXE results in Table 20.*

Exp	Temp (°C)	PGE (ppm)	D_{Rh} (± 1σ)	D_{Pd} (± 1σ)	D_{Pt} (± 1σ)
HU733	1100	500	1.6 (0.3)	0.5 (0.1)	4.1 (0.7)
HU731	1100	2000			4.8 (0.8)
HU393	1000	1000	2.8 (0.1)	0.6 (0.04)	23.2 (5.5)
HU381	1000	2000	4.0 (0.5)	0.7 (0.1)	26.7 (4.5)
HU753	900	1000	4.2 (0.5)	0.8 (0.1)	>14.4
HU429	900	2000	5.5 (0.3)	0.6 (0.03)	>26.8
HU427	900	2000		0.9 (0.03)	
HU469	700	500	5.5 (0.5)	0.5 (0.1)	>4.9
HU471	700	2000			>25.8
HU473	700	2000	9.9 (1.5)		

Table 65. *D (metal/melt) for the PGE determined for Ni metal and melt assemblages from the micro-PIXE results in Table 27.*

Exp	Temp (°C)	PGE (ppm)	D_{Rh} (± 1σ)	D_{Pd} (± 1σ)	D_{Pt} (± 1σ)
HU441	1100	2000	2.7 (0.1)	0.5 (0.02)	19.9 (1.0)
HU437	1100	2000		0.7 (0.03)	
HU393	1000	1000	4.7 (0.1)	0.8 (0.03)	49.3 (3.4)
HU394	1000	6000	4.4 (0.07)	0.6 (0.01)	45.6 (2.4)
HU395	1000	10000	3.9 (0.05)	0.6 (0.01)	56.2 (1.0)
HU412	1000	10000	3.8 (0.1)	0.7 (0.01)	44.7 (1.3)
HU392	1000	?	7.1 (0.1)	0.9 (0.1)	219 (29)
HU429	900	2000	5.3 (0.1)	0.7 (0.01)	84 (8)
HU426	900	2000			97 (34)
HU427	900	2000		0.7 (0.02)	
HU428	900	2000	5.4 (0.1)		

? = discussed in text, section 5.1.1.1. (separated drop with unplanned composition)

6.1.1.1. Variation of partition coefficients with different instruments

Only experiments HU393, HU427 and HU429 were investigated by both micro- and milli-PIXE, and can be used to compare results from the two instruments. For experiment HU393 D_{Rh} (4.7) and D_{Pt} (49.1) from micro-PIXE analyses are almost twice those from milli-PIXE analyses: D_{Rh} (2.8) and D_{Pt} (22.6). D_{Pd} varies from 0.8 from micro-PIXE to 0.6 from milli-PIXE analyses. This might imply higher sensitivity of the milli-PIXE for PGE in the metal phase, or lower PGE sensitivity in the melt phase. The partition coefficients for experiment HU429 compare better. D_{Rh} varies from 5.5 to 5.3 and D_{Pd} from 0.6 to 0.7. The micro-PIXE value for D_{Pt} is 84 (Table 65), while the milli-PIXE value (Table 64) is > 26.8. The D_{Pd} values for experiment HU427 are 0.7 and 0.9 respectively.

In order to get a clearer indication of the difference in sensitivities between the instruments, the determined PGE contents for the separate phases are shown in Table 66, where the results from milli- and micro-PIXE can be compared directly. The PGE content determined for each phase by milli-PIXE was plotted against the PGE content determined for the same phase by micro-PIXE (Figure 46). From Figure 46 it becomes apparent that at higher concentrations analysed, Pd is over-represented by the milli-PIXE analyses compared to the micro-PIXE analyses, which is not the case at lower Pd concentrations. As a result, the Pd ratio, which was determined in this system by dividing the lower concentration by the higher concentration, would be somewhat lower for milli-PIXE – as was seen to be the case. Pt, on the other hand, is slightly over-represented in the micro-PIXE analysis. When the higher Pt ratio is determined by dividing the higher concentration by the lower concentration, a too-high ratio will be obtained, as was observed in the present situation.

Table 66. *PGE contents in nickel and sulphide melt determined by both milli- and micro-PIXE.*

Exp		Milli-PIXE			Micro-PIXE		
		Rh wt% (± 3σ)	Pd wt% (± 3σ)	Pt wt% (± 3σ)	Rh wt% (± 3σ)	Pd wt% (± 3σ)	Pt wt% (± 3σ)
HU393	Nickel	0.391(0.024)	0.111(0.020)	0.555(0.026)	0.349(0.014)	0.096(0.013)	0.737(0.025)
	Melt	0.141(0.014)	0.184(0.017)	0.025(0.015)	0.075(0.002)	0.124(0.003)	0.015(0.001)
HU427	Nickel		0.304(0.023)			0.159(0.008)	
	Melt		0.352(0.026)			0.215(0.008)	
HU429	Nickel	0.737(0.032)	0.219(0.023)	0.778(0.029)	0.606(0.020)	0.151(0.009)	0.919(0.020)
	Melt	0.134(0.017)	0.344(0.024)	*0.006*(0.016)	0.115(0.004)	0.225(0.004)	0.011(0.002)

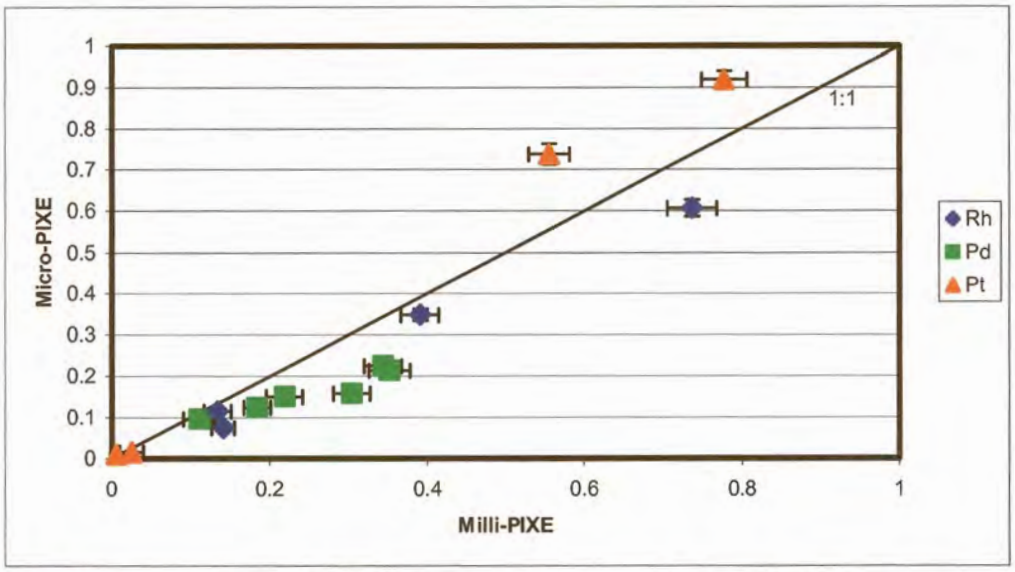

Figure 46. *Comparison of PGE contents determined by milli-PIXE and micro-PIXE in corresponding phases from experiments HU393, HU427 and HU429. Error bars show 3σ standard deviations.*

An alternative explanation could be the influence of the two different software packages (GUPIX and GEOPIXE) used to analyse the spectra from the two instruments, and the deviations in D could be software-related. In a recent study of Pt-Pd-Ni-S phases (Merkle *et al.*, in print), EPMA results and milli-PIXE results using GUPIX were comparable. However, the results from GEOPIXE analyses of the spectra differed significantly (R. Merkle, personal communications). The effect of different software packages used to

interpret spectra would probably vary with the composition of the matrix analysed, but requires further evaluation. As a result of these observations, the Milli-PIXE (GUPIX) results are preferred to the micro-PIXE (GEOPIXE) results.

The differences in results between the two instruments suggest that the determination of partition coefficients is influenced by many factors and that results from different instruments cannot be directly compared. The magnitude of the fractionation of a PGE into a specific phase in an assemblage remains within the same order of magnitude for both instruments.

6.1.1.2. Variation of partition coefficients with equilibration temperature

D tends to decrease with increasing temperature. Figure 47 shows the milli-PIXE D (from Table 64) of experiments HU733 and HU469, plotted against equilibration temperature. Both experiments contained 500 ppm of each of Rh, Pd and Pt. D_{Rh} decreases very clearly, D_{Pd} remains constant, and D_{Pt} at 700°C is a minimum value, higher than D_{Pt} at 1100°C.

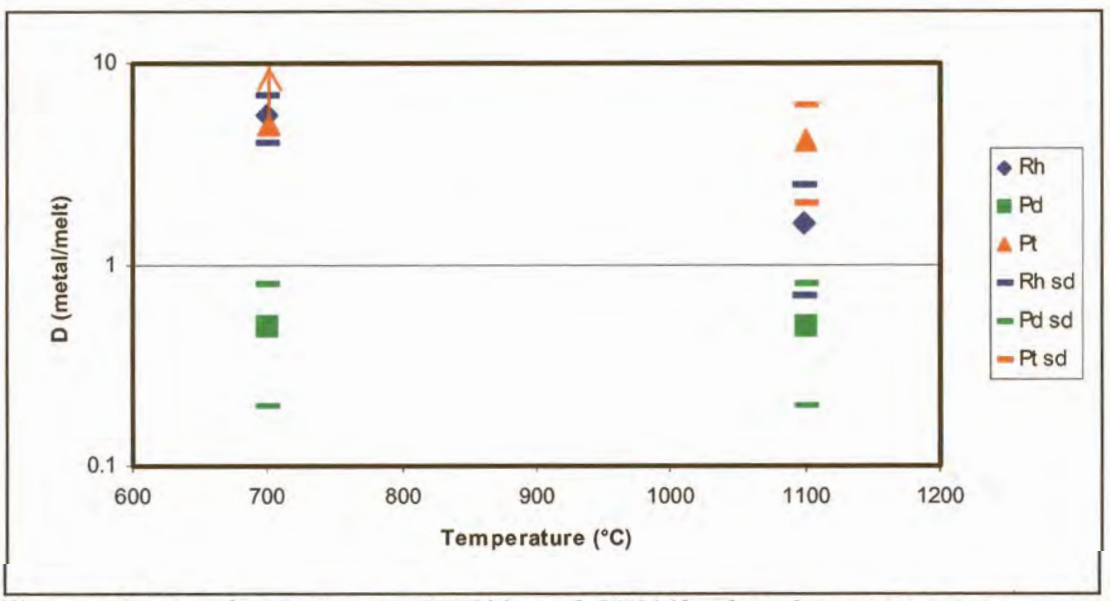

Figure 47. *D of experiments HU733 and HU469 plotted against temperature. Both experiments contained 500 ppm of each PGE. D_{Pt} at 700°C (HU469) is a minimum value (arrow indicates possible higher values). Error bars show 3σ standard deviations.*

Figure 48 shows the D of experiments HU381 and HU429 plotted against equilibration temperature (from Table 64). Both experiments contained 2000 ppm of each PGE. The decrease of D_{Rh} over the 100°C temperature increase is clear. The apparent increase of D_{Pd} from 900°C to 1000°C is not significant, considering the associated errors. D_{Pt} at 900°C is a minimum value, but suggests a decrease in the partition coefficient.

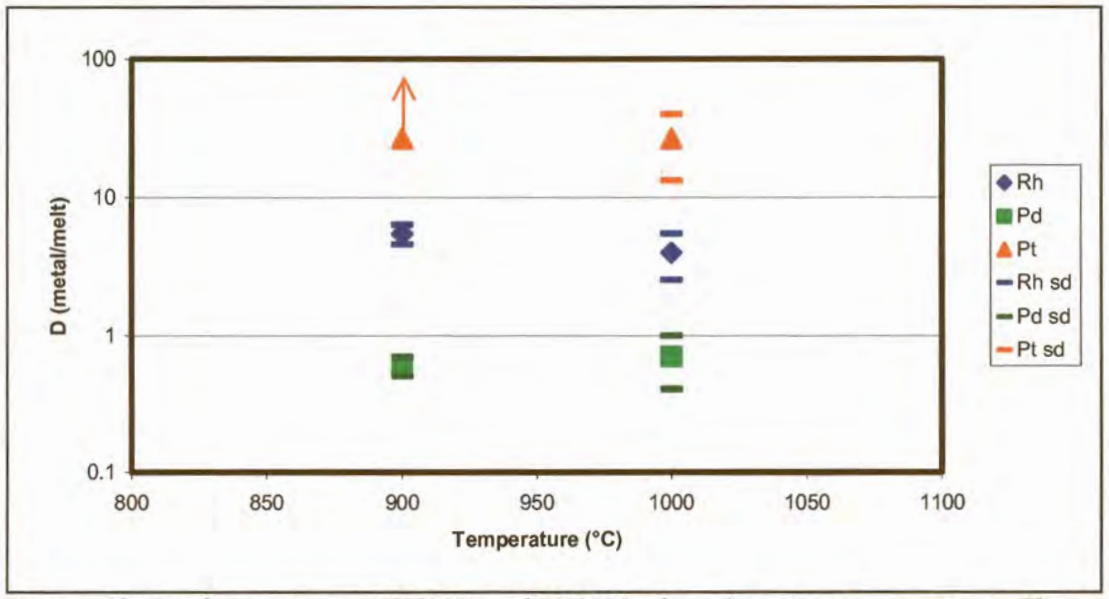

Figure 48. *D of experiments HU381 and HU429 plotted against temperature. The trend of the Pd values is overshadowed by their associated errors. The 900°C Pt value is a minimum value (the arrow indicates possible higher values). Error bars show 3σ standard deviations.*

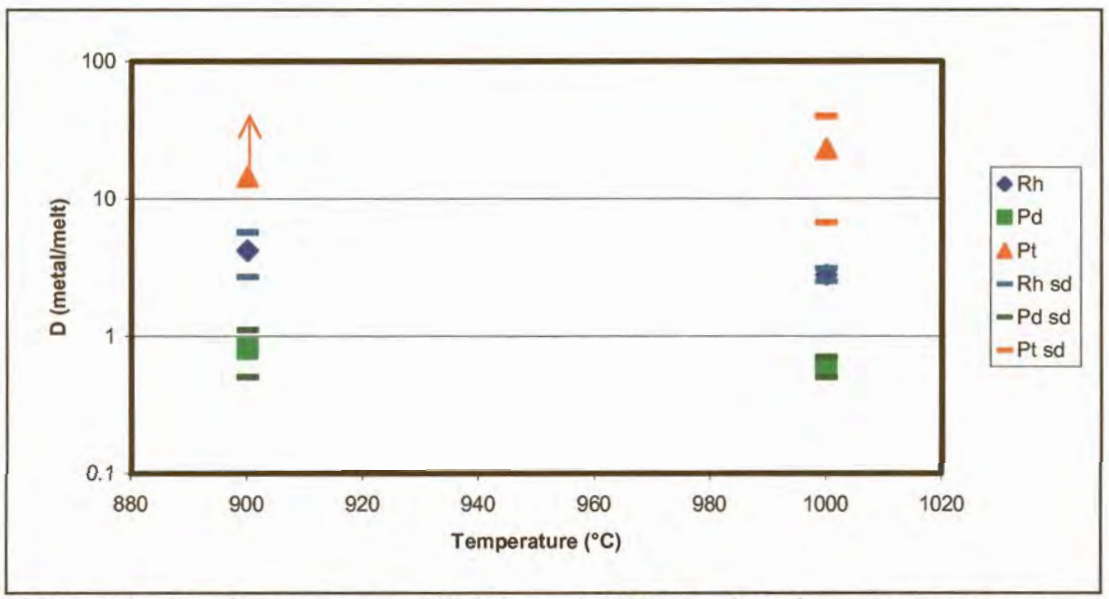

Figure 49. *D of experiments HU393 and HU753 plotted against temperature. Both experiments contained 1000 ppm of each PGE. Error bars show 3σ standard deviations, and the arrow possible higher values. The trend displayed by D_{Pt} is insignificant.*

The D for experiments HU393 and HU753 are plotted against temperature in Figure 49. Both experiments contained of 1000 ppm of each PGE. D_{Rh} and D_{Pd} decrease with increasing temperature. As the 900°C D_{Pt} is a minimum value and the 1000°C D_{Pt} has a very large associated error, no trend can be deduced.

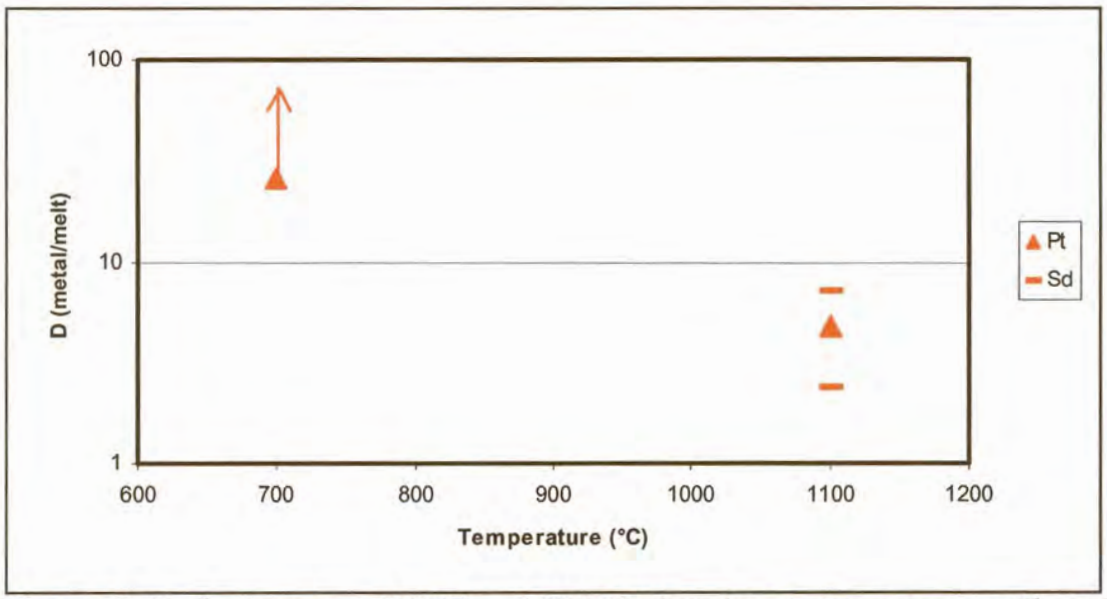

Figure 50. *D of experiments HU731 and HU471 plotted against temperature. The value at 700°C is a minimum value (the arrow indicates possible higher values). Error bars show 3σ standard deviations.*

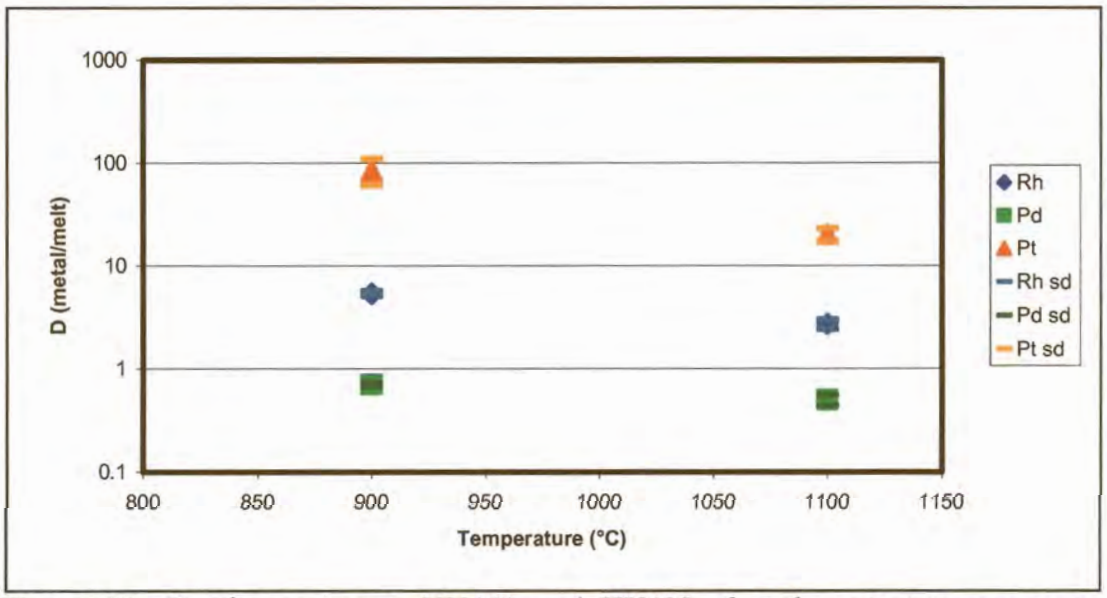

Figure 51. *D of experiments HU441 and HU429 plotted against temperature. Both experiments contained 2000 ppm of each PGE. Error bars show 3σ standard deviations.*

Experiments HU731 and HU471 both contained 2000 ppm of only Pt in addition to Ni and S, and the D are compared in Figure 50. The 700°C partition coefficient is a minimum value, but still much larger than the 1100°C coefficient, including its error.

Figure 51 illustrates the dependency of D on temperature from the micro-PIXE data in Table 65, for experiments HU441 (1100°C) and HU429 (900°C). Both contained 2000 ppm of each PGE.

6.1.1.3. Variation of partition coefficients with PGE content

The PGE contents of the experiments apparently do not significantly influence the partition coefficients at these concentrations. Partition coefficients for experiments HU393 and HU381 determined by milli-PIXE (Table 64) are plotted in Figure 52. Both experiments were reacted at 1000°C, but HU393 contained 1000 ppm of each PGE while HU381 contained 2000 ppm of each PGE. The D's for the two experiments are very similar. Figure 53 shows the D of experiments HU753 (1000 ppm) and HU429 (2000 ppm), equilibrated at 900°C. The D_{Pt} are both minimum values.

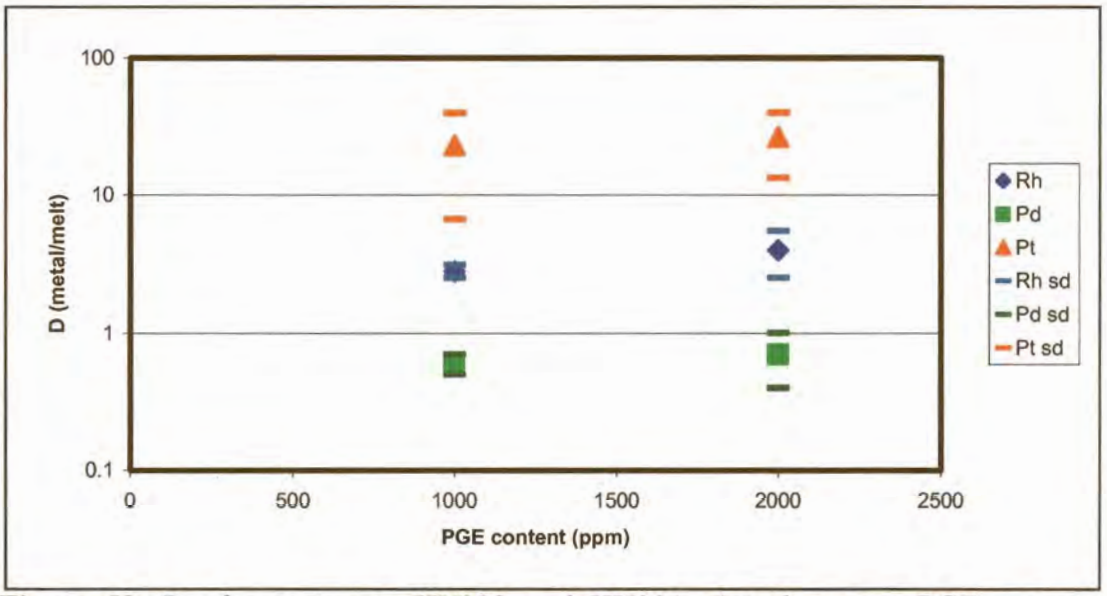

Figure 52. *D of experiments HU393 and HU381 plotted against PGE content. Both experiments were equilibrated at 1000°C. Error bars show 3σ errors.*

The D calculated for experiments HU393, HU394, HU395 and HU412 from micro-PIXE data (Table 65) are plotted in Figure 54. Experiment HU393 contained 1000 ppm of each PGE, HU394 contained 6000 ppm of each PGE, and HU395 and HU412 each contained 10000 ppm of each PGE. At these concentrations, PGE content does not influence the partition coefficients.

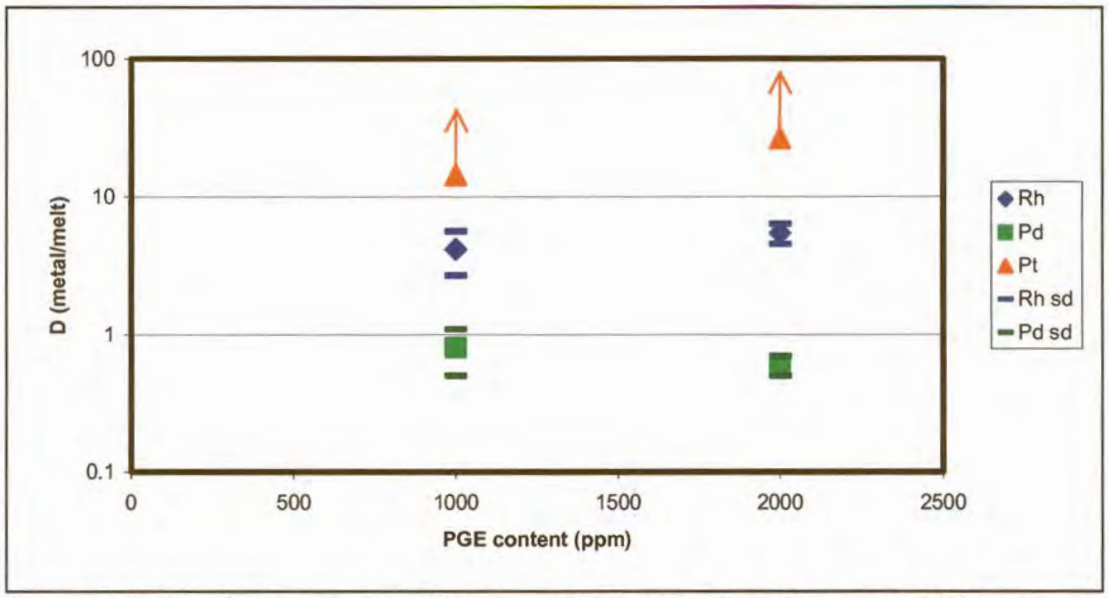

Figure 53. *D of experiments HU753 and HU429 plotted against PGE content. Both experiments were equilibrated at 900°C. Error bars show 3σ standard deviations. The arrows indicate possible higher D values.*

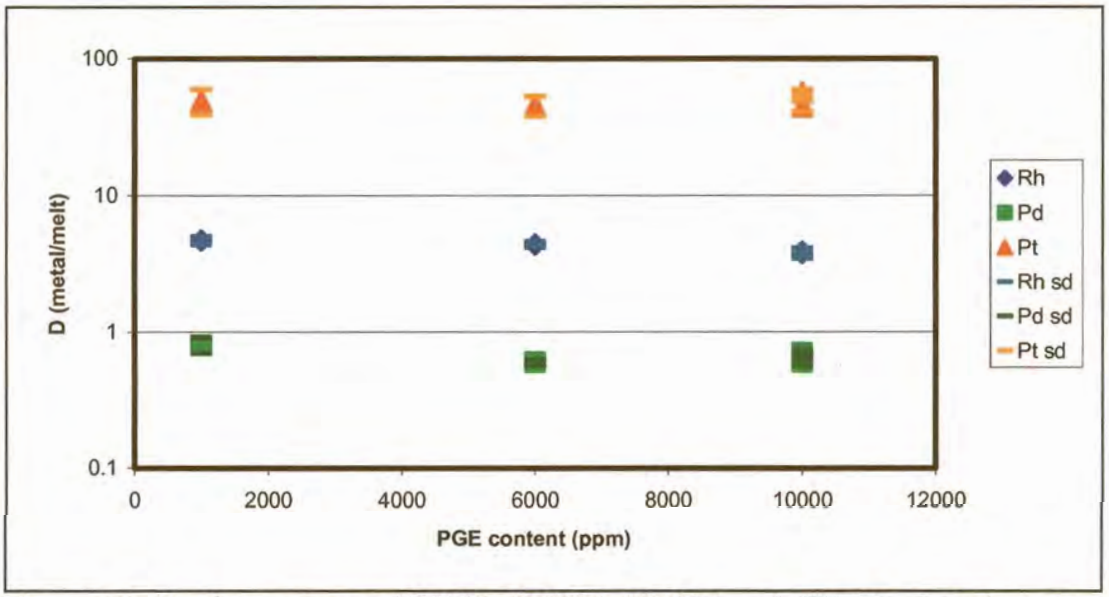

Figure 54. *D of experiments HU393, HU394, HU395 and HU412 plotted against PGE content. All these experiments were equilibrated at 1000°C. Error bars show 3σ standard deviations.*

6.1.1.4. Variation of partition coefficients resulting from the effect of PGE on each other

The influence of PGE on each other during partitioning is not unambiguous. According to the micro-PIXE analyses, partition coefficients appear to increase slightly when a PGE is in isolation from the other PGE, especially for Pd (compare values from experiments HU426, HU427, HU428 and HU429 – Table 65). The milli-PIXE D_{Pd} (Table 64) for experiments HU427 and HU429 also suggests stronger differentiation of Pd into metal in the absence of other PGE (D value closer to 1). It seems that in the absence of other PGE the partitioning behaviour of the remaining PGE is amplified, but D drops when there is competition from other PGE.

6.1.1.5. In conclusion

Pt, and to a lesser extent Rh, partition into the nickel, while Pd prefers to remain in the sulphide melt. Partition coefficients determined by different PIXE instruments vary, but remain in the same order of magnitude. The influence of equilibration temperature is most prominent with Pt and least with Pd. The amount of PGE in the experiments did not influence the partition coefficients, but the PGE partitioned more strongly into the preferred phase in the absence of other PGE.

6.2. The Cu-S system

6.2.1. Cu-rich melt - S-rich melt assemblage (1200°C)

Nernst partition coefficient: D = (PGE content in Cu-rich melt) / (PGE content in S-rich melt).

D were calculated from the milli-PIXE analyses discussed in section 5.2.1.2. (Table 31). The ratios and confidence intervals were obtained with resampling statistics (as discussed in

section 4.3.). Table 67 contains the D calculated from milli-PIXE results. Influence of initial bulk PGE contents, and presence or absence of other PGE in the systems, were investigated.

Table 67. *D(Cu-rich melt/S-rich melt) for the PGE determined for the Cu-rich melt and S-rich melt from milli-PIXE results in Table 31.*

Exp	Temp (°C)	PGE (ppm)	D_{Rh} (± 1σ)	D_{Pd} (± 1σ)	D_{Pt} (± 1σ)
HU442	1200	1000	>9.2	~14 (~100)	>6.0
HU443	1200	2000			>11.1
HU444	1200	2000		7.5 (1.0)	
HU445	1200	2000	>34.9		
HU450	1200	2000	>21.4	>6.3	>3.3

6.2.1.1.Variation of partition coefficients with PGE content

Both experiments HU442 and HU450 contained all three PGE, but HU442 contained 1000 ppm of each PGE while HU450 contained 2000 ppm of each PGE. Five of the six coefficients are, however, minimum coefficients, and the associated error determined for the remaining D_{Pd} with resampling statistics is extremely large, due to the large standard deviation of 0.01 wt% for Pd in S-rich melt.. The coefficients are plotted in Figure 55. No trends can be determined from this data set.

6.2.1.2. Variation of partition coefficients resulting from the effect of PGE on each other

Experiment HU450 contained 2000 ppm of each PGE, and experiments HU443, HU444 and HU445 each contained 2000 ppm of one PGE only (Table 67). Five of the six values are minimum values, and no deductions can be made.

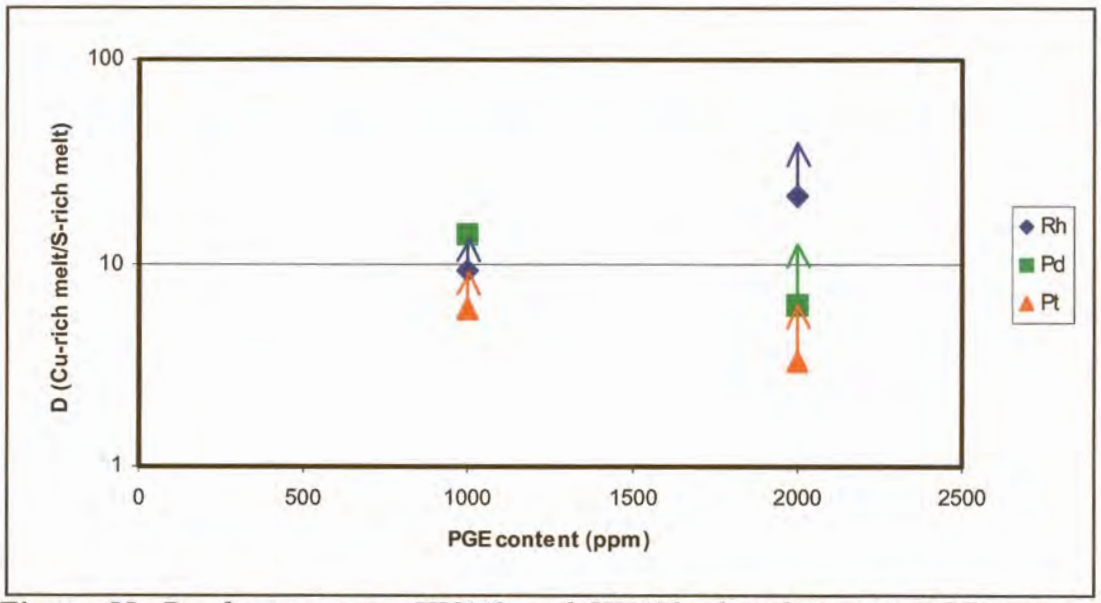

Figure 55. *D of experiments HU442 and HU450 plotted against PGE content. Both experiments were equilibrated at 1200°C. Five of the six values are minimum values, as shown by the arrows, and the error of the remaining D value is too large to plot.*

6.2.1.3.In conclusion

All three PGE strongly prefer the Cu-rich melt phase to the S-rich melt phase, with the consequence that precise PGE concentrations in the latter phase could not be determined. Only minimum detection limits could be obtained for most of the analyses of the S-rich melt. As a result, influence of PGE content and the effect of the absence and/or presence of other PGE, could not be determined.

6.2.2. Copper - digenite assemblage (1000°C and 800°C)

Nernst partition coefficient: D = (PGE content in metal) / (PGE content in digenite).

D were calculated from milli-PIXE analyses (Table 38) and micro-PIXE analyses (Table 41) discussed in section 5.2.2.2. The partition coefficients and confidence intervals were obtained with resampling statistics (as discussed in section 4.3.). Table 68 contains the D calculated from milli-PIXE results and Table 69 the D calculated from micro-PIXE results.

The effect of different PIXE instruments, the influence of PGE contents, and the presence or absence of other PGE in the experiments, were investigated.

Table 68. *D(copper/digenite) for the PGE determined for copper and digenite from milli-PIXE results in Table 38. Values in italics are statistically unreliable.*

Exp	Temp (°C)	PGE (ppm)	D_{Rh} (± 1σ)	D_{Pd} (± 1σ)	D_{Pt} (± 1σ)
HU382	1000	4000			>15.0
HU384	1000	3000	>58.7		
HU385	1000	2000	>23.9	>29.2	>13.5
HU387	1000	1000	>15.0	23 (4.8)	*>1.2*
HU465	1000	10000	>167.5	100 (8)	>55.6
HU482	800	1000	45 (6)	>43.4	>21.6

Table 69. *D(copper/digenite) for the PGE determined for copper and digenite from micro-PIXE results in Table 41.*

Exp	Temp (°C)	PGE (ppm)	D_{Rh} (± 1σ)	D_{Pd} (± 1σ)	D_{Pt} (± 1σ)
HU385	1000	2000	>588.3	675 (80)	#

= standard deviations for analyses are too large to allow for reliable resampling

6.2.2.1.Variation of partition coefficients with different instruments

D_{Pd} for experiment HU385 in both Tables 68 and 69 is the largest partition coefficient of the three PGE, followed by D_{Rh}, with D_{Pt} being the lowest. As most of these values are minimum values, it is not possible to quantify real differences between the two data sets.

6.2.2.2.Variation of partition coefficients with equilibration temperature

Experiment HU387 was equilibrated at 1000°C and experiment HU482 at 800°C, but both contained 1000 ppm of each PGE. The PGE were difficult to detect in the digenite, therefore three of the values are minimum values. There is a decrease in the D_{Pd} and D_{Rh} from 800°C to 1000°C (Figure 56).

6.2.2.3.Variation of partition coefficients with PGE content

Experiments HU385, HU387 and HU465 were all equilibrated at 1000°C. HU387 contained 1000 ppm of each PGE, HU385 contained 2000 ppm of each PGE and HU465 contained 10000 ppm of each PGE. D appears to increase with increasing PGE content (Figure 57), but because so many of the values are minimum values, the trend is not conclusive.

6.2.2.4.Variation of partition coefficients resulting from the effect of PGE on each other

The influence of the PGE on each other during partitioning can be seen in experiments HU382, HU384 and HU385, all of which were equilibrated at 1000°C. D_{Rh} and D_{Pt} are minimum values, but Pt and Rh appear to partition more strongly into the metal in the absence of other PGE.

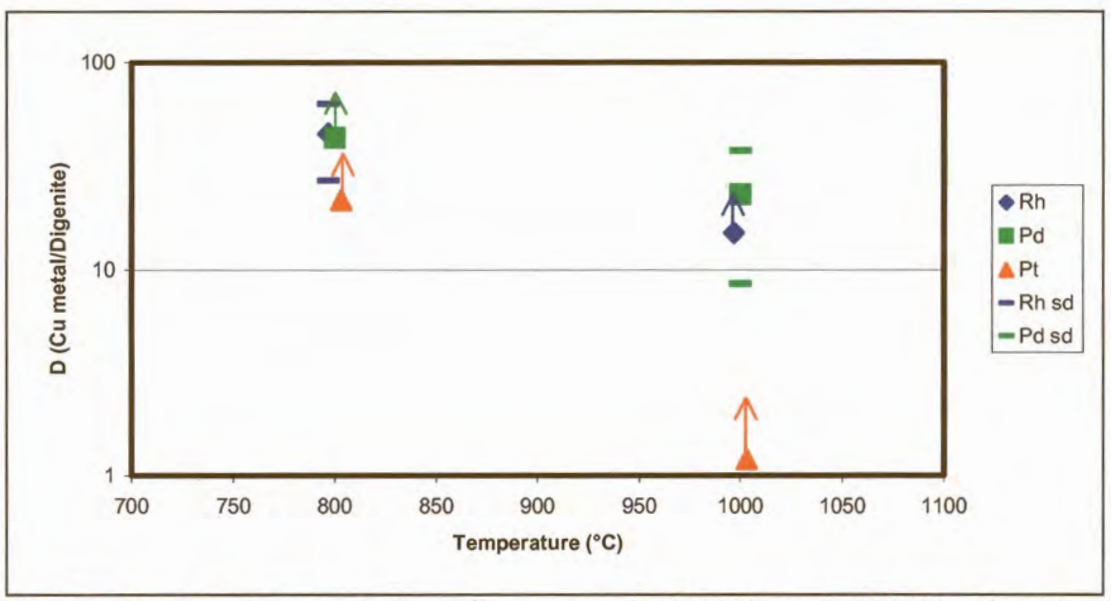

Figure 56. *D_{Rh}, D_{Pd} and D_{Pt} of experiments HU387 and HU482 plotted against equilibration temperature. Both experiments contained 1000 ppm of each PGE. Four of the six values are minimum values, as shown by the arrows. Error bars show 3σ standard deviations.*

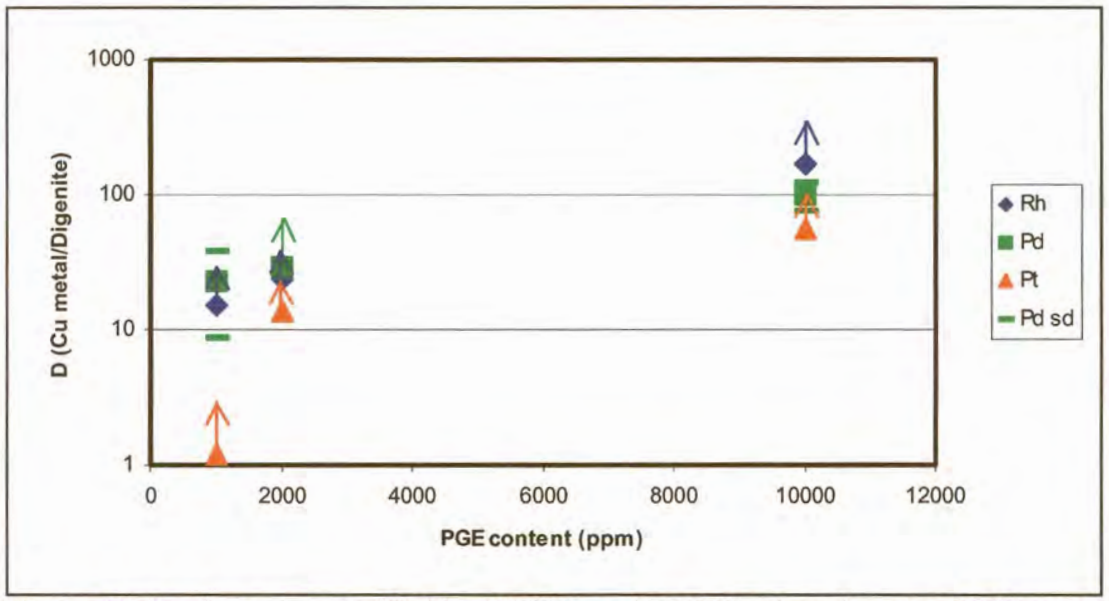

Figure 57. *D of experiments HU385, HU387 and HU465, plotted against PGE content. All were equilibrated at 1000°C. Arrows indicate possible higher values for D, and error bars 3σ standard deviations.*

6.2.2.5.In conclusion

All PGE strongly prefer the copper to the digenite. Because most of the partition coefficients are minimum values, the trends can only be surmised. There are no definite differences between results from the two PIXE instruments, and it is uncertain whether PGE content, and the presence of other PGE, play a role during PGE partitioning. Temperature does influence the coefficients – they decrease with increasing temperature.

6.2.3. Digenite - melt assemblage (1000°C)

Nernst partition coefficient: D = (PGE content in melt) / (PGE content in digenite).

D were calculated from micro-PIXE analyses (Table 45) discussed in section 5.2.3.2. The partition coefficients and confidence intervals were obtained with resampling statistics (as discussed in section 4.3.). Table 70 presents the D's calculated from micro-PIXE results. The influence of PGE contents and presence or absence of other PGE in the experiments, were investigated.

Table 70. *D(melt/digenite) for the PGE determined for the melt and digenite from micro-PIXE results in Table 45.*

Exp	Temp (°C)	PGE (ppm)	D_{Rh} (± 1σ)	D_{Pd} (± 1σ)	D_{Pt} (± 1σ)
HU397	1000	?6000	3.8 (2.0)	4.8 (0.4)	17.4 (2.4)
HU398	1000	10000	6.1 0.5 ()	4.0 (0.1)	12.7 (1.0)
HU411	1000	2000	43.1 (0.9)	4.0 (0.1)	23.6 (1.5)
HU413	1000	1000	62.8 (3.1)	2.9 (0.1)	14.5 (2.2)
HU418	1000	3000			12.7 (0.6)
HU420	1000	2000	9.8 (0.4)		

? – A very PGE-rich drop separated from this experiment – discussed in 5.2.3.1 – remaining PGE content uncertain.

6.2.3.1. Variation of partition coefficients resulting from the effect of PGE on each other

Experiment HU411 contained 2000 ppm of each PGE, while experiment HU418 contained 3000 ppm Pt and HU420 2000 ppm Rh. The partition coefficients for the experiments that contain one PGE in isolation are lower than those where the PGE were combined.

6.2.3.2. Variation of partition coefficients with PGE content

The effect of PGE content on the partition coefficient is unclear in this case. When the D are plotted against the PGE contents (experiments HU398, HU411, HU413), there is a clear negative trend for Rh, and a suggestion of a negative trend for Pt. Pd remains constant (Figure 58).

6.2.3.3. In conclusion

All three PGE prefer the sulphide melt as opposed to the digenite, and Rh and Pt more so than Pd. D_{Rh} and D_{Pt} are higher when accompanied by other PGE than when in isolation. Higher PGE content correlates with a decrease in D_{Rh}.

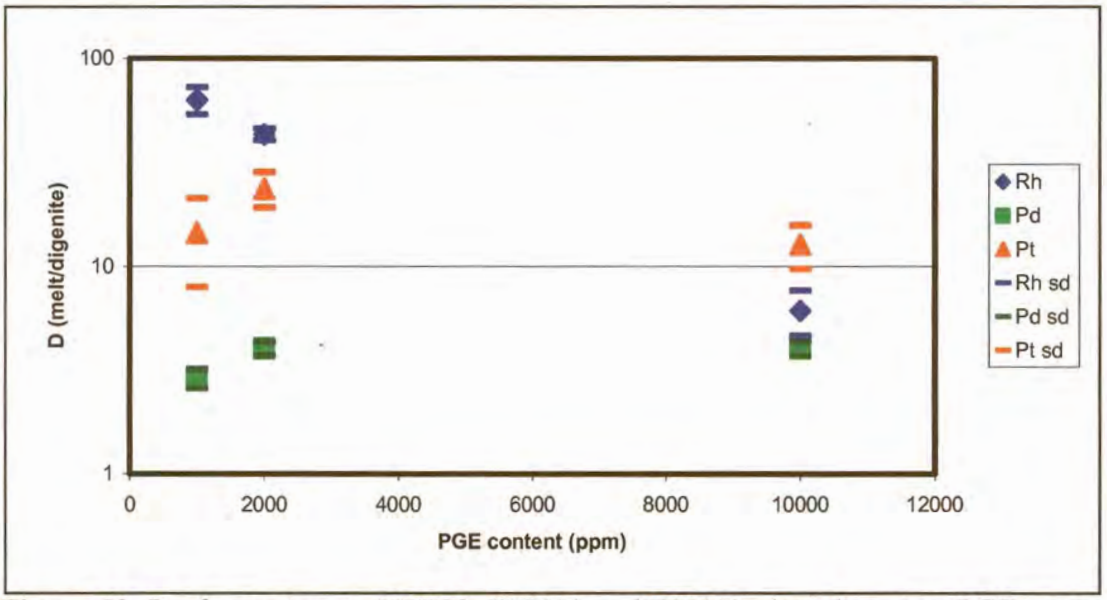

Figure 58. *D of experiments HU398, HU411 and HU413 plotted against PGE content. All were reacted at 1000°C. Error bars show 3σ standard deviations.*

6.3. The Fe-S system

6.3.1. Iron – Fe-S melt assemblage (1200°C to 1000°C)

Nernst partition coefficient: D = (PGE content in metal) / (PGE content in melt).

D were calculated from milli-PIXE analyses (Table 55), discussed in section 5.3.1.2. The partition coefficients and confidence intervals were obtained with resampling statistics (as discussed in section 4.3.). Table 71 contains the D calculated from milli-PIXE results. The standard deviations of these partition coefficients are very large, and it is very difficult to observe any trends or to compare different coefficients. Rh and Pt show a preference for the iron. D_{Pd} changes from slightly incompatible at higher temperatures to slightly compatible to iron at lower temperatures.

The presence of oxygen in these experiments makes it possible to determine the exact fO_2 and fS_2 conditions under which the experiments were reacted, as O, S and Fe were all present and equilibrated. Phase stability diagrams from HSC software were consulted, and log pO_2 - log pS_2 coordinates of the Fe-FeO-FeS triple points at 1200°C, 1100°C and

1000°C transformed to fO_2- fS_2 coordinates. At 1200°C an fO_2 of 2.79 x 10^{-13} and a fS_2 of 1.63 x 10^{-5} would have prevailed, at 1100°C an fO_2 of 1.13 x 10^{-14} and a fS_2 of 2.71 x 10^{-6}, and at 1000°C an fO_2 of 2.73 x 10^{-16} and a fS_2 of 3.21x10^{-7}. At lower temperatures smaller amounts of oxygen are required to form oxides with Fe, which explains why the 1000°C experiments contain the most oxides.

Table 71. *D(iron/melt) for the PGE determined from milli-PIXE results in Table 55.*

Exp	Temp (°C)	PGE (ppm)	D_{Rh} (± 1σ)	D_{Pd} (± 1σ)	D_{Pt} (± 1σ)
HU825	1200	2200			*214.0 (#)*
HU826	1200	2600		*0.98(0.69)*	
HU827	1200	2000	*4.27(#)*		
HU734	1100	2400			-
HU735	1100	2400		*0.8(~4.0)*	
HU736	1100	2000	*1.2(#)*		
HU843	1000	2200		*1.92(#)*	
HU844	1000	2000	>2.0		
HU845	1000	2000	>2.1	>1.2	-
HU849	1000	6000	>2.2	-	>1.1
HU850	1000	10000	*8(#)*	*1.8*	*1.6*

= standard deviations for analyses are too large to allow for reliable resampling

6.3.2. Pyrrhotite – sulphide melt assemblage (1100°C)

Nernst partition coefficient: D = (PGE content in melt) / (PGE content in pyrrhotite).

D were calculated from milli-PIXE analyses (Table 59) discussed in section 5.3.2.2. The partition coefficients were obtained with resampling statistics (as discussed in section 4.3.). Table 72 contains the D calculated from milli-PIXE results. Minimum partition coefficients were determined for Rh, Pd and Pt. All PGE prefer the sulphide melt.

Table 72. *D(melt/pyrrhotite) for the PGE determined from milli-PIXE results in Table 59.*

Exp	Temp (°C)	PGE (ppm)	D_{Rh} (± 1σ)	D_{Pd} (± 1σ)	D_{Pt} (± 1σ)
HU737	1100	2000			>3.8
HU738	1100	2000		>10.5	
HU739	1100	2000	>3.7		

6.3.3. Iron - troilite assemblage (900°C)

Nernst partition coefficient: D = (PGE content in metal) / (PGE content in troilite).

D were calculated from milli-PIXE analyses (Table 63) discussed in section 5.3.3.2. The partition coefficients and confidence intervals were obtained with resampling statistics (as discussed in section 4.3.). Table 73 contains the D calculated from milli-PIXE results. All PGE favour the metal as opposed to troilite.

Table 73. *D(iron/troilite) for the PGE determined from milli-PIXE results in Table 63.*

Exp	Temp (°C)	PGE (ppm)	D_{Rh} (± 1σ)	D_{Pd} (± 1σ)	D_{Pt} (± 1σ)
HU434	900	1800			>2.8
HU435	900	2600		-	
HU436	900	2200	*>2.1*		
HU756	900	1000	>3.5	*1.2(0.7)*	>1.6

6.4. Mass balance calculations

Mass balances were calculated by using the EPMA analyses of co-existing phases, the PGE content in both phases as determined by PIXE, starting compositions, and the lever-rule. Mass balances were calculated for experiments in which:

- PGE contents in both co-existing phases were above the detection limit.
- Major element compositions of both phases in the experiment could be determined accurately in terms of the two major elements concerned (i.e. no accidental contamination).

The mass balance errors - expressed as percentages in relation to the initial amount of PGE weighed into the experiments - for experiments of the Ni-S system are shown in Tables 74 and 75. The Ni-S system was selected for testing and interpreting sources of error, as it contained the largest number of analysed experiments of a single assemblage. The mass balances indicate that surplus PGE were detected in almost all of the experiments, with few exceptions.

Table 74. *Mass balance errors calculated from micro-PIXE analyses of PGE contents of the Ni-S system, expressed as percentages of the original PGE content.*

Exp	Temp (°C)	Rh - % error	Pd - % error	Pt - % error
HU441	1100	9.64	16.71*	29.00
HU437	1100	-	32.33*	-
HU393	1000	42.40	38.33*	75.10
HU394	1000	40.39	5.59	95.50
HU395	1000	40.93	60.16	64.75
HU412	1000	20.80	1.36	25.75
HU429	900	27.71	1.92	35.34
HU426	900	-	-	51.90*
HU427	900	-	0.51*	-
HU428	900	11.07*	-	-

* - Element under-represented by PIXE measurements.

Table 75. *Mass balance errors calculated from milli-PIXE analyses of PGE contents of the Ni-S system, expressed as percentages of the original PGE content.*

Exp	Temp (°C)	Rh - % error	Pd - % error	Pt - % error
HU733	1100	100.42	46.06	3.51*
HU731	1100	-	-	33.34*
HU393	1000	102.50	27.72	41.25
HU381	1000	93.67	88.36	86.65
HU753	900	56.31	6.58*	-
HU429	900	53.23	54.13	-
HU427	900	-	69.14	-
HU469	700	71.07	3.12	-
HU473	700	31.33	-	-

* - Element under-represented by PIXE measurements.

Overall the mass balance errors are very large, averaging more than 50% for the milli-PIXE data and more than 30% for the micro-PIXE data. To evaluate whether the mass balance errors are dependent on analytical uncertainty, the relationship between the mass balance percentage errors and the partition coefficient standard deviations as percentage errors of the partition coefficients was evaluated. The standard deviations of the partition coefficients were determined from the analytical errors of the PIXE data, and are therefore known to be solely dependent on analytical error. Figure 59 shows this relationship for the micro-PIXE data, and Figure 60 for the milli-PIXE data.

The positive correlation between analytical error and mass balance percentage error for the micro-PIXE data (Figure 59) indicates that the mass calibration error is reflected in the errors of the partition coefficients for this data. It is therefore implied that the mass balance errors are mainly dependent on analytical error, and not experimental error.

However, there is no positive correlation between percentage analytical error and percentage error from mass balance calibration for the milli-PIXE data (Figure 60). As errors other than analytical error have been eliminated by the positive relationship for the

micro-PIXE data (Figure 59), and errors are implied to be mainly analytical, it is clear that the analytical error in the milli-PIXE data is more random and unpredictable.

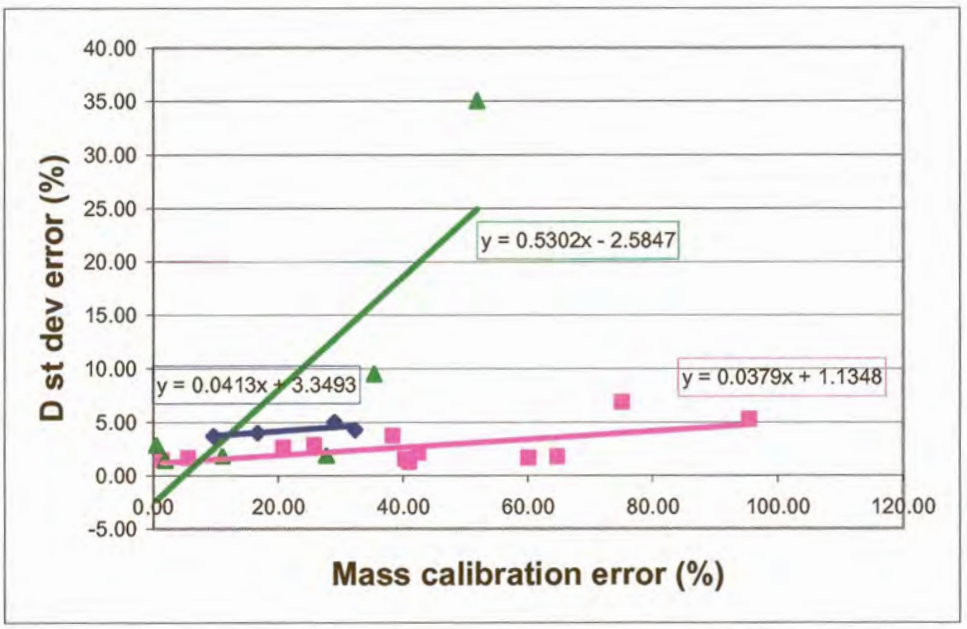

Figure 59. *The linear relationship between mass calibration errors and standard deviation errors for micro-PIXE data at 1100°C (●), 1000°C (■) and 900°C (▲) are indicated by the regression lines. The R value for the 1100°C data is 0.77, for the 1000°C data 0.60, and for the 900°C data 0.82.*

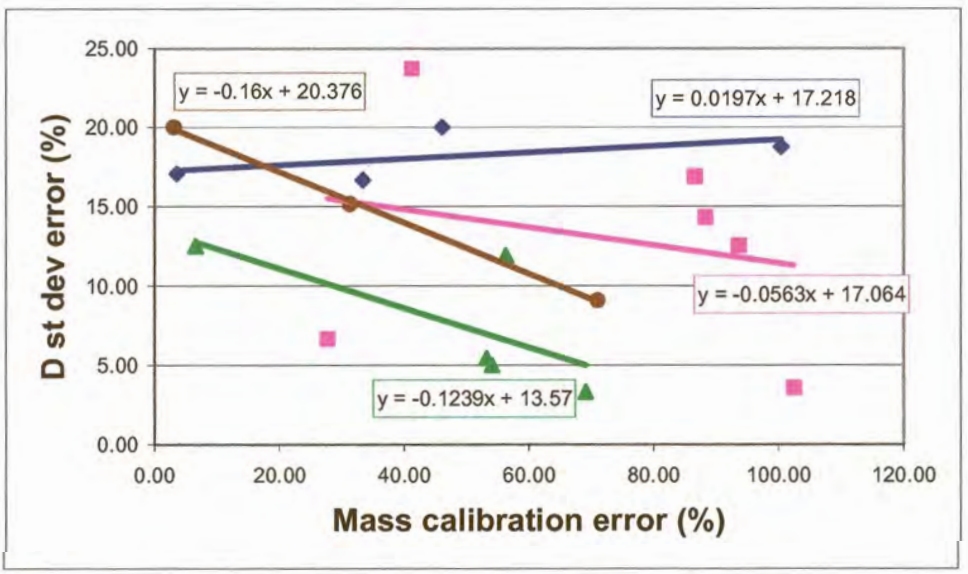

Figure 60. *The linear relationship between mass calibration errors and standard deviation errors for milli-PIXE data at 1100°C (●), 1000°C (■), 900°C(▲) and 700°C (●) are indicated by the regression lines. The R value for the 1100°C data is 0.52, for the 1000°C data 0.24, for the 900°C data 0.70, and for the 700°C data 1.00.*

In hindsight, analytical errors on both instruments could have been checked more thoroughly, for example by the compilation of correlation curves for one or more sets of standards with increasing contents of an element, or the analysis of standards with known trace contents. However, as PIXE is frequently portrayed to be standard independent (Ryan *et al.*, 1990), further evaluation of this problem was not considered a necessity at the time of analysis. Development of the milli-PIXE line at the AEC for the analysis of matrixes as investigated in this study is ongoing, but resolving fundamental problems of PIXE analysis, as encountered in this study, goes way beyond the scope of this project. The instrument is presently not accessible for analytical work, and the root of the problem cannot be evaluated at present. However, future measurements aimed at resolving these problems will include preparation of appropriate standards, as well as re-evaluation of the collected spectra and a refinement of the partition coefficients.

The mass balance errors should reflect all possible introduced errors, such as weighing errors, sample separation during equilibration, and analytical error, but the latter is believed to predominate.

7. Conclusions

7.1. The Ni-S system

The partition coefficients of Rh, Pd and Pt between metallic nickel and sulphide melt were discussed in Section 6.1.1. and are presented in Tables 64 and 65.

- Pt and Rh are compatible with nickel (partition coefficients > 1), while Pd is incompatible. Partition coefficients vary from 2 to 10 for Rh, from 0.5 to 0.9 for Pd and from 4 to 220 for Pt. These results compare favourably with the investigation by Urban *et al.* (1995), who reported Pt to prefer alloys with Ni and PGE, and Pd to favour the sulphides. Rh, however, was reported also to prefer PGE sulphides, whereas it prefers the nickel in this investigation. This is probably because the PGE content in the melt in the present investigation is too low to form PGE sulphides. Fleet and Stone (1991) also reported enrichment of Pt in alloy in the Fe-Ni-S system, and relative enrichment of Pd in sulphide liquid as opposed to alloy. They found Pd partitioning into Fe alloy, but in the absence of Fe in the alloys it favoured the sulphide. As their partition coefficients were determined between iron and sulphide liquid, they cannot be compared to the coefficients determined for the Ni-S system. Fleet *et al.* (1999) reported partition coefficients in the Fe-Ni-S system between solid metal and liquid metal sulphide of 40 – 300 for Pt and 0.7 – 1.47 for Pd, which compares favourably with this investigation. The absence of Fe in the alloy in these Ni-S experiments probably influences Pd to partition into the melt, so that the coefficients remain smaller than 1.

- As shown in Tables 64 and 65, there are significant differences between the partition coefficients from the two different PIXE instruments. It is generally accepted that errors of PGE partition coefficients determined at low PGE contents are large. According to Barnes *et al.* (1997) errors on PGE partition coefficients are

in the order of 20 – 50%. Such errors could eliminate the difference between the two PIXE instruments in this investigation.

- The partition coefficients are temperature dependent – they decrease as the temperature increases. Fleet *et al.* (1999) stated that PGE partition coefficients in the Fe-Ni-S system are much less dependent on temperature than on the S content in the melt, and that with increasing S content in the melt the PGE become more siderophile. At lower temperatures the S content in the Ni-S melt in this investigation is higher than at high temperatures (see phase diagram in Figure 11). For the Ni-S system in this investigation it is not possible to determine whether it is the temperature or the S content in the melt that is responsible for the change of the partition coefficients.

- The partition coefficients are not significantly influenced by the PGE contents investigated in this study. This supports the statement by Barnes *et al.* (1997) that at low PGE contents the partition coefficients are independent of their concentration.

- The PGE partition significantly more strongly into metal in the absence of other PGE, especially Pd.

7.2. The Cu-S system

Partition coefficients for Rh, Pd and Pt between Cu-rich melt and S-rich melt were discussed in Section 6.2.1. and are presented in Table 67. Partition coefficients between copper and digenite were determined in Section 6.2.2. and are shown in Tables 68 and 69, and partition coefficients between digenite and melt were determined in Section 6.2.3. and are presented in Table 70.

- Rh, Pd and Pt all partition into the Cu-rich melt as opposed to the sulphide melt (partition coefficients > 1), but these coefficients are mostly minimum values, and the exact values are unknown. The partition coefficients determined in the present

investigation for Rh are generally larger than 10, for Pd about 7 and for Pt larger than 3. Gerlach *et al.* (1972) determined a coefficient of 2000 for Pt into Cu, Schlitt and Richards (1975) determined partition coefficients of 167 for Pd and 2500 for Pt into Cu. Taylor (1983) determined an experimental partition coefficient of 110 for Rh, and calculated coefficients of 11 for Rh, 25 for Pd and 6800 for Pt. Burylev *et al.* (1974) determined partition coefficients of 80 for Pd and 2000 for Pt. The Rh partition coefficients from this investigation compare favourably, while the Pd coefficients are a little low and the Pt coefficients should be very high.

- The partition coefficients between metal and digenite for this investigation are generally larger than 15 for Rh, larger than 20 for Pd and larger than 10 for Pt - all three PGE are compatible with the metal.

- Partition coefficients of between about 4 and 60 for Rh, between 3 and 5 for Pd and between 12 and 24 for Pt were determined between melt and digenite in this investigation - all PGE favouring the melt. Spectra were interpreted with the GEOPIXE software, and these coefficients could be questionable (see Section 6.1.1.1.).

- For the copper-digenite assemblage there is an indication that the partition coefficient increases as the bulk PGE content increases, but for the other two assemblages it is not possible to draw any conclusions.

7.3. The Fe-S(±O) system

Partition coefficients for PGE between iron and melt, pyrrhotite and melt and iron and troilite were discussed in Sections 6.3.1., 6.3.2. and 6.3.3., and the coefficients are presented in Tables 71, 72 and 73. The partition coefficients determined for this system are very unreliable, due to experimental difficulties and the presence of O in most of the experiments.

- Most of the partition coefficients determined for the metal-melt assemblage are statistically unreliable. The Rh coefficient is apparently larger than 2, favouring the metal, the Pd coefficient varies from slightly compatible to slightly incompatible in the metal, and the Pt coefficients are larger than 1, favouring the metal, but are very unreliable. Fleet and Stone (1991) reported alloy/sulphide liquid partition coefficients of 1 to 2 for Pd, 30 to 110 for Rh and > 1000 for Pt. Chabot and Drake (1997) determined a Pd partition coefficient of between 0.5 and 2 for metal / liquid. With increasing S content of the liquid the Pd became more compatible with the solid metal – as was also determined in this investigation. This finding supports the statements by Fleet *et al.* (1999) and Li *et al.* (1996) that PGE partitioning is dependent on the S content of the melt.

- In the melt-pyrrhotite assemblage the partition coefficients are all larger than 1 - all PGE are compatible with the melt. The Rh and Pt partition coefficients are larger than about 4, and the Pd partition coefficient larger than 10. Fleet and Stone (1991) found Rh the only PGE to be slightly compatible with the sulphide.

- In the metal-troilite assemblage all three PGE favour the metal - all partition coefficients are larger than 1. The Rh and Pt coefficients are larger than 2, and the Pd coefficient larger than 1. Jones *et al.* (1986) reported a metal/troilite partition coefficient of 150 for Pd.

- No assumptions on the influence of bulk PGE content, temperature or the influence of other PGE can be made, due to the unreliability of the partition coefficients.

7.4. PGE partitioning in general

In assemblages with alloy, such as copper – digenite, Cu-rich melt – sulphide melt, iron – sulphide melt, iron – troilite and nickel – sulphide melt, Pt and Rh are always concentrated in the alloy phases. In the nickel – sulphide melt assemblage, Pd is the only PGE that is not compatible in the metal, and is concentrated in the melt, and in the iron – sulphide melt

assemblage, Pd varies from slightly incompatible at higher temperatures to slightly compatible at lower temperatures in the metal. Pt partitioning into iron is surprisingly low, but can possibly be attributed to the presence of O. All PGE avoid the sulphide phases – digenite, pyrrhotite and troilite – and are being concentrated in the co-existing sulphide melt or alloy.

Acknowledgements

I thank my research supervisor, Prof. R.K.W. Merkle, for providing me with this opportunity, for his confidence in my abilities to complete this research, for his interest, patience, suggestions and criticism and for all his support. My appreciation also to our microprobe operator, Peter Gräser, for many helpful suggestions and support, my fellow student Willemien Viljoen and the rest of the Applied Mineralogy Group, for their contributions.

This research was sponsored by Amplats Research Centre. I would like to thank their staff, and specifically Juliana Bruwer, for their helpful contributions and ideas, and the use of two of their furnaces. Sincere thanks also to Dr. J.R. Taylor for helpful discussions and his continued interest.

The staff at the National Accelerator Centre, in particular Dr. V. Prozesky, were very kind, patient and helpful in providing PIXE analyses at a special rate. I would also like to thank the staff at the Van De Graaf Accelerator of the Atomic Energy Corporation, Dr. C.B. Franklyn and G.T. Young, for giving me access to their PIXE, and for all the time and effort they have so kindly spent on helping me. Without their support the whole investigation could have failed.

Many thanks to Roger Dixon for editing this work, and for his interest and support.

Lastly, but very importantly, I would like to thank my family and Karel, for their loving support and patience, without which I would not have been able to finish this thesis.

References

Barnes, S.-J., Naldrett, A.J. and Gorton, M.P. (1985). The origin of the fractionation of platinum-group elements in terrestrial magmas. *Chemical Geology*, **53**, 303-323.

Barnes, S.-J., Makovicky, E., Karup-Møller, S., Makovicky, M. and Rose-Hansen, J. (1994). Partition coefficients for Ni, Cu, Pd, Pt, Rh and Ir between monosulphide solid solution and sulphide liquid and the implications for the formation of compositionally zoned Ni-Cu sulphide bodies by fractional crystallisation of sulphide liquid. *Mineralogical Magazine*, **58A**, 51-52.

Barnes, S.-J., Makovicky, E., Makovicky, M., Rose-Hansen, J. and Karup-Møller, S. (1997). Partition coefficients for Ni, Cu, Pd, Pt, Rh and Ir between monosulfide solid solution and sulfide liquid and the formation of compositionally zoned Ni-Cu sulfide bodies by fractional crystallisation of sulfide liquid. *Canadian Journal of Earth Sciences*, **34**, 366-374.

Blum, J.D., Wasserburg, G.J., Hutcheon, I.D., Beckett, J.R. and Stolper, E.M. (1989). Diffusion, phase equilibria and partitioning experiments in the Ni-Fe-Ru system. *Geochimica et Cosmochimica Acta*, **53**, 483-489.

Bruwer, J.S. (1996). *Experimental investigation of the system Cu-Ni-S in the temperature interval 1200°C to 700°C*. M.Sc. thesis (unpublished), University of Pretoria, South Africa, 157pp.

Bryukvin, V.A., Shekhter, L.N., Reznichenko, V.A., Kuvinov, V.E., Blokhina, L.I. and Kukoyev, V.A. (1985). Phase equilibria in the system Fe-Pd-S. *Izvest. Akad. Nauk SSSR, Metally*, **4**, 25-28. (in Russian)

Burylev, B.P., Mechev, V.V., Tsemekhan, L.Sh., Romanov, V.D. and Vaisburd, S.E. (1974). Distribution of palladium and platinum between the metal and sulphide in Cu-S and Cu-Ni-S melts. *Izvest. Akad. Nauk SSSR, Metally*, 82-86. (in Russian)

Cabri, L.J. (1988). Application of proton and nuclear microprobes in ore deposit mineralogy and metallurgy. *Nuclear Instruments and Methods in Physics Research B*, **30**, 459-465.

Cabri, L.J. and Campbell, J.L. (1998). The proton microprobe in ore mineralogy (Micro-PIXE technique). *In: Modern Approaches to Ore and Environmental Mineralogy*. Ed: Cabri, L.J. and Vaughan, D.J. Mineralogical Association of Canada, Short Course Series, 27, Chapter 7, 181-198.

Cabri, L.J., Harris, D.C. and Nobiling, R. (1984a). Trace silver analyses by proton microprobe in ore evaluation. *In: Precious metals: Mining, extraction and processing*, Ed: Kudryk, V., Corrigan, D.A. and Liang, W.W. The Metallurgical Society of AIME, New York, 93-100.

Cabri, L.J., Blank, H., El Goresy, A., Laflamme, J.H.G., Nobiling, R., Sizgoric, M.B. and Traxel, K. (1984b). Quantitative trace-element analyses of sulphides from Sudbury and Stillwater by proton microprobe. *Canadian Mineralogist*, **22**, 521-542.

Campbell, J.L., Maxwell, J.A., Teesdale, W.J. and Wang, J.-X. (1990). Micro-PIXE as a compliment to electron probe microanalysis in mineralogy. *Nuclear Instruments and Methods in Physics Research B*, **44**, 347-356.

Campbell, J.L., Teesdale, W.J., Kjarsgaard, B.A. and Cabri, L.J. (1996). Micro-PIXE analysis of silicate reference standards for trace Ni, Cu, Zn, Ga, Ge, As, Rb, Sr, Y, Zr, Nb, Mo and Pb, with emphasis on Ni for application of the Ni-in-garnet geothermometer. *Canadian Mineralogist*, **34**, 37-48.

Cemic, L. and Kleppa, O.J. (1986). High temperature calorimetry of sulphide systems. I. Thermochemistry of liquid and solid phases of Ni + S. *Geochimica et Cosmochimica Acta*, **50**, 1633-1641.

Chabot, N.L. and Drake, M.J. (1997). An experimental study of silver and palladium partitioning between solid and liquid metal, with applications to iron meteorites. *Meteoritics and Planetary Science*, **32**, 637-645.

Chakrabarti, D.J. and Laughlin, D.E. (1986). Cu-S. *In: Binary Alloy Phase diagrams*, Volume 1, Massalski, T.B. (Editor). American Society for Metals, Ohio, 953-957.

Chuang, Y. –Y, Hsieh, K.-C., and Austin Chang, Y. (1985). Thermodynamics and phase relationships of transition metal-sulfur systems: Part V. A re-evaluation of the Fe-S system using an associated solution model for the liquid phase. *Metallurgical Transactions*, **16B**, 277-285.

Cousens, D.R., French, D.H., Ramsden, A.R., Griffin, W.L., Ryan, C.G. and Sie, S.H. (1989). Application of the proton microprobe to the partitioning of Platinum Group Elements in sulphide and oxide phases. *Mineralogy-Petrology Symposium*, Sydney NSW, 45-49.

Crocket, J.H., Fleet, M.E. and Stone, W.E. (1997). Implications of composition for experimental partitioning of platinum-group elements and gold between sulfide liquid and basalt melt: The significance of nickel content. *Geochimica et Cosmochimica Acta*, **61**, 4139-4149.

Czamanske, G.K., Kunilov, V.E., Zientek, M.L., Cabri, L.J., Likhachev, A.P., Calk, L.C. and Oscarson, R.L. (1992). A proton-microprobe study of magmatic sulfide ores from the Noril'sk-Talnakh district, Siberia. *Canadian Mineralogist*, **30**, 249-287.

Czamanske, G.K., Sisson, T.W., Campbell, J.L. and Teesdale, W.J. (1993). Micro-PIXE analysis of silicate reference standards. *American Mineralogist*, **78**, 893-903.

Distler, V.V. (1980). Solid solutions of platinoids in sulphides. *In: Sulphosalts, platinum minerals and ore microscopy*. Proceedings of the General Meeting IMA, Novosibirsk 1978. IGEM Akad. Nauk SSSR, Nauka, 191-200. (in Russian)

Distler, V.V., Malevskiy, A. Yu. and Laputina, I.P. (1977). Distribution of platinoids between pyrrhotite and pentlandite in crystallisation of a sulphide melt. *Geochemistry International*, **14**, 30-40.

Fleet, M.E. (1987). Structure of godlevskite, Ni_9S_8. *Acta Crystallography*, **C43**, 2255-2257.

Fleet, M.E. (1988). Stoichiometry, structure and twinning of godlevskite and synthetic low-temperature Ni-excess nickel sulphide. *Canadian Mineralogist*, **26**, 283-291.

Fleet, M.E. and Stone, W.E. (1991). Partitioning of platinum-group elements in the Fe-Ni-S system and their fractionation in nature. *Geochimica et Cosmochimica Acta*, **55**, 245-253.

Fleet, M.E., Chryssoulis, S.L., Stone, W.E. and Weisener, C.G. (1993). Partitioning of platinum-group elements and Au in the Fe-Ni-Cu-S system: experiments on the

fractional crystallisation of sulphide melt. *Contributions to Mineralogy and Petrology*, **115**, 36-44.

Fleet, M.E., Liu, M and Crocket, J.H. (1999). Partitioning of trace amounts of highly siderophile elements in the Fe-Ni-S system and their fractionation in nature. *Geochimica et Cosmochimica Acta*, **63**, 2611-2622.

Franklyn, C.B. and Merkle, R.K.W. (1999). Milli-PIXE of co-existing cooperite and braggite - a comparison with electron microprobe analysis. *Nuclear Instruments and Methods in Physics Research B*, **158**, 550-555.

Franklyn, C.B. and Merkle, R.K.W. (2001) Surface contamination by smearing during polishing – a PIXE study. *Nuclear Instruments and Methods in Physics Research B*, **181**, 140-144.

Franklyn, C.B., Ueckermann, H. and Merkle, R.K.W. (2001) Accidental surface contamination – the effect on trace element analysis. *Nuclear Instruments and Methods in Physics Research B*, **181**, 145-149.

Gerlach, von J., Hennig, U. and Park, H.S. (1972). Über die Edelmetallverteilung auf Stein und Speise. *Erzmetall*, **25**, 69-77.

Gueddari, K., Piboule, M. and Amosse, J. (1996). Differentiation of platinum-group elements (PGE). and of gold during partial melting of peridotites in the lherzolitic massifs of the Betico-Rifean Range (Ronda and Beni Bousera). *Chemical Geology*, **134**, 181-197.

Halden, N.M., Campbell, J.L. and Teesdale, W.J. (1995). PIXE analysis in mineralogy and geochemistry. *Canadian Mineralogist*, **33**, 293-302.

Johansson, S.A.E. (1992). Particle Induced X-ray Emission and Complementary Nuclear Methods for trace element determination. *Analyst*, **117**, 259-265.

Jones, J.H. and Drake, M.J. (1983). Experimental investigations of trace element fractionation in iron meteorites, II: The influence of sulfur. *Geochimica et Cosmochimica Acta*, **47**, 1199-1209.

Jones, J.H. and Drake, M.J. (1986). Geochemical constraints on core formation in the earth. *Nature*, **322**, 221-228.

Jones, J.H. and Malvin, D.J. (1990). A non metal interaction model for the segregation of trace metals during solidification of Fe-Ni-S, Fe-Ni-P, and Fe-Ni-S-P alloys. *Metallurgical Transactions*, **21B**, 697-706.

Jones, J.H., Benjamin, T.M., Maggiore, C.M., Duffy, C.J. and Hart, S.R. (1986). Experimental partitioning of Ag, Mo, Pb and Pd between iron metal and troilite. *Proceedings of the 17th Lunar Planetary Science Conference*, 400-401.

Karup-Møller, S. and Makovicky, E. (1993). The system Pd-Ni-S at 900°, 725°, 550° and 400°C. *Economic Geology*, **88**, 1261-1268.

Karup-Møller, S. and Makovicky, E. (1999). The phase system Cu-Pd-S at 900°C, 725°C, 550°C and 400°C. *Neues Jahrbuch fur Mineralogie, Monatshefte*, 551-567.

Kolonin, G.R., Peregoedova, A.V. and Sinyakova, E.F. (1997). The physical-chemical model of fractionation of Pt, Ir and light PGE during crystallisation of sulphide melts. *The Betekhtin Symposium* (Moscow), Abstracts 270-271. (in Russian)

Kulagov, E.A., Evstigneeva, T.L. and Yushko-Zakharova, O.E. (1969). The new nickel sulphide, godlevskite. *Geol. Rudnykh. Mestorozhderii*, **11**, 115-121. (in Russian)

Kullerud, G. (1960). The Cu-S system. *Carnegie Institution of Washington Year Book*, **59**, 110-111.

Kullerud, G. (1961). Two-liquid field in the Fe-S system. *Carnegie Institution of Washington Year Book*, **60**, 174-176.

Kullerud, G. (1971). Experimental techniques in dry sulphide research. *In: Research techniques for high pressure and high temperatures.* Editor: G.C. Ulmer, Springer-Verlag, Berlin Heidelberg New York, 289-315.

Kullerud, G. and Yoder, H.S. (1959). Pyrite stability relations in the Fe-S system. *Economic Geology*, **54**, 533-572.

Kullerud, G. and Yund R.A. (1962). The Ni-S system and related minerals. *Journal of Petrology*, **3**, 126-175.

Legendre, O. and Auge, T. (1986). Mineralogy of platinum-group mineral inclusions in chromitites from different ophiolitic complexes. *In: Metallogeny of basic and ultrabasic rocks*. Editors: M.J. Gallagher *et al.*, Institute of Mining and Metallurgy, 361-372.

Li, C. and Barnes, S.-J. (1996). Partitioning of platinum-group elements and Au in the Fe-Ni-Cu-S system: experiments on the fractional crystallisation of sulphide melt – a discussion. *Contributions to Mineralogy and Petrology*, **123**, 435-437.

Li, C., Barnes, S.-J., Makovicky, E., Rose-Hansen, J.R. and Makovicky, M. (1996). Partitioning of Ni, Cu, Ir, Rh, Pt and Pd between monosulfide solid solution and sulfide liquid: effects on composition and temperature. *Geochimica et Cosmochimica Acta*, **60**, 1231-1238.

Lin, R.Y., Hu, D.C. and Chang, Y.A. (1978). Thermodynamics and phase relations of transition metal - sulfur systems. II. The nickel-sulfur system. *Metallurgical Transactions*, **9B**, 531-538.

Makovicky, E. and Karup-Møller, S. (1993). The system Pd-Fe-S at 900°, 725°, 550° and 400°C. *Economic Geology*, **88**, 1269-1278.

Makovicky, E. and Karup-Møller, S. (1994). The phase system Cu-Rh-S at 900°C, 725°C and 500°C. *7th International Platinum Symposium* (Moscow, Russia), Abstracts, 70-71.

Makovicky, E. and Karup-Møller, S. (1995). The system Pd-Fe-Ni-S at 900 and 725°C. *Mineralogical Magazine*, **59**, 685-702.

Makovicky, M., Makovicky, E. and Rose-Hansen, J. (1986). Experimental studies on the solubility and distribution of platinum group elements in base-metal sulphides in platinum deposits. *In: Metallogeny of basic and ultrabasic rocks*. Editors: M.J. Gallagher *et al.*, Institute of Mining and Metallurgy, 415-425.

Makovicky, M., Makovicky, E. and Rose-Hansen, J. (1988). Experimental evidence of the formation and mineralogy of platinum and palladium ore deposits. *In: Mineral Deposits within the European Community.* Editors: J. Boissonnas and P. Omenetto. Berlin-Heidelberg, Springer-Verlag, 303-317.

Makovicky, E., Karup-Møller, S., Makovicky, M. and Rose-Hansen, J. (1990). Experimental studies on the phase systems Fe-Ni-Pd-S and Fe-Pt-Pd-As-S applied to PGE deposits. *Mineralogy and Petrology*, **42**, 307-319.

Maxwell, J.A., Campbell, J.L. and Teesdale, W.J. (1989). The Guelph PIXE software package. *Nuclear Instruments and Methods in Physics Research B*, **43**, 218-230.

Maxwell, J.A., Teesdale, W.J. and Campbell, J.L. (1994). Compensation schemes for peak-tailing uncertainties in PIXE spectra, using the GUPIX code. *Nuclear Instruments and Methods in Physics Research B*, **94**, 172-179.

Maxwell, J.A., Teesdale, W.J. and Campbell, J.L (1995). The Guelph PIXE software package II. *Nuclear Instruments and Methods in Physics Research B*, **95**, 407-421.

Merkle, R.K.W. and Franklyn, C.B. (1999). Milli-PIXE determination of trace elements in osmium-rich platinum-group minerals from the Witwatersrand basin, South Africa. *Nuclear Instruments and Methods in Physics Research B*, **158**, 556-561.

Merkle, R.K.W., Franklyn, C.B., Przybylowicz, W. and Verryn, S.M.C. (in print). Submitted to *Nuclear Instruments and Methods in Physics Research B.*

Morimoto, N. and Gyobu, A. (1971). The composition and stability of digenite. *American Mineralogist*, **56**, 1889-1909.

Naldrett, A.J. (1981). Nickel sulphide deposits: Classification, composition, and genesis. *Economic Geology 75th Anniversary Volume*, 628-685.

Naldrett, A.J. (1989). Magmatic sulphide deposits. *Oxford Monographs on Geology and Geophysics*, Number 14, Clarendon Press, New York.

Naldrett, A.J., Gasparrini, E., Buchan, R. and Muir, J.E. (1972). Godlevskite (β-Ni_7S_6). from the Texmont mine, Ontario. *Canadian Mineralogist*, **11**, 879-885.

Naldrett, A.J., Hoffman, E.L., Green, A.H., Chou, C.-L. and Naldrett, S.R. (1979). The composition of Ni-sulfide ores, with particular reference to their content of PGE and Au. *Canadian Mineralogist*, **17**, 403-415.

Naldrett, A.J., Innes, D.G., Sowa, J. and Gorton, M.P. (1982). Compositional variations within and between five Sudbury ore deposits. *Economic Geology*, **77**, 1519-1534.

Noddack, Von W, Noddack, I. and Bohnstedt, U. (1940). Die Teilungskoeffizienten der Schwermetalle zwischen Eisensulfid und Eisen. I. *Zeitschrift für Anorganische und Allgemeine Chemie*, **244**, 252-280.

Page, N.J. and Talkington, R.W. (1984). Palladium, platinum, rhodium, ruthenium and iridium in peridotites and chromitites from ophiolite complexes in Newfoundland. *Canadian Mineralogist*, **22**, 137-149.

Paktunc, A.D., Hulbert, L.J. and Harris, D.C. (1990). Partitioning of the platinum-group and other trace elements in sulfides from the Bushveld Complex and Canadian occurrences of nickel-copper sulfides. *Canadian Mineralogist*, **28**, 475-488.

Palme, H. and Wlotzka, F. (1976). A metal particle from a Ca, Al-rich inclusion from the meteorite Allende, and the condensation of refractory siderophile elements. *Earth and Planetary Science Letters*, **33**, 45-60.

Pattou, L., Lorand, J.P. and Gros, M. (1996). Non-chondritic platinum-group element ratios in the earth's mantle. *Nature*, **379**, 712-715.

Peregoedova, A. (1997). The experimental study of Pt and Pd behaviour during crystallisation of Fe-Cu-Ni sulphide melts. *European Journal of Geosciences Conference 9*, Abstract 58/5P11.

Remond, G., Cesbron, F., Traxel, K., Campbell, J.L. and Cabri, L.J. (1987). Electron Microprobe analysis and Proton Induced X-ray Spectrometry applied to trace

element analysis in sulfides: problems and prospects. *Scanning Microscopy*, **1**, 1017-1037.

Rogers, P.S.Z., Duffy, C.J. and Benjamin, T.M. (1987). Accuracy of standardless nuclear microprobe trace element analyses. *Nuclear Instruments and Methods in Physics Research B*, **22**, 133-137.

Romanov, V.D., Mechev, V.V., Vaisburd, S.E. and Tsemekhan, L.Sh. (1973). Iridium, ruthenium and osmium in systems Cu-Cu_2S and Cu-Cu_2O. *Soviet Journal of Non-Ferrous Metals*, **14**, 13-14.

Rudashevskiy, N.S., Mochalov, A.G., Shkursky, V.V., Shumskaya, N.I. and Men'shikov, Y.P. (1984). The first discovery of malanite $Cu(Pt,Ir,Rh)_2S_4$ in the USSR. *Mineralogicheskiy Zhurnal*, **6**, 93-97. (in Russian with English abstract)

Rudashevskiy, N.S., Menachikov, Y.N., Mochalov, A.G., Trubkin, N.V., Shumskaya, N.I. and Zhdanov, V.V. (1985). Cuprorhodsite $CuRh_2S_4$ and cuproiridsite $CuIr_2S_4$, new natural thiospinels of platinum-group elements. *Zapiski Vsesoyuznogo Mineralogicheskogo Obshchestva*, **114**, 187-195. (in Russian)

Ryan, C.G., Cousens, D.R., Sie, S.H., Griffin, W.L. and Suter, G.F. (1990). Quantitative PIXE microanalysis of geological material using the CSIRO proton microprobe. *Nuclear Instruments and Methods in Physics Research B*, **47**, 55-71.

Schlitt, W.J. and Richards, K.J. (1973). The behaviour of selenium and tellurium in metal-matte systems. *Metallurgical Transactions*, **4**, 819-825.

Schlitt, W.J. and Richards, K.J. (1975). The distribution of silver, gold, platinum and palladium in metal-matte systems. *Metallurgical Transactions*, **6B**, 237-243.

Schmitt, W., Palme, H., and Wänke, H. (1989). Experimental determination of metal/silicate partition coefficients for P, Co, Ni, Cu, Ga, Ge, Mo, and W and some implication for the early evolution of the earth. *Geochimica et Cosmochimica Acta*, **53**, 173-185.

Sharma, R.C. and Chang, Y.A. (1980). Thermodynamics and phase relationships of transition metal-sulfur systems: IV. Thermodynamic properties of the Ni-S liquid phase and the calculation of the Ni-S phase diagram. *Metallurgical Transactions*, **11B**, 139-146.

Sie, S.H., Ryan, C.G., Cousens, D.R. and Griffin, W.L. (1989a). A Proton Microprobe for the Geosciences. *In: Ward, C.R. (Editor), Minpet 89: Mineralogy-Petrology Symposium.* Australasian Institute of Mining and Metallurgy, Sydney, 7-10.

Sie, S.H., Ryan, C.G., Suter, G.F., Cousens, D.R. and Griffin, W.L. (1989b). Determination of noble metals at crustal abundances. *In: Ward, C.R. (Editor), Minpet 89: Mineralogy-Petrology Symposium.* Australasian Institute of Mining and Metallurgy, Sydney, 33-35.

Simon, J.L. (1997). *Resampling: The "New Statistics"*. 2nd edition. Resampling Stats Inc. Arlington, VA, 436pp.

Skinner, B.J., Luce, F.D., Dill, J.A., Ellis, D.E., Hagen, H.A., Lewis, D.M., Odell, D.A., Sverjensky, D.A. and Williams, N. (1976). Phase relations in ternary portions of the system Pt-Pd-Fe-As-S. *Economic Geology*, **71**, 1469-1475.

Stone, W.E., Crocket, J.H. and Fleet, M.E. (1990). Partitioning of palladium, iridium, platinum and gold between sulphide liquid and basalt melt at 1200°C. *Geochimica et Cosmochimica Acta*, **54**, 2341-2344.

Taylor, J.R. (1983). A thermodynamic study of the distribution of metals between copper matte and bullion. *Advances in sulfide smelting*, 1, TMS-AIME, New York, 217-229.

Urban, H., Zereini, F., Skerstupp, B. and Tarkian, M. (1995). The determination of platinum-group elements (PGE). by nickel sulfide fire-assay: Coexisting PGE-phases in the nickel sulfide button. *Fresenius' Journal of Analytical Chemistry*, **352**, 537-543.

Walker, R.J., Hanski, E., Vuollo, J., and Liipo, J. (1996). The Os isotopic composition of Proterozoic upper mantle: evidence for chondritic upper mantle from the Outokumpu ophiolite, Finland. *Earth and Planetary Science Letters*, **141**, 161-173.

Willis, J. and Goldstein, J.I. (1982). The effects of C, P and S on trace element partitioning during solidification in Fe-Ni alloys. *Proceedings of the 13th Lunar Planetary Science Conference Part 1: Journal of Geophysical Research 87*, Supplement, A435-A445.

Appendix: Tables of experimental compositions and conditions.

Table A1. Ni-S charges for the 1200°C isothermal section.

Charge nr	Weight measured (g)					Weight %					Exp	Pre-reaction		Melt		1200°C	Remarks
	Ni	S	Pt	Pd	Rh	Ni	S	Pt	Pd	Rh		°C	Days	°C	Days	Days	
136	1.6974	0.2996	0.0012	0.0010	0.0010	84.862	14.979	0.060	0.050	0.050		800	13			9	Separated, resealed
																2	Separated
142	0.4225	0.0746	0.0010	0.0010	0.0010	84.483	14.917	0.200	0.200	0.200	HU446	800	13			9	
143	0.4245	0.0740	0.0010			84.985	14.815	0.200	0.000	0.000	HU447	800	13			9	
144	0.4241	0.0749		0.0011		84.803	14.977	0.000	0.220	0.000	HU448	800	13			9	
145	0.4241	0.0750			0.0011	84.786	14.994	0.000	0.000	0.220	HU449	800	13			9	
146	0.8475	0.1499	0.0010	0.0010	0.0010	84.716	14.984	0.100	0.100	0.100	HU824	800	13			9	Separated, resealed
																2	

Table A2. Ni-S charges for the 1100°C isothermal section.

Charge nr	Weight measured (g)					Weight %					Exp	Pre-reaction		Melt		1100°C	Remarks
	Ni	S	Pt	Pd	Rh	Ni	S	Pt	Pd	Rh		°C	Days	°C	Days	Days	
124	1.6974	0.2996	0.0010	0.0011	0.0010	84.866	14.979	0.050	0.055	0.050		800	47			13	Separated, resealed.
												800	4			13	Cracked in furnace, oxidised.
125	0.8479	0.1500	0.0011	0.0011	0.0010	84.697	14.984	0.110	0.110	0.100	HU466	800	47			13	Separated, resealed
												800	4			13	
126	0.4243	0.0751	0.0010			84.792	15.008	0.200	0.000	0.000		800	47			13	Separated, resealed.
												800	4			13	Cracked in furnace, oxidised.
127	0.4241	0.0753		0.0010		84.752	15.048	0.000	0.200	0.000	HU437	800	47			13	
132	0.4243	0.0749			0.0010	84.826	14.974	0.000	0.000	0.200	HU440	800	47			13	
133	0.4226	0.0748	0.0010	0.0010	0.0010	84.452	14.948	0.200	0.200	0.200	HU441	800	47			13	
594	1.6972	0.2996	0.0010	0.0013	0.0010	84.856	14.979	0.050	0.065	0.050	HU733	700	5			8	Duplicate of 124
595	0.4242	0.0749	0.0010			84.823	14.977	0.200	0.000	0.000	HU731	700	5			8	Duplicate of 126

Table A3. Ni-S charges for the 1000°C isothermal section.

Charge nr	Weight measured (g)					Weight %					Exp	Pre-reaction		Melt		1000°C	Remarks
	Ni	S	Pt	Pd	Rh	Ni	S	Pt	Pd	Rh		°C	Days	°C	Days	Days	
5	0.4245	0.0750	0.0014			84.747	14.973	0.279	0.000	0.000	HU378	800	14	1200	10	42	
6	0.4245	0.0753		0.0013		84.714	15.027	0.000	0.259	0.000	HU379	800	14	1200	10	42	
7	0.4242	0.0750			0.0011	84.789	14.991	0.000	0.000	0.220	HU380	800	14	1200	10	42	
8	0.4226	0.0746	0.0010	0.0010	0.0010	84.486	14.914	0.200	0.200	0.200	HU381	800	14	1200	10	42	
25	1.6975	0.2996	0.0010	0.0010	0.0012	84.862	14.978	0.050	0.050	0.060	HU392	800	48			35	
26	0.8480	0.1499	0.0011	0.0013	0.0010	84.690	14.971	0.110	0.130	0.100	HU393	800	33			35	
31	0.4174	0.0739	0.0030	0.0034	0.0032	83.330	14.753	0.599	0.679	0.639	HU394	800	33			35	
32	0.4123	0.0728	0.0050	0.0050	0.0050	82.444	14.557	1.000	1.000	1.000	HU395	800	33			35	Quenched slower
48	0.4226	0.0749	0.0010	0.0016	0.0011	84.318	14.944	0.200	0.319	0.219	HU399	800	26			35	Duplicate of 8
95	0.4122	0.0730	0.0050	0.0050	0.0050	82.407	14.594	1.000	1.000	1.000	HU412	700	14	1100	5hrs	15	Duplicate of 32
96	0.3743	0.1248	0.0020			74.696	24.905	0.399	0.000	0.000	HU461	700	14	1100	5hrs	15	Separated, resealed
												700	3	1200	3	14	
106	0.3746	0.1248		0.0010		74.860	24.940	0.000	0.200	0.000	HU462	700	14	1100	5hrs	15	Separated, resealed
												700	3	1200	3	14	
107	0.3742	0.1249			0.0011	74.810	24.970	0.000	0.000	0.220	HU463	700	14	1100	5hrs	15	Separated, resealed
												700	3	1200	3	14	
108	0.3727	0.1243	0.0010	0.0010	0.0010	74.540	24.860	0.200	0.200	0.200	HU464	700	14	1100	5hrs	15	Separated, resealed
												700	3	1200	3	14	
109	0.3682	0.1232	0.0030	0.0030	0.0030	73.581	24.620	0.600	0.600	0.600	HU414	700	14	1100	5hrs	15	
110	0.3637	0.1213	0.0055	0.0050	0.0050	72.687	24.236	1.099	0.999	0.999	HU415	700	14	1100	5hrs	15	
111	0.7478	0.2495	0.0018	0.0010	0.0010	74.698	24.923	0.180	0.100	0.100	HU416	700	14	1100	5hrs	15	
118	1.4978	0.4992	0.0010	0.0016	0.0010	74.868	24.953	0.050	0.080	0.050		700	14	1100	5hrs	15	Separated, resealed.
												700	3	1100	3	14	Cracked during reaction, oxidised.

Table A4. Ni-S charges for the 900°C isothermal section.

Charge nr	Weight measured (g)					Weight %					Exp	Pre-reaction		Melt		900°C	Remarks
	Ni	S	Pt	Pd	Rh	Ni	S	Pt	Pd	Rh		°C	Days	°C	Days	Days	
161	0.8474	0.1496	0.0010	0.0010	0.0011	84.732	14.959	0.100	0.100	0.110	HU753	800	43	1100	4	51	Separated, resealed
														1050	3	20	
162	1.6975	0.2995	0.0010	0.0010	0.0010	84.875	14.975	0.050	0.050	0.050		800	36	1100	4	51	Separated, resealed
														1050	3	20	Cracked in furnace, oxidised.
163	0.4241	0.0749	0.0011			84.803	14.977	0.220	0.000	0.000	HU426	800	43	1100	4	51	
164	0.4245	0.0752		0.0010		84.781	15.019	0.000	0.200	0.000	HU427	800	43	1100	4	51	
165	0.4241	0.0750			0.0014	84.735	14.985	0.000	0.000	0.280	HU428	800	43	1100	4	51	
166	0.4224	0.0746	0.0010	0.0010	0.0010	84.480	14.920	0.200	0.200	0.200	HU429	800	43	1100	4	51	
167	1.4978	0.4992	0.0011	0.0010	0.0012	74.879	24.956	0.055	0.050	0.060		800	36	1100	4	51	Separated, resealed
														1050	3	20	Cracked in furnace, oxidised.
168	0.7478	0.2492	0.0011	0.0010	0.0010	74.773	24.918	0.110	0.100	0.100		800	36	1100	4	51	Separated, resealed
														1050	3	20	Cracked in furnace, oxidised.
169	0.3729	0.1245	0.0010	0.0010	0.0014	74.461	24.860	0.200	0.200	0.280		800	43	1100	4	51	Separated, resealed
														1050	3	20	Cracked in furnace, oxidised.
173	0.3744	0.1250	0.0015			74.745	24.955	0.299	0.000	0.000	HU754	800	43	1100	4	51	Separated, resealed
														1050	3	20	
174	0.3742	0.1248		0.0010		74.840	24.960	0.000	0.200	0.000	HU433	800	43	1100	4	51	
175	0.3746	0.1249			0.0014	74.785	24.935	0.000	0.000	0.279	HU755	800	43	1100	4	51	Separated, resealed
														1050	3	20	
190	1.6975	0.2996	0.0010	0.0010	0.0010	84.871	14.979	0.050	0.050	0.050		800	4	1050	3	20	Duplicate of 162, oxidised in furnace.
191	0.8475	0.1496	0.0010	0.0011	0.0011	84.725	14.956	0.100	0.110	0.110		800	4	1050	3	20	Duplicate of 161, oxidised in furnace.

Table A5. Ni-S charges for the 800°C isothermal section.

Charge nr	Weight measured (g)					Weight %					Exp	Pre-reaction		Melt		800°C	Remarks
	Ni	S	Pt	Pd	Rh	Ni	S	Pt	Pd	Rh		°C	Days	°C	Days	Days	
46	0.4241	0.0749		0.0010		84.820	14.980	0.000	0.200	0.000	HU481	800	56			52	
67	1.6975	0.2998	0.0011	0.0010	0.0010	84.858	14.987	0.055	0.050	0.050		800	30			52	Cracked in PRF, resealed, failed
68	0.8474	0.1500	0.0010	0.0012	0.0010	84.689	14.991	0.100	0.120	0.100		800	30			52	Cracked in PRF, resealed, failed

Table A6. Ni-S charges for the 700°C isothermal section.

Charge nr	Weight measured (g)					Weight %					Exp	Pre-reaction		Melt		700°C	Remarks
	Ni	S	Pt	Pd	Rh	Ni	S	Pt	Pd	Rh		°C	Days	°C	Days	Days	
43	1.6975	0.2996	0.0010	0.0012	0.0010	84.862	14.978	0.050	0.060	0.050		800	56	1000	5hrs	23	Cracked in PRF, resealed, failed
44	0.8475	0.1496	0.0018	0.0012	0.0011	84.648	14.942	0.180	0.120	0.110		800	56	1000	5hrs	23	Cracked in PRF, resealed, failed
45	0.4246	0.0750	0.0010			84.818	14.982	0.200	0.000	0.000	HU470	800	56	1000	5hrs	23	
47	0.4246	0.0749			0.0012	84.801	14.959	0.000	0.000	0.240		800	56	1000	5hrs	23	Cracked in PRF, resealed, failed
59	0.4243	0.0750	0.0012			84.775	14.985	0.240	0.000	0.000	HU471	800	30	1000	5hrs	23	Duplicate of 45
60	0.4241	0.0751		0.0011		84.769	15.011	0.000	0.220	0.000	HU472	800	30	1000	5hrs	23	
61	0.4241	0.0749			0.0010	84.820	14.980	0.000	0.000	0.200	HU473	800	30	1000	5hrs	23	Duplicate of 47
62	0.4224	0.0748	0.0010	0.0010	0.0011	84.429	14.951	0.200	0.200	0.220	HU474	800	30	1000	5hrs	23	
79	0.4230	0.0745	0.0011	0.0010	0.0010	84.499	14.882	0.220	0.200	0.200	HU475	700	10	1000	5hrs	23	
94	1.6980	0.2998	0.0012	0.0010	0.0012	84.849	14.981	0.060	0.050	0.060	HU469	800	50	1000	5hrs	23	Duplicate of 43
187	0.4242	0.0750			0.0010	84.806	14.994	0.000	0.000	0.200	HU776	700	5	1050	1	12	Duplicate of 47, 61. Separated, resealed.
																18	
188	1.6975	0.2996	0.0010	0.0012	0.0010	84.862	14.978	0.050	0.060	0.050	HU777	700	5	1050	1	12	Duplicate of 43, 94. Separated, resealed.
																18	

Table A7. Cu-S charges for the 1200°C isothermal section.

Charge nr	Weight measured (g)					Weight %					Exp	Pre-reaction		Melt		1200°C	Remarks
	Cu	S	Pt	Pd	Rh	Cu	S	Pt	Pd	Rh		°C	Days	°C	Days	Days	
137	1.7975	0.1997	0.0012	0.0011	0.0012	89.844	9.982	0.060	0.055	0.060		800	13			9	Cracked during reaction, oxidised.
138	0.8973	0.0997	0.0010	0.0010	0.0010	89.730	9.970	0.100	0.100	0.100	HU442	800	13			9	
139	0.4491	0.0499	0.0010			89.820	9.980	0.200	0.000	0.000	HU443	800	13			9	
140	0.4491	0.0499		0.0010		89.820	9.980	0.000	0.200	0.000	HU444	800	13			9	
141	0.4492	0.0499			0.0010	89.822	9.978	0.000	0.000	0.200	HU445	800	13			9	
147	0.4473	0.0497	0.0012	0.0010	0.0010	89.424	9.936	0.240	0.200	0.200	HU450	800	13			9	

Table A8. Cu-S charges for the 1100°C isothermal section.

Charge nr	Weight measured (g)					Weight %					Exp	Pre-reaction		Melt		1100°C	Remarks
	Cu	S	Pt	Pd	Rh	Cu	S	Pt	Pd	Rh		°C	Days	°C	Days	Days	
128	0.4491	0.0500	0.0010			89.802	9.998	0.200	0.000	0.000		800	47			13	Separated, resealed.
												800	4			13	Cracked during reaction, oxidised.
129	0.4493	0.0499		0.0010		89.824	9.976	0.000	0.200	0.000	HU438	800	47			13	
130	0.4491	0.0499			0.0010	89.820	9.980	0.000	0.000	0.200	HU439	800	47			13	
131	0.4477	0.0499	0.0010	0.0011	0.0010	89.415	9.966	0.200	0.220	0.200	HU467	800	47			13	Separated, resealed
												800	4			13	
134	1.7972	0.1997	0.0012	0.0010	0.0011	89.851	9.984	0.060	0.050	0.055		800	47			13	Cracked during reaction.
135	0.8977	0.0997	0.0010	0.0011	0.0010	89.725	9.965	0.100	0.110	0.100	HU468	800	47			13	Separated, resealed
												800	4			13	
211	1.7979	0.1997	0.0015	0.0013	0.0010	89.832	9.978	0.075	0.065	0.050		800	4			13	Duplicate of 134, separated, resealed
																8	Separated again.

Table A9. Cu-S charges for the 1000°C isothermal section

Charge nr	Weight measured (g)					Weight %					Exp	Pre-reaction		Melt		1000°C	Remarks
	Cu	S	Pt	Pd	Rh	Cu	S	Pt	Pd	Rh		°C	Days	°C	Days	Days	
9	0.4494	0.0498	0.0018			89.701	9.940	0.359	0.000	0.000	HU382	800	14	1200	10	42	
10	0.4494	0.0498		0.0016		89.736	9.944	0.000	0.319	0.000	HU383	800	14	1200	10	42	
11	0.4492	0.0499			0.0015	89.732	9.968	0.000	0.000	0.300	HU384	800	14	1200	10	42	
12	0.4473	0.0497	0.0011	0.0015	0.0010	89.353	9.928	0.220	0.300	0.200	HU385	800	14	1200	10	42	
17	0.3888	0.1099	0.0011	0.0013	0.0011	77.419	21.884	0.219	0.259	0.219		800	59				Failed in PRF
18	1.7975	0.1997	0.0010	0.0011	0.0011	89.857	9.983	0.050	0.055	0.055	HU386	800	59			35	
19	0.8973	0.0995	0.0010	0.0010	0.0015	89.703	9.947	0.100	0.100	0.150	HU387	800	59			35	
20	0.3892	0.1098	0.0012			77.809	21.951	0.240	0.000	0.000	HU388	800	12			40	Cracked during quenching
21	0.3899	0.1098		0.0010		77.871	21.929	0.000	0.200	0.000	HU389	800	12			40	Cracked during quenching
22	0.3898	0.1098			0.0010	77.867	21.934	0.000	0.000	0.200	HU390	800	12			40	Cracked during quenching
23	0.7777	0.2193	0.0012	0.0012	0.0010	77.739	21.921	0.120	0.120	0.100		800	18				Failed in PRF
24	1.5580	0.4398	0.0010	0.0014	0.0015	77.834	21.971	0.050	0.070	0.075	HU391	800	48			35	
33	0.4460	0.0494	0.0030	0.0030	0.0030	88.422	9.794	0.595	0.595	0.595	HU396	800	40			35	
34	0.4378	0.0485	0.0050	0.0049	0.0050	87.350	9.677	0.998	0.978	0.998		800	40				Failed in PRF
35	0.3829	0.1080	0.0030	0.0030	0.0034	76.534	21.587	0.600	0.600	0.680	HU397	800	40			35	
36	0.3785	0.1065	0.0052	0.0051	0.0051	75.639	21.283	1.039	1.019	1.019	HU398	800	40			35	
54	0.7777	0.2193	0.0010	0.0011	0.0014	77.731	21.919	0.100	0.110	0.140	HU400	800	26			35	Duplicate of 23
91	0.4365	0.0487	0.0050	0.0050	0.0053	87.213	9.730	0.999	0.999	1.059		700	14	1100	5hrs	15	Duplicate of 34, failed in furnace.
92	0.3880	0.1093	0.0010	0.0010	0.0015	77.476	21.825	0.200	0.200	0.300	HU411	700	14	1100	5hrs	15	Duplicate of 17
102	0.7777	0.2193	0.0010	0.0010	0.0010	77.770	21.930	0.100	0.100	0.100	HU413	700	14	1100	5hrs	15	Duplicate of 23, 54
183	0.4492	0.0499		0.0010		89.822	9.978	0.000	0.200	0.000	HU417	700	14	1100	5hrs	15	Duplicate of 10
184	0.3898	0.1100	0.0017			77.727	21.934	0.339	0.000	0.000	HU418	700	14	1100	5hrs	15	Duplicate of 20
185	0.3895	0.1098		0.0010		77.853	21.947	0.000	0.200	0.000	HU419	700	14	1100	5hrs	15	Duplicate of 21
186	0.3892	0.1098			0.0010	77.840	21.960	0.000	0.000	0.200	HU420	700	14	1100	5hrs	15	Duplicate of 22
210	0.4367	0.0490	0.0050	0.0055	0.0050	87.131	9.777	0.998	1.097	0.998	HU365	700	3	1200	3	14	Duplicate of 34, 91

Table A10. Cu-S charges for the 900°C isothermal section.

Charge nr	Weight measured (g)					Weight %					Exp	Pre-reaction		Melt		900°C	Remarks
	Cu	S	Pt	Pd	Rh	Cu	S	Pt	Pd	Rh		°C	Days	°C	Days	Days	
152	1.7973	0.1997	0.0010	0.0010	0.0010	89.865	9.985	0.050	0.050	0.050		800	35	1100	4	51	Separated, resealed
														1050	3	20	Oxidised in furnace.
153	0.8973	0.0999	0.0010	0.0010	0.0010	89.712	9.988	0.100	0.100	0.100		800	43	1100	4	51	Separated, resealed
														1050	3	20	Separated again.
154	0.4493	0.0500	0.0010			89.806	9.994	0.200	0.000	0.000		800	43	1100	4	51	Separated, resealed
														1050	3	20	Oxidised in furnace.
155	0.4491	0.0499		0.0010		89.820	9.980	0.000	0.200	0.000	HU421	800	43	1100	4	51	
156	0.4494	0.0502			0.0015	89.683	10.018	0.000	0.000	0.299	HU422	800	43	1100	4	51	
157	0.4474	0.0497	0.0012	0.0011	0.0010	89.408	9.932	0.240	0.220	0.200	HU423	800	43	1100	4	51	
159	0.7777	0.2193	0.0010	0.0010	0.0010	77.770	21.930	0.100	0.100	0.100	HU424	800	43	1100	4	51	Cracked in PRF, resealed
160	0.3878	0.1093	0.0011	0.0010	0.0012	77.498	21.843	0.220	0.200	0.240	HU425	800	43	1100	4	51	
170	0.3892	0.1098	0.0013			77.793	21.947	0.260	0.000	0.000	HU430	800	43	1100	4	51	
171	0.3891	0.1098		0.0010		77.836	21.964	0.000	0.200	0.000	HU431	800	43	1100	4	51	
172	0.3894	0.1098			0.0010	77.849	21.951	0.000	0.000	0.200	HU432	800	43	1100	4	51	
179	1.5579	0.4397	0.0012	0.0010	0.0010	77.864	21.976	0.060	0.050	0.050		800	35	1050	3	20	Cracked in PRF, resealed, failed in furnace.

Table A11. Cu-S charges for the 800°C isothermal section.

Charge nr	Weight measured (g)					Weight %					Exp	Pre-reaction		Melt		800°C	Remarks
	Cu	S	Pt	Pd	Rh	Cu	S	Pt	Pd	Rh		°C	Days	°C	Days	Days	
38	0.4494	0.0499	0.0010			89.826	9.974	0.200	0.000	0.000	HU483	800	70			52	
39	0.4493	0.0499		0.0010		89.824	9.976	0.000	0.200	0.000	HU484	800	56			52	
40	0.4490	0.0500			0.0013	89.746	9.994	0.000	0.000	0.260	HU485	800	56			52	
42	0.8973	0.0997	0.0015	0.0011	0.0010	89.676	9.964	0.150	0.110	0.100	HU482	800	56			52	
71	0.4477	0.0497	0.0013	0.0010	0.0012	89.379	9.922	0.260	0.200	0.240		800	30			52	Cracked, oxidised.
78	1.7973	0.1999	0.0010	0.0010	0.0010	89.856	9.994	0.050	0.050	0.050		700	51			52	Cracked, oxidised.

Table A12. Cu-S charges for the 700°C isothermal section.

Charge nr	Weight measured (g)					Weight %					Exp	Pre-reaction		Melt		700°C	Remarks
	Cu	S	Pt	Pd	Rh	Cu	S	Pt	Pd	Rh		°C	Days	°C	Days	Days	
41	0.4473	0.0500	0.0010	0.0010	0.0012	89.371	9.990	0.200	0.200	0.240		800	56	1000	5hrs	23	Cracked, oxidised.
49	1.7973	0.1999	0.0012	0.0011	0.0010	89.843	9.993	0.060	0.055	0.050		800	26				Failed in PRF
65	0.4493	0.0499	0.0014			89.752	9.968	0.280	0.000	0.000	HU779	800	30	1000	5hrs	23	Separated
												700	5	1050	1	12	
69	0.4493	0.0499		0.0010		89.824	9.976	0.000	0.200	0.000	HU477	800	30	1000	5hrs	23	
70	0.4491	0.0499			0.0011	89.802	9.978	0.000	0.000	0.220	HU478	800	30	1000	5hrs	23	
77	0.8973	0.0997	0.0010	0.0012	0.0010	89.712	9.968	0.100	0.120	0.100	HU476	700	20	1000	5hrs	23	
100	1.7975	0.1997	0.0010	0.0013	0.0011	89.848	9.982	0.050	0.065	0.055		800	50	1000	5hrs	23	Duplicate of 49, failed

Table A13. Fe-S charges for the 1200°C isothermal section.

Charge nr	Weight measured (g)					Weight %					Exp	Pre-reaction				Melt		1200°C	Remarks
	Fe	S	Pt	Pd	Rh	Fe	S	Pt	Pd	Rh		°C	Days	°C	Days	°C	Days	Days	
212	0.3927	0.0999	0.0011			79.542	20.235	0.223	0.000	0.000	HU825	800	41	700	149			2	Cracked in PRF, resealed, cracked and resealed 2nd time.
213	0.3933	0.0986		0.0013		79.745	19.992	0.000	0.264	0.000	HU826	800	41	700	149			2	Cracked in PRF, resealed
214	0.3919	0.0987			0.0010	79.719	20.077	0.000	0.000	0.203	HU827	800	41	700	149			2	Cracked in PRF, resealed
215	0.3219	0.1733	0.0011			64.860	34.918	0.222	0.000	0.000		800	41	700	149			2	Cracked in PRF, resealed, cracked and resealed 2nd time, oxidised at 1200°C.
216	0.3238	0.1744		0.0013		64.825	34.915	0.000	0.260	0.000		800	41	700	149			2	Cracked in PRF, resealed, oxidised at 1200°C
217	0.3212	0.1729			0.0012	64.850	34.908	0.000	0.000	0.242		800	41	700	149			2	Cracked in PRF, resealed, cracked and resealed 2nd time, oxidised at 1200°C.

Table A14. Fe-S charges for the 1100°C isothermal section.

Charge nr	Weight measured (g)					Weight %					Exp	Pre-reaction				Melt		1100°C	Remarks
	Fe	S	Pt	Pd	Rh	Fe	S	Pt	Pd	Rh		°C	Days	°C	Days	°C	Days	Days	
218	0.3914	0.0982	0.0012			79.747	20.008	0.244	0.000	0.000	HU734	700	149					8	Uncertain of equilibrium conditions.
219	0.3921	0.0980		0.0012		79.809	19.947	0.000	0.244	0.000	HU735	700	149					8	
220	0.3906	0.0979			0.0010	79.796	20.000	0.000	0.000	0.204	HU736	700	149					8	Uncertain of equilibrium conditions.
221	0.3207	0.1727	0.0010			64.867	34.931	0.202	0.000	0.000	HU737	700	149					8	Uncertain of equilibrium conditions.
222	0.3212	0.1730		0.0010		64.863	34.935	0.000	0.202	0.000	HU738	700	149					8	Resealed after prereaction.
223	0.3198	0.1724			0.0010	64.842	34.955	0.000	0.000	0.203	HU739	700	149					8	Cracked during prereaction.

Table A15. Fe-S charges for the 1000°C isothermal section.

Charge nr	Weight measured (g)					Weight %					Exp	Pre-reaction				Melt		1000°C	Remarks
	Fe	S	Pt	Pd	Rh	Fe	S	Pt	Pd	Rh		°C	Days	°C	Days	°C	Days	Days	
1	0.3993	0.0999	0.0012			79.796	19.964	0.240	0.000	0.000		800	15			1200	10	2	Completely oxidised in furnace.
2	0.3999	0.0999		0.0013		79.804	19.936	0.000	0.259	0.000		800	15			1200	10	2	Completely oxidised in furnace.
3	0.3994	0.1002			0.0010	79.784	20.016	0.000	0.000	0.200		800	15			1200	10	2	Completely oxidised in furnace.
4	0.3985	0.1005	0.0010	0.0014	0.0014	79.256	19.988	0.199	0.278	0.278		800	15			1200	10	2	Completely oxidised in furnace.
13	0.3242	0.1746	0.0010			64.866	34.934	0.200	0.000	0.000		800	89						Failed in PRF
14	0.3242	0.1748		0.0010		64.840	34.960	0.000	0.200	0.000		800	89						Failed in PRF
15	0.3246	0.1748			0.0010	64.868	34.932	0.000	0.000	0.200		800	89						Failed in PRF
16	0.3232	0.1745	0.0012	0.0013	0.0013	64.447	34.796	0.239	0.259	0.259		800	89						Failed in PRF
27	0.3946	0.0984	0.0032	0.0028	0.0031	78.590	19.598	0.637	0.558	0.617		800	32						Failed in PRF
28	0.3880	0.0970	0.0050	0.0050	0.0050	77.600	19.400	1.000	1.000	1.000		800	32						Failed in PRF
29	0.3199	0.1719	0.0030	0.0030	0.0029	63.891	34.332	0.599	0.599	0.579		800	32						Failed in PRF
30	0.3153	0.1698	0.0050	0.0050	0.0050	63.047	33.953	1.000	1.000	1.000		800	32						Failed in PRF
37	1.2980	0.6999	0.0015	0.0017	0.0015	64.816	34.950	0.075	0.085	0.075		800	21						Failed in PRF
64	0.7976	0.1995	0.0010	0.0010	0.0010	79.752	19.948	0.100	0.100	0.100		800	56						Failed in PRF
66	1.5976	0.3994	0.0010	0.0010	0.0010	79.880	19.970	0.050	0.050	0.050		800	56						Failed in PRF
98	0.7977	0.1994	0.0010	0.0010	0.0010	79.762	19.938	0.100	0.100	0.100		800	41						Duplicate of 64, failed in PRF
104	0.6442	0.3464	0.0010	0.0011	0.0015	64.796	34.842	0.101	0.111	0.151		800							Exploded in PRF
105	0.3958	0.0990	0.0010			79.831	19.968	0.202	0.000	0.000		800	41						Duplicate of 1, failed in PRF
112	0.3979	0.0995		0.0011		79.819	19.960	0.000	0.221	0.000	HU843	800	41	700	149			15	Duplicate of 2, cracked in PRF, resealed twice
113	0.3975	0.0995			0.0010	79.819	19.980	0.000	0.000	0.201	HU844	800	41	700	149			15	Duplicate of 3, cracked in PRF, resealed
114	0.3948	0.0987	0.0011	0.0010	0.0010	79.501	19.875	0.222	0.201	0.201	HU845	800	41	700	149			15	Duplicate of 4, cracked in PRF, resealed
115	0.3230	0.1739	0.0010			64.872	34.927	0.201	0.000	0.000	HU846	800	41	700	149			15	Duplicate of 13, cracked in PRF, resealed twice
116	0.3216	0.1732		0.0011		64.852	34.926	0.000	0.222	0.000	HU847	800	41	700	149			15	Duplicate of 14, cracked in PRF, resealed
117	0.3235	0.1747			0.0010	64.804	34.996	0.000	0.000	0.200	HU848	800	41	700	149			15	Duplicate of 15, cracked in PRF, resealed
119	0.3929	0.0982	0.0030	0.0031	0.0030	78.549	19.632	0.600	0.620	0.600	HU849	800	41	700	149			15	Duplicate of 27, cracked in PRF, resealed
120	0.3885	0.0971	0.0050	0.0050	0.0054	77.545	19.381	0.998	0.998	1.078	HU850	800	41	700	149			15	Duplicate of 28, cracked in PRF, resealed
121	0.3176	0.1710	0.0030	0.0035	0.0030	63.762	34.330	0.602	0.703	0.602		800	41						Duplicate of 29, failed in PRF
122	0.3157	0.1700	0.0050	0.0051	0.0050	63.039	33.946	0.998	1.018	0.998	HU851	800	41	700	149			15	Duplicate of 30, cracked in PRF, resealed
123	0.3232	0.1741	0.0010	0.0010	0.0010	64.601	34.799	0.200	0.200	0.200	HU852	800	41	700	149			15	Duplicate of 16, cracked in PRF, resealed twice
150	1.5918	0.3980	0.0010	0.0014	0.0010	79.862	19.968	0.050	0.070	0.050		800							Duplicate of 66, exploded in PRF
151	1.2940	0.6968	0.0010	0.0012	0.0011	64.891	34.943	0.050	0.060	0.055		800							Duplicate of 37, exploded in PRF

Table A16. Fe-S charges for the 900°C isothermal section.

Charge nr	Weight measured (g)					Weight %					Exp	Pre-reaction				Melt		900°C	Remarks
	Fe	S	Pt	Pd	Rh	Fe	S	Pt	Pd	Rh		°C	Days	°C	Days	°C	Days	Days	
176	0.3923	0.0980	0.0009			79.866	19.951	0.183	0.000	0.000	HU434	800	43			1100	4	51	
177	0.3992	0.0981		0.0013		80.064	19.675	0.000	0.261	0.000	HU435	800	43			1100	4	51	
178	0.3937	0.0986			0.0011	79.793	19.984	0.000	0.000	0.223	HU436	800	43			1100	4	51	
180	0.7880	0.1970	0.0014	0.0010	0.0010	79.725	19.931	0.142	0.101	0.101	HU756	800	34			1050	3	20	Cracked in PRF, resealed, separated, not equilibrium.
181	0.3909	0.0977	0.0012	0.0011	0.0010	79.467	19.862	0.244	0.224	0.203		800	34			1050	3	20	Cracked in PRF, resealed, oxidised in furnace.
182	1.5758	0.3940	0.0011	0.0010	0.0010	79.872	19.971	0.056	0.051	0.051		800	6			1050	3	20	Cracked in PRF, resealed, oxidised in furnace.

Table A17. Fe-S charges for the 800°C isothermal section.

Charge nr	Weight measured (g)					Weight %					Exp	Pre-reaction				Melt		800°C	Remarks
	Fe	S	Pt	Pd	Rh	Fe	S	Pt	Pd	Rh		°C	Days	°C	Days	°C	Days	Days	
85	0.3992	0.0996	0.0010			79.872	19.928	0.200	0.000	0.000	HU785	800	93					12	Cracked in PRF, resealed
86	0.3991	0.0996		0.0010		79.868	19.932	0.000	0.200	0.000	HU784	800	93					12	Cracked in PRF, resealed
87	0.3993	0.1000			0.0012	79.780	19.980	0.000	0.000	0.240		800	93						Failed in PRF
88	0.3936	0.0988	0.0010	0.0010	0.0013	79.403	19.931	0.202	0.202	0.262	HU783	800	93					12	Cracked in PRF, resealed
97	0.7686	0.1971	0.0010	0.0010	0.0011	79.753	19.933	0.101	0.101	0.111	HU786	800	62					12	Cracked in PRF, resealed
99	1.5876	0.3969	0.0010	0.0013	0.0010	79.867	19.967	0.050	0.065	0.050	HU782	800	62					12	Failed in PRF
149	1.5893	0.3977	0.0010	0.0010	0.0010	79.864	19.985	0.050	0.050	0.050		800							Duplicate of 99, exploded in PRF

Table A18. Fe-S charges for the 700°C isothermal section.

Charge nr	Weight measured (g)					Weight %					Exp	Pre-reaction				Melt		700°C	Remarks
	Fe	S	Pt	Pd	Rh	Fe	S	Pt	Pd	Rh		°C	Days	°C	Days	°C	Days	Days	
55	0.3992	0.0998	0.0012			79.808	19.952	0.240	0.000	0.000		800	56						Failed in PRF
56	0.3992	0.0998		0.0010		79.840	19.960	0.000	0.200	0.000		800	56						Failed in PRF
57	0.3992	0.0998			0.0010	79.840	19.960	0.000	0.000	0.200		800	56						Failed in PRF
58	0.3976	0.0994	0.0010	0.0015	0.0010	79.441	19.860	0.200	0.300	0.200		800	56						Failed in PRF
82	0.3992	0.0998	0.0015			79.760	19.940	0.300	0.000	0.000		800	93	700	5	1050	1	12	Duplicate of 55, cracked in PRF, resealed, oxidised
83	0.3995	0.1000		0.0010		79.820	19.980	0.000	0.200	0.000		800	93						Duplicate of 56, failed
84	0.3992	0.0998			0.0010	79.840	19.960	0.000	0.000	0.200		800	93	700	5	1050	1	12	Duplicate of 57, cracked in PRF, resealed, oxidised
89	0.3941	0.0985	0.0010	0.0014	0.0010	79.456	19.659	0.202	0.282	0.202		800	93						Duplicate of 58, failed in PRF
93	0.7916	0.1980	0.0010	0.0011	0.0010	79.742	19.946	0.101	0.111	0.101		800	63						Failed in PRF
103	1.5934	0.3984	0.0010	0.0013	0.0010	79.866	19.969	0.050	0.065	0.050		800	31						Failed in PRF
148	1.5888	0.3972	0.0010	0.0013	0.0010	79.867	19.967	0.050	0.065	0.050		800							Duplicate of 103, exploded in PRF

Abstract

Partitioning of platinum-group elements between metal and sulphide melt in the Cu-S and Ni-S systems.

By

Henriëtte Ueckermann

Study leader: Prof. R. K. W. Merkle

Degree: M. Sc. Applied Mineralogy

The partitioning behaviour of the three platinum-group elements (PGE), Rh, Pd and Pt, was investigated at trace concentrations between phases in the systems Cu-S and Ni-S at low S contents. Additional exploratory investigations of partitioning in the Fe-S system were also performed. Experiments were equilibrated in quartz tubes at temperatures between 1200°C and 700°C, and were analysed by Electron Probe Micro Analyser for the major elements and Particle Induced X-ray Emission for the trace elements. Quantitative data on the partitioning of PGE at temperatures relevant to the formation and development of PGE deposits are of great importance in the exploration, ore beneficiation, and metallurgy of PGE.

Both Pt and Rh are compatible with nickel as opposed to sulphide melt at all temperatures investigated. D_{Rh} increases from 1.6 at 1100°C to 9.9 at 700°C, and similarly D_{Pt} from 4 to 200. Pd is concentrated in the melt, with D_{Pd} similarly increasing from 0.5 to 0.9. All three become more compatible with nickel as the temperature decreases. As the sulphur content of the melt increases at lower temperatures, other researchers (e.g. Li *et al.*, 1996; Fleet *et al.*, 1999) have suggested that partition coefficients are more dependent on the S content in the melt than on temperature itself, but in this investigation the two factors could not be discriminated.

Rh, Pd and Pt were all concentrated in the Cu-rich melt that co-exists with S-rich melt at 1200°C, with $D_{Rh} > 10$, $D_{Pd} \sim 7.5$, and $D_{Pt} > 3$. All three PGE were concentrated in the sulphide melt that co-exists with digenite at 1000°C, with D_{Rh} varying from 4 to 62, D_{Pd} from 2.9 to 4.8, and D_{Pt} from 12.7 to 23.6. All three platinum-group elements also prefer the copper as opposed to the digenite at 1000°C, with $D_{Rh} > 15$ at 1000°C and ~45 at 800°C, D_{Pd} varying from 23 to 675 – differing between instruments - and $D_{Pt} > 13$.

Rh and Pt preferably partition into iron that co-exists with sulphide melt at 1200°C, 1100°C and 1000°C. $D_{Rh} > 2$ and $D_{Pt} > 1.1$, and probably much larger. D_{Pd} changes from slightly incompatible at 1200°C (0.98) to compatible at 1000°C (>1.2). All three PGE partition into sulphide melt that co-exists with pyrrhotite at 1100°C, with $D_{Rh} > 3.7$, $D_{Pd} > 10.5$, and $D_{Pt} > 3.8$. At 900°C all three PGE partition into iron as opposed to troilite, with $D_{Rh} > 2.1$, $D_{Pd} \sim 1.2$, and $D_{Pt} > 1.6$.

Uittreksel

Skeiding van platinum-groep elemente tussen metaal en sulfied smeltsels in die Cu-S and Ni-S sisteme.

Deur

Henriëtte Ueckermann

Studie leier: Prof. R. K. W. Merkle

Graad: M. Sc. Applied Mineralogy

Die verdelingsgedrag van die drie platinum-groep elemente (PGE), Rh, Pd en Pt, in spoor hoeveelhede, is by lae S inhoude in die Cu-S en Ni-S stelsels ondersoek. Bykomende eksploratoriese ondersoeke van verdeling is ook in die Fe-S stelsel gedoen. Eksperimente is ge-ekwilibreer in kwarts glasbuisies by temperature tussen 1200°C en 700°C. Hoofelemente is bepaal deur wyse van elektron mikrosonde analises en spoorelemente deur Partikel geinduseerde X-straal emissie analises. Kwantitatiewe data van die skeidingsgedrag van PGE by temperature relefant tot die vorming en ontwikkeling van PGE afsettings is van groot belang vir die eksplorasie, benefisiering en metallurgie van PGE.

Beide Rh en Pt verkies nikkel teenoor die sulfied smeltsel by al die temperature wat ondersoek is. D_{Rh} neem toe van 1.6 by 1100°C tot 9.9 by 700°C, en soortgelyk D_{Pt} van 4 tot 200. Pd konsentreer in die smeltsel, met D_{Pd} wat soortgelyk toeneem van 0.5 tot 0.9. Al drie PGE konsentreer tot 'n hoër mate in die nikkel by laer temperature. Aangesien die S inhoud van die smeltsel toeneem by laer temperature, is daar deur ander navorsers (bv. Li *et al.*, 1996; Fleet *et al.*, 1999) voorgestel dat verdelingskoëffisiente eerder meer afhanklik is van die S inhoud van die smeltsel as die temperatuur, maar in die huidige studie kan daar nie tussen hierdie twee faktore onderskei word nie.

Rh, Pd en Pt is almal gekonsentreer in die Cu-ryke smeltsel wat saam met die S-ryke smeltsel voorkom by 1200°C, met $D_{Rh} > 10$, $D_{Pd} \sim 7.5$, en $D_{Pt} > 3$. Al drie PGE is in die sulfied smeltsel wat saam met digeniet by 1000°C voorkom gekonsentreer, met D_{Rh} wisselend van 4 tot 62, D_{Pd} van 2.9 tot 4.8, en D_{Pt} van 12.7 tot 23.6. Al drie PGE verkies ook koper bo digeniet by 1000°C, met $D_{Rh} > 15$ by 1000°C en ~45 by 800°C, D_{Pd} wisselend van 23 tot 675 – en verskillend van instrument tot instrument – en $D_{Pt} >13$.

Rh and Pt verdeel eerder in die yster wat saam met sulfied smeltsel voorkom by 1200°C, 1100°C and 1000°C. D_{Rh} is > 2 en $D_{Pt} > 1.1$, en waarskynlik baie groter. Pd verander van effens gekonsentreer in die smeltsel by 1200°C (0.98) tot meer gekonsentreerd in die yster by 1000°C (>1.2). Al drie PGE verkies die sulfied smeltsel bo pyrrhotiet by 1100°C, met $D_{Rh} > 3.7$, $D_{Pd} > 10.5$, en $D_{Pt} > 3.8$. By 900°C verkies al drie PGE yster teenoor troiliet, met $D_{Rh} > 2.1$, D_{Pd} ongeveer 1.2, en $D_{Pt} > 1.6$.